CRANFIELD UNIVERSITY

LUIGI SERIO

A CRYOGENIC HELIUM MASS FLOWMETER FOR THE LARGE HADRON COLLIDER

SCHOOL OF ENGINEERING

PhD

CRANFIELD UNIVERSITY

SCHOOL OF ENGINEERING

DEPARTMENT OF PROCESS AND SYSTEMS ENGINEERING

Ph.D. THESIS

Academic Year 2007-2008

LUIGI SERIO

A CRYOGENIC HELIUM MASS FLOWMETER FOR THE LARGE HADRON COLLIDER

Supervisor: Dr. J. Hemp

September 2007

This thesis is submitted in partial fulfilment of the requirements for the degree of Doctor of Philosophy

TO ANNA-CARLA, BIANCA AND MARICA

Abstract

This thesis is concerned with the design, development and testing of helium mass flowmeters based on different technologies to be used as diagnostic tools for the cryogenic system of the Large Hadron Collider at CERN, the European laboratory for particle physics. The flowmeters were designed and the performance assessed for liquid, supercritical and superfluid helium down to 1.8 K and with pressures up to 0.3 MPa.

A testing regime and equipment to enable the performance of a range of developed flowmeters to be validated at working cryogenic temperatures and pressures is described in the thesis. In particular a novel cryogenic flow test facility with 1.5 % accuracy as well as an irradiation test station designed, constructed and used as part of the evaluation work are described in the thesis. The final validation with metrological certification down to 0.5 % accuracy was performed in collaboration with the Colonnetti metrological laboratory in Italy.

Devices based on the thermal exchange and transport properties of the fluid were developed and proven to be reliable and inexpensive but with accuracy poorer than 10 %. As part of this work a new empirical heat transfer correlation for supercritical helium in the piping geometry and operating conditions of the LHC was established.

Industrially available Coriolis meters which had not been employed before at such low temperatures were extensively investigated. It was found that with some minor modifications in the electronics (drive system) and in the elasticity modulus (Young's modulus) value for the flow tubes material at low temperature, accuracy down to 0.5 % could be achieved. Additional features in the mechanical and electrical design were also introduced to improve robustness and reliability at

cryogenic temperatures. They mainly consisted in purging the meters secondary containment with helium to avoid gas freezing at low temperatures and increasing the internal gauge wire to improve its fatigue strength. The elasticity modulus of 316 L stainless steel below 20 K was characterised and compared to available literature data.

The successful Coriolis flowmeters were validated to meter the cryogenic power distribution in the 27-km long superfluid helium system of the future collider and are now extensively and successfully used in superconducting devices test facilities at CERN and in companion laboratories.

ACKNOWLEDGMENTS

I wish to acknowledge the Department of Process and Systems Engineering of Cranfield University for having sponsored this research and in particular Prof. M.L. Sanderson for accepting and supporting my thesis project and my supervisor, Dr. J. Hemp, for his valuable advice and guidance.

Special thanks to J. Casas-Cubillos and A. Rivetti for their expertise, advice and fruitful discussion throughout the research work.

The experimental part of this work has been conducted mainly at CERN, in the Cryogenics for Accelerators Group, Accelerator Technology Department, and at IMGC Turin, in the framework of my work project to identify methods and instruments to meter supercritical helium flow for the Large Hadron Collider machine. I wish to acknowledge the support of my various supervisors over the years, A. Bezaguet, W. K. Erdt and L. J. Tavian, and my department head Ph. Lebrun for giving me the opportunity to work on this project.

Final but not least, I must acknowledge the support given to me by my two daughters and my wife who kindly allowed me to work and study on this subject over evenings, week-ends and holidays.

TABLE OF CONTENTS

LIST OF FIGURES

LIST OF TABLES

NOMENCLATURE

The unit system used is the SI unless otherwise specified. The least used symbols and notation are described in the text and therefore not listed below.

Symbols

A	cross sectional area [m^2]
A_c	cross sectional area [m^2]
A_t	cross sectional area [m^2]
C_d	discharge coefficient factor
C_p	specific heat at constant pressure [J kg^{-1} K^{-1}]
C_v	specific heat at constant volume [J kg^{-1} K^{-1}]
d	orifice bore or wire/element diameter [m]
D	internal pipe diameter [m]
e	thickness [m]
E	spring constant of the tube or elastic modulus [GPa]
f	rotational frequency [s^{-1}]
g	acceleration due to gravity [m s^{-2}]
h	heat transfer coefficient [W m^{-2} K^{-1}]
H	enthalpy [J kg^{-1}]
k	thermal conductivity [W m^{-1} K^{-1}]
K	constant, allows for the fact that the twist of the tube will not form a straight integration
l	length [m]
L	latent heat [J g^{-1}]
m	mass [kg]
$\dot{m}$	mass flow rate [kg s^{-1}]
p	pressure [Pa]
$\dot{q}$	rate of heat transfer per unit area [W m^{-2}]
$\dot{q}_L$	rate of heat transfer per unit length [W m^{-1}]
$\dot{q}_h$	specific rate of heat transfer [J kg^{-1}]
Q_c	cooling power [W]
Q_h	heat flow [W]
Re	Reynolds number
s	entropy per unit mass [J kg^{-1} K^{-1}]
S	pipe inner cross-sectional area [m^2]
t	time [s]
T	temperature [K]
u	velocity component [m s^{-1}]

$\vec{u}$	velocity vector [m s^{-1}]
$\tilde{u}$	average velocity in the flow cross-section [m s^{-1}]
U	specific internal energy [J kg^{-1}]
v	velocity component [m s^{-1}]
V_{OL}	volumetric flow [m^3 s^{-1}]
Y	gas expansion factor
θ	deflection or twist angle [rad]
μ	absolute viscosity [kg m^{-1} s^{-1}]
υ	kinematic viscosity[m^2 s^{-1}]
ρ	density [kg m^3]
ω	driving frequency [s^{-1}]
ω_s	natural frequency of tube in twisting oscillation [s^{-1}]
$\vec{\Omega}$	angular velocity [rad s^{-1}]

Units not in the SI system

eV	electron charge (1 eV = 1.6 10^{-19} J)
bar	pressure (1 bar = 10^5 Pa)

Chapter 1

1. INTRODUCTION

CERN's mission is to create new knowledge in the field of particle physics and to study the constituents of matter and the nature of fundamental forces. Fundamental research is an investment in the future which adds to the culture heritage of our civilization and to the quality of our life. It is also the source of concrete progress and of practical inventions, with an impact on everyday life, because progress in fundamental research is only possible through the development of technology and technology advances only through progress in understanding/knowledge.

CERN is currently engaged in a difficult and exciting enterprise, the realization of a new accelerator, the Large Hadron Collider (LHC), where high-intensity proton beams will collide head-on at unprecedented energies. The extreme conditions will give new research possibilities, to test predicted but as yet unobserved phenomena and to search for the unknown. The LHC will fulfil a world-wide scientific mission and will enhance international scientific co-operation to reduce its overall technical cost.

In the framework of the design and construction of the LHC a vigorous R&D activity was launched to advance technologies in the field of superconductivity, cryogenics and vacuum physics in order to push the accelerator energy frontier up by an order of magnitude while remaining economically feasible. This required research, development and industrial collaboration in several fields, one of which, mass flow metering of cryogenic fluids, is reported herewith. The work aim was

to complement the instrumentation available for low temperature physics. The objective is now fulfilled with a technology transfer in industry for use also in other applications: superconductivity R&D laboratories, space propulsion and nuclear fusion superconducting technologies. Furthermore, one of the developed and tested flowmeters is now a certified secondary standard for mass flow measurements at cryogenic temperatures.

1.1 CERN

CERN is the European Organization for Nuclear Research, the world's largest particle physics centre. Founded in 1954, the laboratory was one of Europe's first joint ventures, and is an example of international collaboration. From the original 12 signatories of the CERN convention, membership has grown to the present 20 Member States (figure 1).

Figure 1: The twenty Member States of CERN

The CERN accelerator complex and facilities are based in Geneva, Switzerland and the 27-km long accelerator ring stretches across the Swiss-French border between the Lake of Geneva and the Jura mountains (figure 2).

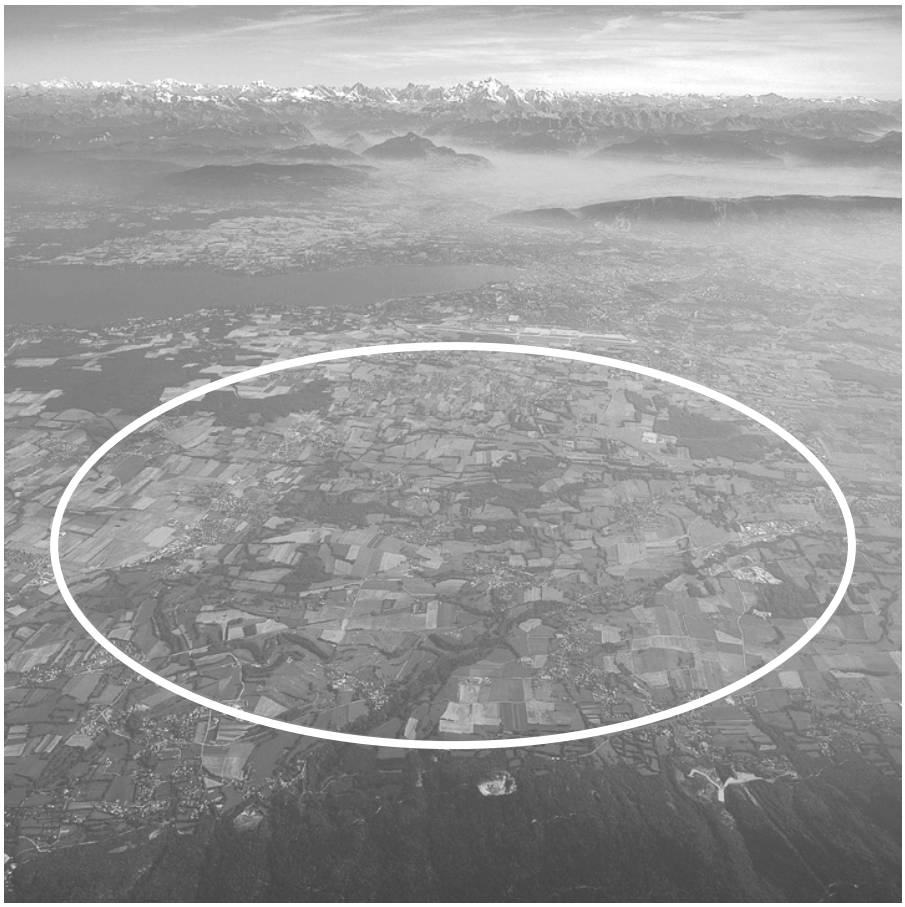

Figure 2: Aerial view of the position of CERN main accelerator ring in Geneva suburban area

Today CERN has become the largest and leading Laboratory in High Energy Particle physics and a worldwide centre of excellence by providing researchers with unique instruments for their experiments. Some 7000 particle physicists, representing 500 universities and over 80 nationalities, have access to CERN experiments and facilities. For this community of physicists, CERN staff designs

and builds intricate machinery and ensures its smooth operation. It helps prepare, run, analyse and interpret the complex scientific experiments and carries out the variety of tasks required. It produces scientific results that are occasionally rewarded by Nobel Prize. CERN is a non-profit-making organization whose annual budget, comparable to that of a large European university, is funded by its Member States.

CERN employs some 2500 people, encompassing a wide range of skills and trades - physicists, engineers, programmers, technicians, craftsmen, administrators, secretaries, workmen.

1.2 The Large Hadron Collider

The LHC is the particle accelerator built to serve the world's high-energy physics community at CERN. Completed at the end of 2007, it will begin operation in 2008 to investigate proton-proton collision at higher energy (up at least one order of magnitude) than any existing accelerator worldwide. Proton collisions at 14 TeV will be used to search for the Higgs boson of unknown mass, predicted by the Standard Model (Coughlan and Dodd, 1991) to be the carrier particles of the Higgs field which is thought to permeate the universe and to give mass to other particles.

The Standard Model, universally recognized, assesses that the coupling between forces and matter is achieved via particles of integer spin called bosons. Photons are the bosons for the electromagnetic force (atom, light), the W± and Z for the nuclear weak force (neutron, sun combustion), the gluons for the nuclear strong force (nucleons), the graviton for gravitational force (yet to be discovered) and the Higgs for the Higgs field (Zeppenfeld, Nikitenko, Richter-Was, 2000).

To investigate matter and forces, beams of elementary particles (protons – electrons) are accelerated by means of electromagnetic fields in long underground installations (safety and radiation screening) at speeds approaching that of light. After collision the kinetic energy is transformed into new particles which are detected and analyzed by large, in size and complexity, detectors.

The LHC will therefore accelerate proton beams to energy levels never obtained before and, following the laboratory tradition of re-investment in its previous infrastructure, will make use of the previous accelerator complex (figure 3) for injection and the 27-km long existing tunnel previously used for the electron-positron machine (LEP). As the cost of civil engineering makes up for almost half of the accelerator costs, this makes the LHC a valuable re-investment for the particle physics world community.

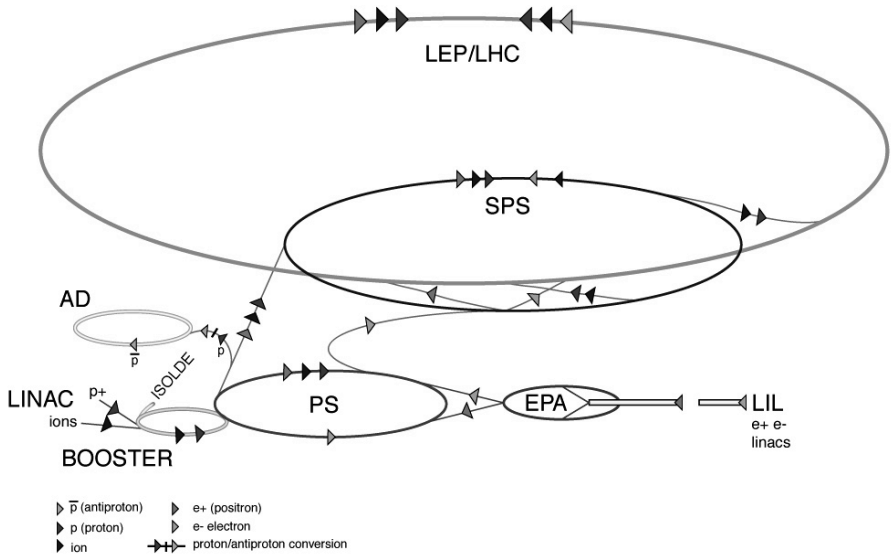

Figure 3: CERN accelerator complex

The 7 TeV protons circulating in the ring will require bending by magnetic fields of 8.4 T (more than hundred thousand times the earth magnetic field) all around

the 27-km circumference. As demonstrated in the last twenty-years all the above can be achieved, technically and economically, by R&D in the field of superconducting technology and related low-temperature cooling systems.

1.3 The superconducting magnets and the cryogenic system

The LHC accelerator as been designed to achieve the required machine performances to explore the particle physics world at the required energy as from the Standard Model. The main technical parameters of the machine as a proton collider are listed in table 1.

Energy at collision	7	TeV
Energy at injection	450	GeV
Dipole field at 7 TeV	8.33	T
Coil inner diameter	56	mm
Distance between aperture axes (1.9 K)	194	mm
Luminosity	1	E34 $cm^{2}s^{1}$
Beam beam parameter	3.6	E-3
DC beam current	0.56	A
Bunch spacing	7.48	m
Bunch separation	24.95	ns
Number of particles per bunch	1.1	E11
Normalized transverse emittance (r.m.s.)	3.75	μm
Total crossing angle	300	μrad
Luminosity lifetime	10	h
Energy loss per turn	7	keV
Critical photon energy	44.1	eV
Total radiated power per beam	3.8	kW
Stored energy per beam	350	MJ
Filling time per ring	4.3	min

Table 1: LHC general parameters

The basic technological key to the LHC is the development and industrial production of high-field superconducting accelerator dipole and quadrupole magnets in the 8 to 9 T range.

The superconductor chosen is Nb-Ti operating in superfluid helium at the temperature of 1.9 K. Nb-Ti has been preferred to other alternative compounds such as Nb_3Sn because of brittleness problems, limited industrial availability (LHC requirements are on the order of 1200 t of superconductor) and costs. The operating temperature is dictated by the decreasing of the critical current with temperature (figure 4).

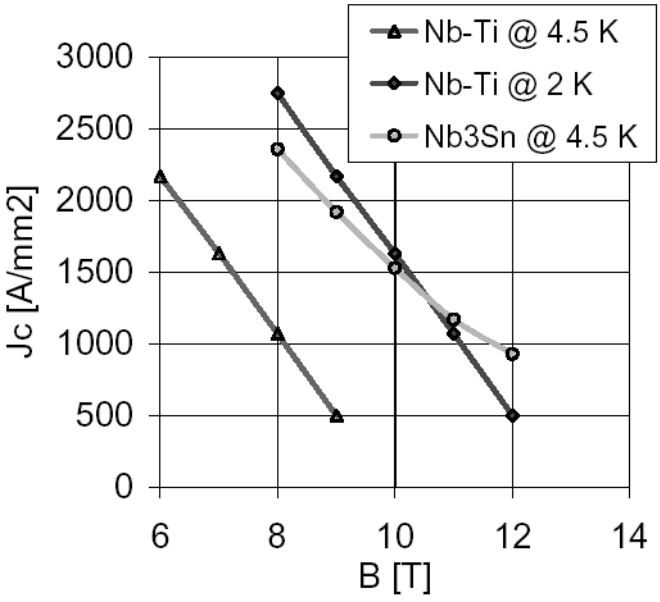

Figure 4: Critical current density of superconductors (Wilson, 1983)

The superconducting coils are made with the so called Rutherford type multi-strand cable made of Nb-Ti filaments inside a resistive and twisted matrix. Non-magnetic collars resting against a stiff iron yoke take the large electromagnetic

forces acting on the conductors. The all is contained in an all-welded shrinking cylinder that also acts as helium enclosure and pressure vessel (figure 5).

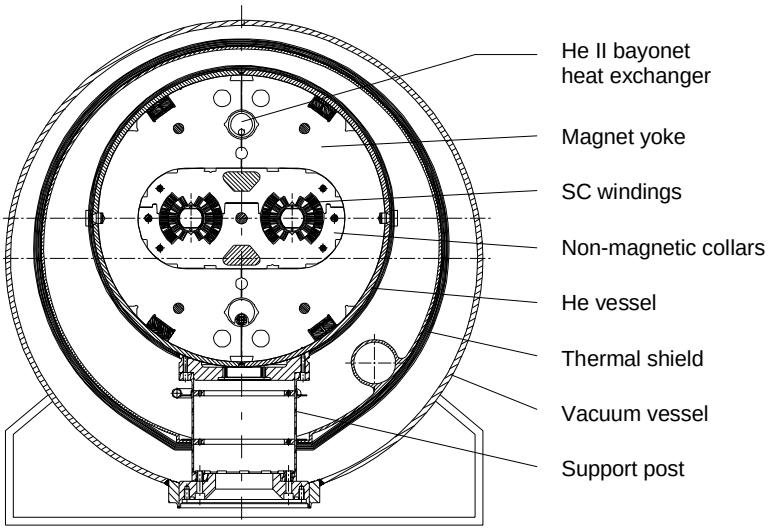

Figure 5: LHC dipole cross section

Another specific feature of the LHC main magnets system is the twin-aperture design. Two sets of windings in a common mechanical and magnetic structure produce the anti-parallel fields required to guide the counter-rotating particle beams. The two in one structure is more compact (space in the underground tunnel) and more efficient as the stray flux of one aperture contributes to increasing the fields in the neighbouring one.

Besides the 1232 main 15-m long dipoles and 392 main quadrupoles, the LHC makes use of auxiliary corrector magnets to correct for multipoles and orbit errors. A total of 8000 superconducting magnets will therefore maintain the particles in their precise circular orbits.

All superconducting magnets, representing 30 000 t of material along the 27-km long tunnel, are cooled in a bath of 700 000 litres of superfluid helium at 1.9 K (-271 deg C).

Lowering the magnet temperatures below 2 K brings other advantages related to the quantum fluid characteristics of helium at this temperature. Its high specific heat (about 2000 times that of copper per unit volume) and low viscosity (permeation) enhance dramatically the windings stability against thermal disturbances. Furthermore, its high thermal conductivity (about 1000 times that of OFHC[1] copper) permits to extract and transport heat over long distances with minimum temperature differences.

The thermodynamic drawback of extracting heat at such low temperatures is limited by an appropriate staging of heat loads. Intermediate cooled thermal shields and heat intercepts are employed together with high efficiency refrigeration cycles. Long-term development on cryogenics technology has given effective solutions for the LHC. Nevertheless, the requirement of high efficiency, extensive thermal testing of components, distribution over long distances of cooling capacity, has shown the lack of robust and accurate instruments to assess thermal loads and meter cooling power distribution via mass flow rate metering.

1.4 Layout of the LHC machine

The LHC is composed of two synchrotrons installed in the 27-km long tunnel of the previous LEP machine (electron-positron collider). Proton beams will be delivered from a smaller and existing synchrotron where they will be accelerated to 450 GeV. The two injection systems are localized in point 2 and 8 (see figure 6). Superconducting magnet strings will guide and focalize the accelerated protons up to 7 TeV. The two beams will run in opposite directions and will

[1] Oxygen Free High Conductivity

collide in the 4 experiment regions where huge detectors are installed underground in the caverns. The experiment detectors ATLAS, ALICE, CMS and LHC-b are located in the 500-m long short straight sections in points 1, 2, 5 and 8. The other four short straight sections house collimation systems in points 3 and 7, a beam dump system in point 6 and radiofrequency cavities for acceleration of the protons in point 4. In these 8 short straight sections there are the so-called inner triplets and non-standard cryostats to collimate and make collide or deviate the high energy beams.

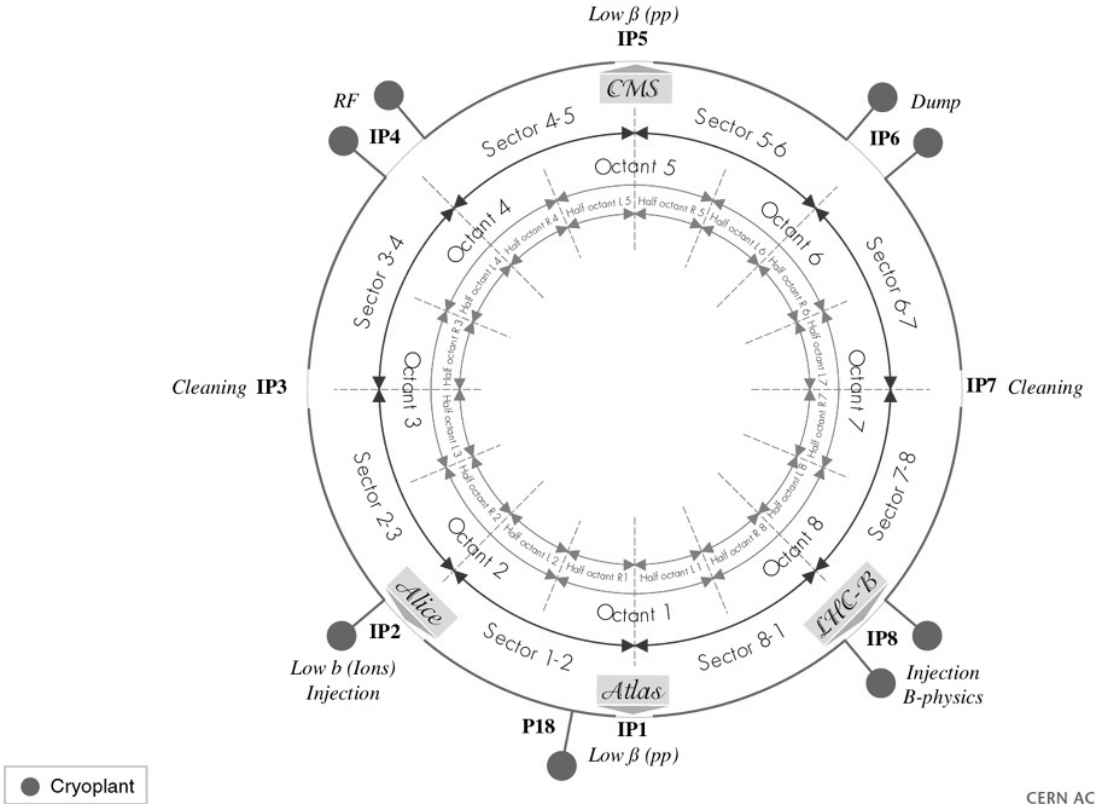

Figure 6: Schematic layout of the LHC machine with cryogenic and vacuum architecture (cryoplants and sectorization valves)

The lattice or periodic pattern of the machine is made of eight identical arcs (or sectors) of 2460 m length, each composed of 23 full cells. Each cell is of the

FODO (focalizing, de-focalizing) type and is made of two half cells of 53.45 m length (see figure 7). The full cell is composed of several superconducting magnets: 6 bending dipoles (14.30 m each), one focalizing and one de-focalizing quadrupole (3.1 m each), some orbit and multipole field correctors.

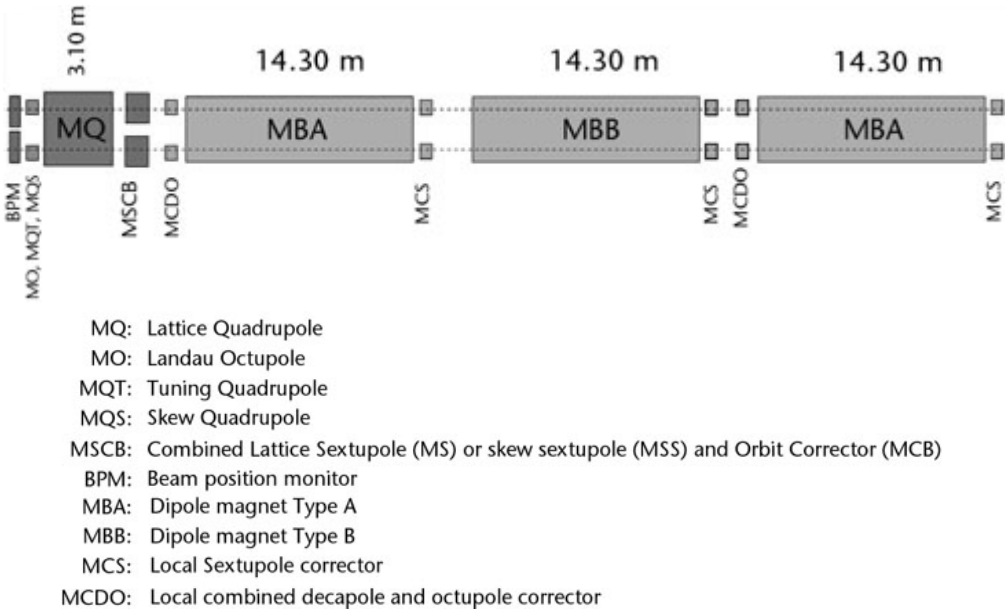

Figure 7: LHC arc half cell

1.5 Aim and objectives

The aim of this work was to find a suitable device to meter cryogenic helium (below 20 K) flow in the LHC machine for diagnostic purposes and to measure precisely (better than 2.5 % accuracy) the thermal performances of LHC components. The objectives were to find, optimize or design, and then test and validate devices suitable to operate in the accelerator environment. The analysis, design, development, tests and qualification of methods to meter flow of cryogenic helium are the main scope of this project.

The work has required an extensive and difficult (due to the lack of prior research in the field) bibliographic search, analysis of environmental constraints, establishment of a functional specification, project management, external (to CERN) institute and industrial collaboration management, technology transfer, in-depth knowledge of accelerator key technologies (superconductivity and cryogenics), design and construction of novel instruments and cryogenic test facilities, running of experimental test stations, data collection and analysis, validation of the instrument of final choice on the prototype LHC machine taking into account hardware (mechanical and electrical) and operational constraints of an industrial-like installation.

Chapter 2 is a bibliography review of methods and devices available to meter cryogenic helium flow. The search results showed the lack of robust and accurate devices working at cryogenic temperatures, but they also identified methods and instruments available at ambient temperature that could be applied successfully, with minor modifications, at cryogenic temperatures. At the same time a functional specification was established on the basis of the future accelerator operating conditions, the characteristics of the cryogenic distribution system and the environmental conditions (i.e. installation in insulation vacuum, accessibility, radiation, etc.).

Chapter 3 and 4 present the physical properties of helium and the cryogenic system of the LHC machine in order to identify the fluid properties of interest, verify the required performance of the instrument and permit a first selection of possible physical parameters to infer mass flow rates.

The analysis of the properties and heat transfer of the fluid at nominal operating conditions in chapter 5 has allowed the author to identify limitations and drawbacks of some devices and advantages of others.

The design, development and construction of prototype flowmeters are presented in chapter 6.

Chapter 7 describes the design and construction of the dedicated supercritical helium test rig and the calibration test station used to validate the final prototypes to metrological standards.

Chapters 8 presents the experimental results obtained by the author in the various test facilities as well as radiation compatibility tests and long-term testing and reliability in a full scale model of the LHC machine, designed and operated by the author to validate accelerators systems and components prior to installations in the machine tunnel.

Chapter 9 analyzes and interprets the experimental results on the flowmeters, the heat transfer coefficients, the measurement of Young's modulus and the measurements made on density waves in the superconducting helium.

The analysis identifies the Coriolis meter as the most suitable flowmeter for the proposed application. It is capable of measuring cryogenic helium flow having a temperature below 20 K with an accuracy of better than $\pm$ 2 % using room temperature calibration on water and better than $\pm$ 0.5 % with individual calibrations using the working fluid at the working temperatures. The Coriolis flowmeter provides direct measurement of the mass flow rate. It is robust and the sensors are radiation tolerant. The electronics can be installed in shielded areas up to several hundred metres from the sensors. Alternative solutions to meter supercritical helium flows are also discussed and compared to the proposed devices.

The heat transfer correlations based on experimental results used to design the thermal flowmeters are also presented together with a suitable empirical heat transfer law proposed for supercritical helium in our specific geometry.

An alternative and accurate method to measure the Young's modulus at cryogenic temperatures below 20 K is presented.

Density waves provoking pressure and temperature oscillations were encountered during the tests. The author's findings are compared with other work performed at CERN and elsewhere.

Chapter 10 provides the recommendations for future work. These include work to verify the long term behaviour of the Coriolis meters in the accelerator environment and to improve other types of flowmeter, such as the thermal probe flowmeter, performances. The possibility of using Coriolis meters to investigate cryogenic helium density oscillations and to measure the Young's modulus at low temperature is also identified.

Chapter 2

2. LITERATURE REVIEW

Flow rate metering is an essential tool for many industries such as public utilities, chemical or petroleum, that use the information obtained from these devices for control, indication or alarm or for commercial or fiscal purposes. Because of the enormous economic impact of accurate flow measurement there is an important market for flow metering devices and a great effort has been invested to improve their accuracy. Many of the commercially available instruments are used in cryogenic facilities to meter flow at ambient temperature on the outlets of the installations but little information is collected on the flow at cryogenic temperature and the sharing of cooling power. Some of the commercially available instruments could in principle also be used in cryogenic facilities and at cryogenic temperatures but would require some work to adapt the hardware (mechanics and electronics) and the operating principles. Recent and complete reviews of flow measurement at ambient conditions have been published elsewhere (Spitzer, 1991, (a) and Baker, 2000, (a)). While flow metering of cryogens at room temperature is well defined and instruments of various types are industrially available, the same is not valid for flow measurements at low temperature. A rather scarce literature and unavailability of commercial devices makes it difficult to identify and correctly operate a flow meter with helium at cryogenic temperature. Furthermore, the lack of tests and calibration facilities at cryogenic nominal working conditions reduces the chance to measure a cryogenic helium flow with accuracy better than 10 %. Rivetti, Martini and Birello, 1996, published a review of flow measurement at cryogenic temperatures together with an outlook of possible methods. The paper describes devices available (mainly

Venturi and turbine flow meters) together with their intrinsic limitations and needs for calibration. Those devices were built and used in laboratory applications and seemed already not suitable for large scale or industrial cryogenic installations where problems of reliability, lack of instrumentation to identify sufficiently the fluid properties, instabilities of the meter fluid and maintenance were not taken into account. Some possible methods of flow measurements at cryogenic temperature were listed but never tested. The present work starts from that proposal to further investigate the use of new possible methods for cryogenic helium flow metering, design and built prototypes, test and prove their reliability and accuracy at nominal operating conditions.

As far as cryogenics is concerned, flow metering devices are used for (a) assessment of cryogenic loads, (b) process monitoring and control and (c) detection of faults and wear on pumping machinery. Apart from oil contamination in the ambient temperature circuits, most of the gaseous fluids used in cryogenics are pure, clean and are well described by the ideal gas law. However when a fluid rate is to be measured at cryogenic temperatures care is necessary in order to avoid the presence of two-phase flow or cavitation that makes the interpretation of data very difficult and can also compromise the reliability of the flowmeter (Rivetti, Martini and Birello, 1996).

2.1 Fundamentals of flow measurement

When using flow metering devices it is important to become familiar with the various fluid[2] properties and with the equations related to the measurement of matter in motion. The main fluid properties for gas flow rate meters are: temperature, pressure, density and viscosity, and are usually well described by the ideal gas law. It is important to note that the following equations are valid as long

[2] A fluid is a substance, such as liquid or gas, that can flow, has no fixed shape and offers little resistance to an external stress

as the velocity is much lower than the velocity of sound in the medium and thermal exchange is ignored (Landau and Lifchitz, 1971).

The transport of frictionless, incompressible fluid through a pipe is described by the equation of continuity, Bernoulli's theorem and the Reynolds number Re. The equation of continuity states the conservation of mass:

$$\frac{\partial \rho}{\partial t} + \nabla \cdot (\rho \vec{u}) = 0 \tag{2.1a}$$

where ρ is the fluid's density, t the time and $\vec{u}$ the velocity. When considering incompressible fluids flowing along a pipe the previous equation can be simplified and represents the conservation of volumetric flow, V_{OL}:

$$V_{OL} = S_1 \tilde{u}_1 = S_2 \tilde{u}_2 \tag{2.1b}$$

where S is the pipe inner cross-sectional area, $\tilde{u}$ is the average velocity in the flow cross-section and the subscripts refer to different positions along the pipe, see figure 8.

The equation of Bernoulli is the result of the conservation of energy along a line of flow and in the absence of viscosity is:

$$\rho \frac{u^2}{2} + p + \rho\, g\, z = \text{constant} \tag{2.2}$$

where p is the pressure, g is the acceleration due to gravity and z is the vertical distance from a reference horizontal plane. At this point it is possible to introduce the concept of head or energy that is often used by engineers; in equation 2.2 the first term is the velocity head (kinetic energy), the second is the pressure head (static energy) and the last one is the elevation head (potential energy). All

flowmeters based on the measurement of differential pressure apply equation 2.2 to infer the mass flow rate.

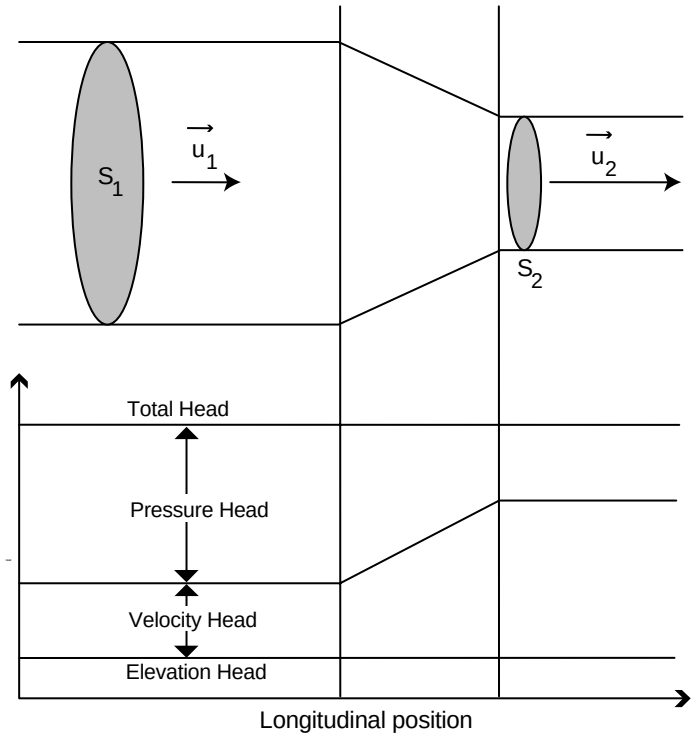

Figure 8: Conservation of volumetric flow and Bernoulli's theorem

When a real fluid flows through a pipe, energy is dissipated by non reversible processes, one of the main causes being the fluid's viscosity that, in a fully developed flow, produces longitudinal velocity gradients in the piping. A dimensionless quantity called the Reynolds number *Re* indicates whether the flow inside a pipe is in laminar, transition or turbulent regime:

$$\mathrm{Re} = \frac{\rho \tilde{u} D}{\mu} = \frac{\tilde{u} D}{\nu} \tag{2.3}$$

where D is the internal pipe diameter, μ is the absolute viscosity and $\nu = \mu/\rho$ is the kinematic viscosity.

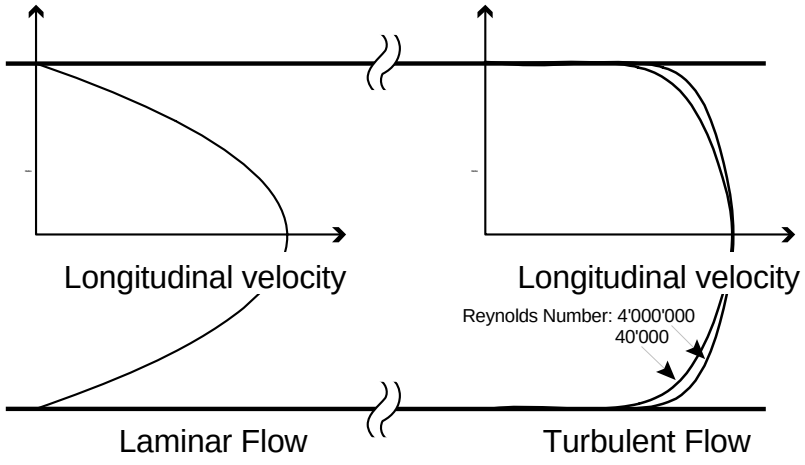

Figure 9: Longitudinal velocity profiles for laminar and turbulent flow

At low Reynolds numbers (below 2000) the flow is laminar with a parabolic velocity profile as shown in figure 9. When reaching a critical Reynolds number, turbulence appears. For Reynolds numbers higher than 4000 the flow is turbulent and the mean velocity profile, still being zero at the pipe wall, is straighter and squared-up (figure 9) with the ratio of the velocity at about the ¾ radius point to the mean velocity being approximately unity. If the Reynolds number is in between 2000 and 4000 the flow may be turbulent or laminar and may change at random from one flow condition to the other.

2.2 Differential pressure flowmeters

Differential pressure flow rate meters are the most commonly employed measuring devices because of the large number of different types industrially

available (Orifice, Venturi, V-Cone, Pitot tube, etc.), the reasonable cost, the accuracy[3] ranging between from 1 % to few % and the intrinsic robustness (simple construction, no moving parts, external instrumentation and low maintenance). International standards lay down precise requirements for constructing, installing and operating differential pressure flowmeters.

Their operating principle is based on the measurement of a differential pressure across a restriction. From Bernoulli's equation (equation 2.2) we can derive that if the velocity (kinetic energy) decreases between two flow cross sections, the pressure (static energy) increases accordingly. Since the equation of continuity for incompressible fluids states that the volumetric flow rate is constant (equation 2.1b), a change in section would give a change in velocity, hence a change in pressure. The volumetric flow rate as a function of pressure is given by:

$$V_{OL} = \frac{\pi}{4} D_2^2 \frac{\sqrt{2(p_1 - p_2)}}{\sqrt{\left[1 - \left(\frac{D_2}{D_1}\right)^4\right]\rho}} \tag{2.4}$$

The volumetric flow rate V_{OL} is then proportional to the square root of the differential head or differential pressure. Equation 4 overestimates the actual flow rate because non-reversible processes are ignored; dimensionless correction factors are then necessary to improve the quality of the measurements and they are: (a) the discharge coefficient factor C_d and (b) the gas expansion factor Y that provides an adjustment factor to the coefficient of discharge for the compressibility of gas (Reader-Harris and Keegans, 1998). Individual calibrations can reduce the uncertainty of the discharge coefficient as defined in the standards.

The differential pressure readout depends on the location of the pressure taps. Pressure taps that are perpendicular and flush with the pipe inner surface are used

[3] Accuracy refers to the truthfulness of the instrument in normal working conditions

to measure static head. Otherwise, if both the kinetic and static heads need to be measured, the pressure tap is parallel to the pipe with an opening opposite to the flow direction.

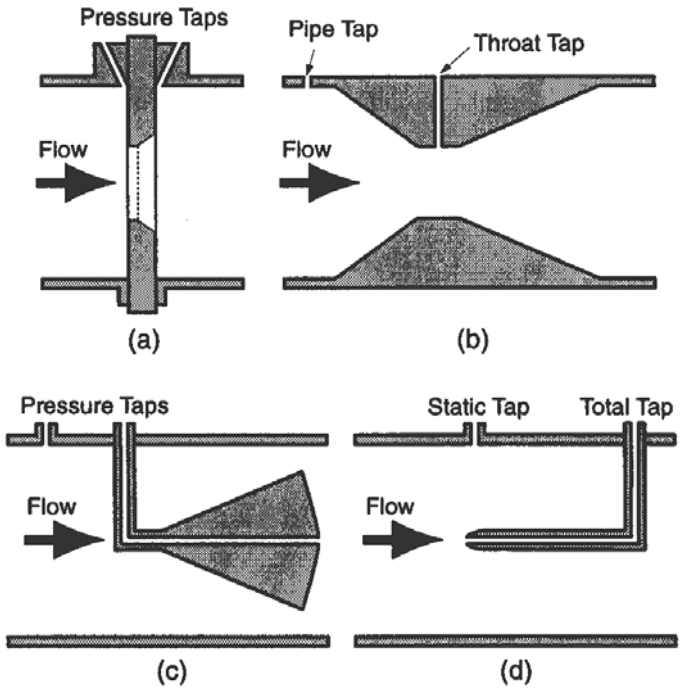

Figure 10: Differential-pressure-type flow rate meters: (a) Orifice, (b) Venturi, (c) V-cone, (d) velocity meter

2.2.1 Orifice flowmeters

Orifice flowmeters (figure 10 a) are probably the most commonly used flowmeters in cryogenic industrial applications because of their robustness, low cost and relatively good accuracy. They consist of a plate with an opening that can be concentric or eccentric depending on the cleanness of the fluid (i.e. a concentric orifice has impaired performance once there is some build-up of dirt at the plate, but is more accurate than an eccentric one that is rarely applied in current practice).

The velocity of the fluid as it passes through the orifice increases and then decreases again after the restriction (equation 2.1b) and from equation 2.2 the increase in kinetic energy (velocity) corresponds to a decrease in static energy (pressure) and viceversa. Since real gases are not perfect fluids, some static energy is lost due to friction (permanent pressure losses) and this is a function of the ratio of the orifice bore *d* to the pipe diameter *D* otherwise called the beta ratio:

$$\beta = \frac{d}{D} \tag{2.5}$$

For a real fluid equation 2.4 thus becomes

$$V_{OL} = \frac{\pi}{4} d^2 \frac{\sqrt{2(\Delta p)}}{\sqrt{(1-\beta^4)\rho}} C_d Y \tag{2.6}$$

The discharge coefficient C_d and the gas expansion factor Y are given by the ISO standards (in particular ISO 5167-1) and can be deduced from laboratory tests. The permanent pressure losses can be expressed as (Baker, 2000, (b)):

$$\Delta p_{loss} = \Delta p(1-\beta^{1.9}) \tag{2.7}$$

where Δp is the pressure drop across the restriction.

Rivetti, Martini, Birello, 1996, claim that these flowmeters have an accuracy of 2 - 5 % of full scale for cryogenic applications depending on how the ISO standard has been followed and implemented. The rangeability is limited by the accuracy of the differential pressure measuring device employed, as for other differential pressure type flowmeters. Flow rangeability of 10:1 can be achieved by using "smart" differential pressure transmitters, i.e. those whose output is proportional to the square root of the measured differential pressure and whose span is automatically adjusted according to the measured pressure.

2.2.2 Venturi flowmeters

Venturi flowmeters are based on the same principle but are made of a relatively long passage with smooth entry, giving the advantage of reduced permanent pressure losses and better working performances in dirty (particles, oils, etc.) fluids (figure 10 b). Of course this makes the flowmeter more expensive to manufacture, but accuracies as good as 1 % of full scale can be achieved (Rivetti, Martini, Birello, 1996).

2.2.3 V-Cone

In this flowmeter the restriction in the fluid stream is achieved by the insertion of a V-shaped cone element at the centre of the pipe (figure 10 c). The beta ratio is in this case:

$$\beta = \frac{\sqrt{D^2 - d^2}}{D} \tag{2.8}$$

and the differential pressure generated is lower than an orifice flowmeter comparable in size, beta ratio and flow rate. Other important advantage is that the V-shaped cone acts also as a flow conditioner increasing the range of Reynolds number exploitable and reducing the required length of upstream and downstream straight piping (Baker, 2000, (c)). They have never been used for low temperature applications and would require testing and calibration at working conditions.

2.2.4 Pitot tube

A Pitot tube is a device that measures the local fluid velocity by pressure difference between the static pressure and the total pressure measured at an impact port (figure 10 d). From equation 2.2, introducing a factor for non-ideal conditions, we can obtain the pressure rise when flow comes to rest in the entrance of a pitot tube, i.e. the dynamic pressure. This type of flowmeter allows local exploration of flow velocities across the pipe. These meters have been used

by the author to observe local flow velocities in pipes discharging liquid helium with 20 % accuracy with respect to simulated values. In order to correctly position it inside the pipe and obtain a representative value for the mean velocity a Pitot device require calibration with the expected velocity profile.

2.3 Thermal Mass flowmeters

In cryogenics, such flowmeters have their direct application for liquid mass flow rate measurements (Serio et al, 2002, (a) and Rivetti, Martini, Birello, 1996), although their use should be considered with care because of their potential impact on the total heat load budget. They are also widely employed to make boil-off measurements of cryogenic fluids in their gaseous form at ambient temperature.

There are two types of such flowmeter, both based on the variation of the thermal characteristics of the measured fluids: those that measure the heat loss from a heated element (resistance wire, thermocouple, etc.) to the flow stream and those that measures the temperature rise of a fluid passing over a heated element (figure 11).

The first type of flowmeter is based on the King equation for a hot wire (reviewed in 5.1.2):

$$\dot{q}_L = \Delta T \left[k + 2\left(k C_p \rho \pi d \tilde{u} \right)^{1/2} \right] \tag{2.9}$$

where $\dot{q}_L$ is the rate of heat loss per unit of time, ΔT and d are respectively the element's mean temperature elevation and diameter, k the conductivity of the fluid stream and C_v the specific heat of the fluid at constant volume. The advantages of this type of sensor are compactness, little power requirement and fast response time; but on the other hand they are nonlinear and depend on the gas thermal conductivity, temperature and velocity profile.

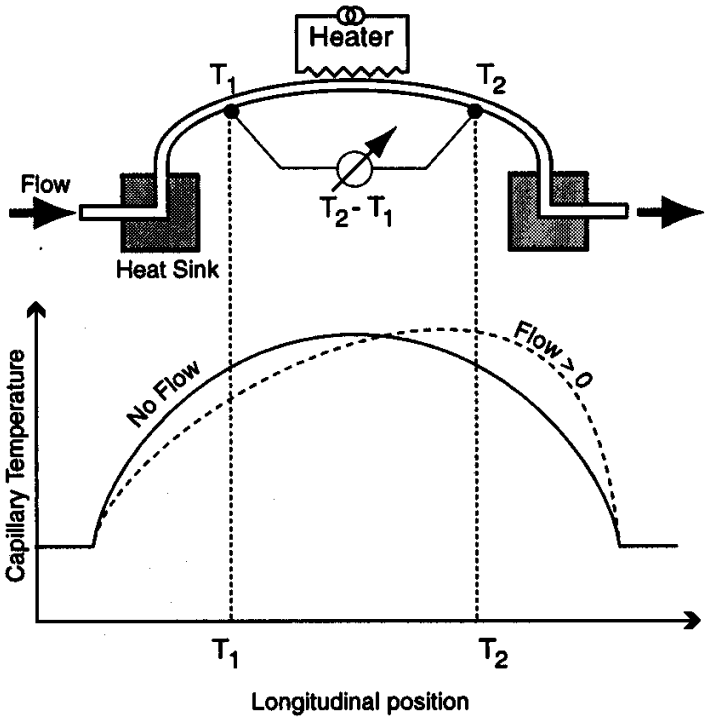

Figure 11: Thermal mass flow rate meter

The second type infer the mass flow rate $\dot{m}$ from the fluid's enthalpy variation ΔH after absorption of a heating power W:

$$\dot{m} = \frac{W}{\Delta H} = \frac{W}{\left(C_p \Delta T\right)} \tag{2.10}$$

where C_p is the specific heat of the fluid at constant pressure and ΔT the temperature increase across the heating element. Usually the heating and sensing elements are placed outside the thin wall of a capillary tube carrying all or a well determined fraction of the fluid (by using a suitable bypass element) thus allowing a wide range of sizes ($0.16\ 10^{-6}$ to 0.25 m^3/s). The small diameter and thin wall capillary tube is necessary to heat homogeneously the fluid and to reduce the

response time, the main drawback being the risk of obstruction while using unclean fluids. The use of heating and sensing elements inserted in the fluid stream is not recommended because of concerns of leak tightness and risk of explosion with hazardous gases. The sensing element is often a thermocouple, while the heating is obtained by either wrapping some insulated resistive heater around the capillary or by inductively heating the capillary. A more sophisticated and compact version is achieved by etching the capillary on an integrated chip whose semiconductor materials act as temperature sensors. The flowmeter body acts as a heat sink keeping both ends of the capillary at ambient temperature. Without flow a symmetrical temperature gradient is established across the heater and as the flow increases the temperature profile is deformed and a measurement of ΔT gives the mass flow (Spitzer, 1991, (b)).

Thermal mass flowmeters in contrast with most of the other devices have the advantage of inferring the mass flow rate of a fluid depending on its thermal and fluid properties. Many of the commercial devices operate at constant ΔT by adjusting the heating power and as a result the time response is improved. In general, thermal flowmeters are comparatively expensive, they give accurate and repeatable results (better than 2 - 3 %) if they are calibrated with the working fluid (being affected by the specific heat of the fluid) and are operated in a clean fluid stream. Care is necessary because the measurement can be affected by oil contamination coming from pumping machinery. Also many of these flowmeters are sold as a single package in conjunction with a flow control valve and a feedback circuit to deliver a programmable steady flow rate.

2.4 Turbine

A turbine flowmeter is among the most accurate flow rate metering device at ambient temperature and it is sometimes available as a transfer standard, i.e. an instrument traceable to a national institute of standards. It has been used to meter

cryogenic fluids, after calibration at working conditions, mainly in laboratory applications (Rivetti, Martini, Birello, 1996). It consists of a rotor mounted on a bearing mechanism, a housing and a device for measuring the rotor rotational frequency that is proportional to the flow rate (figure 12). The turbine blades are designed to operate in a "free-spin" mode and to have a minimal sensitivity to changes in Reynolds's number, resulting in an inefficient blade design with respect to power producing turbines that operate only in a much narrower rotational velocity range. Because a turbine flowmeter has a rotational component it is also very sensitive to swirl flow conditions and therefore care is necessary to condition the fluid flow. Typically at least 10 pipe diameters are required upstream of the meter, keeping in mind that swirl has been measured in a straight pipe after fluid has travelled for more than 100 pipe diameters (Spitzer, 1991, (c)). For gas service this type of device is capable, after calibration, of having an accuracy of 0.3 % of reading and a repeatability of 0.1 %. These instruments have a typical measuring range of 10:1 that on request can be increased to 25:1, or even higher, but the data on the extended range is valid only for the exact viscosity and temperature of the fluid that was used for the calibration and the increased rangeability generally affects the output linearity.

The performance of a turbine flowmeter is often represented by the *K* factor that is defined as the turbine rotational frequency *f* divided by the flow rate, versus the Reynolds number. In order to achieve the ultimate performance it is necessary to take into account the effects of temperature on the meter body; this is done by including in the calibration data the Strouhal Number (Spitzer, 1991, (d)) that gives a correlation between flow rate and frequency taking into account temperature effects on the meters:

$$S_t = \frac{f\ D}{\tilde{u}} = K\ \ D^3 = K\{D_o[1+\alpha(T-T_o)]\}^3 \cong K\, D_o{}^3\,[1+3\alpha(T-T_o)] \quad (2.11)$$

where D_0 is the meter diameter at the reference temperature T_0 and α is the linear expansion coefficient of the meter body (typically 0.003 %/K for austenitic steel).

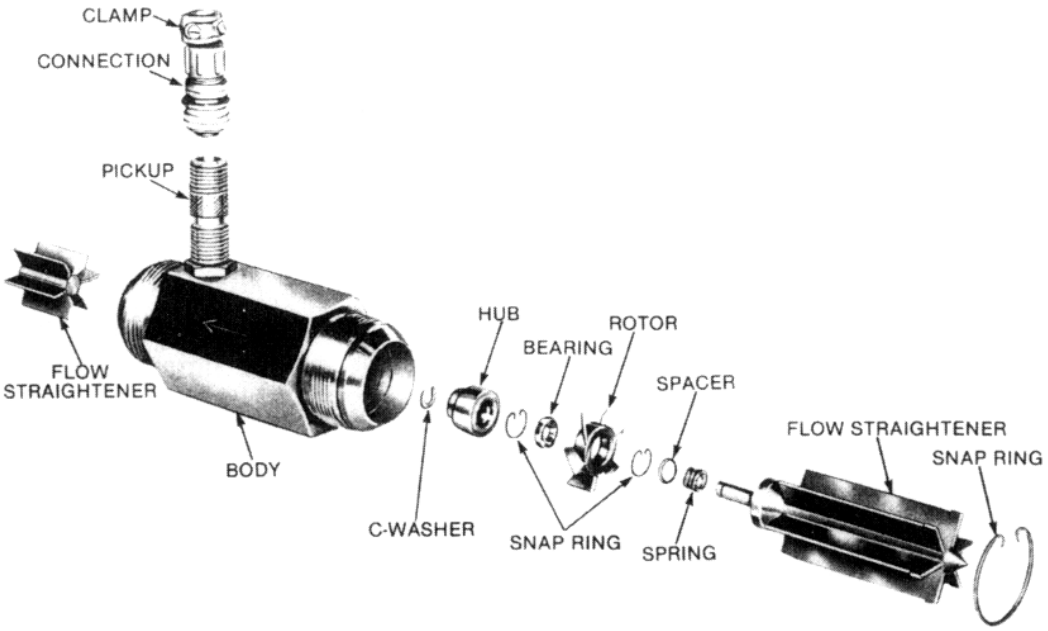

Figure 12: Exploded view of a turbine flowmeter.
(Courtesy of Ketema Inc.)

2.5 Coriolis flowmeters

Coriolis flowmeters (figure 13) can be applied to gas mass flow, where the process pressure is above 5 bar, and liquid metering (Baker, 2000, (d)). The literature does not mention their use at cryogenic temperature mainly because of the requirement, for sensitivity reasons, for high-density fluids. Nowadays, the remarkable progress made in improving the sensitivity and accuracy of Coriolis meters (Baker, 2000, (d)) permits us to consider them as a viable alternative method to measure directly mass flow also at cryogenic temperatures with low density fluids.

Figure 13: Coriolis meter sensor and transmitter

2.5.1 Operating principles

The measuring principle is based on the controlled generation of Coriolis forces that are present when both translation and rotational movement occur simultaneously ($F_C = 2 \cdot m(\vec{\Omega} \times \vec{u})$). The amplitude of the Coriolis force depends both on the moving mass m and its velocity $\vec{u}$, and therefore depends on the mass flow of the fluid. The flowmeter uses an oscillation instead of a constant angular velocity. Usually two parallel measuring tubes (one is sufficient but two are used to remove effects of external vibration), with fluid flowing through them, are made to oscillate. When there is a mass flow, there is some twisting of the tubes. The arm through which fluid flows away from the axis of rotation must exert a force on the fluid to increase its angular momentum, so it is lagging behind the overall vibration. The arm through which fluid is pushed back towards the axis of rotation must exert a force on the fluid to decrease its angular momentum again; hence that arm gets ahead of the overall vibration. As the mass flow increases, the phase shift (inlet/outlet) also increases. The oscillations of the measuring tubes are determined using electrodynamic sensors at the inlet and outlet (figure 14). The measurement principle operates independently of

temperature (the variation of the elastic modulus with temperature and static stress need to be taken into account), pressure, viscosity, conductivity or flow profile. The measuring tubes are continuously excited at the natural resonant frequency, or other resonant mode, of the system (tube + fluid). The frequency of oscillation can be used to measure fluid density. The calibration of the meter is done to take into account mechanical, manufacturing and electronics tolerances. Tube shapes together with resonant frequencies used can vary from manufacturer to manufacturer. The tubes are designed to optimize phase shift between sensor signals and to minimize pressure loss.

Coriolis meters have been used for more than 20 years in a wider range of applications and have proven to be reliable (Baker, 2000, (d)). Typical performances for commercial instruments used for ambient temperature applications are (Baker, 2000, (d)): accuracy between 0.1 and 0.25 % for 20:1 turndown, repeatibility of 0.1 % and accuracy below 1% for 100:1 turndown.

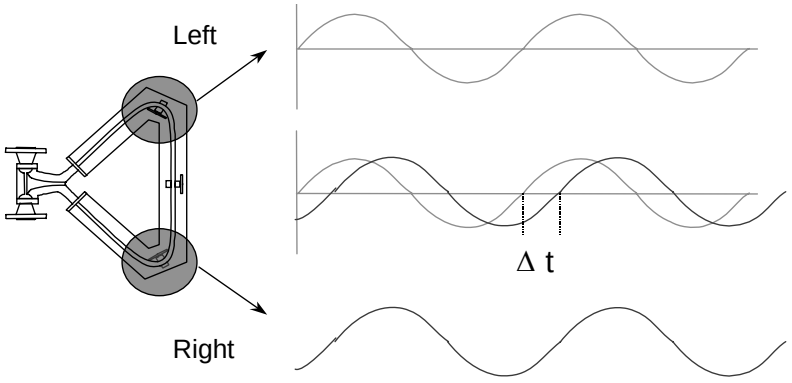

Figure 14: Coriolis flowmeter operation

2.5.2 Theory of operation

For sake of simplicity one should consider only one tube to demonstrate the operating principle. The same can be applied to two oscillating tubes. The

advantage of using two tubes is the rejection of vibrations coming from the meter connection (piping, machinery, etc.).

In figure 15 the principle of operation is schematized. Fluid is flowing in the tube as indicated. The Coriolis forces

$$F_C = 2 \cdot m(\vec{\Omega} \times \vec{u}) \tag{2.12}$$

is experienced by the fluid in the system of coordinates moving with the tube . If the flow velocity is u and the angular velocity Ω is upward, the first half of the tube will experience a downward force due to the Coriolis acceleration. The other half of the tube will experience an equal but opposite force.

Considering the twisting or distorting torque due to the flow and the Coriolis force, introducing the oscillating motion and relating the twisting torque to the twist in the tube θ (see figure 16), it can be demonstrated (Baker, 2000, (e)) that the mass flow in terms of the time of transit of the two sides is equal to

$$\dot{m} = \frac{E \cdot \Delta t \cdot (1 - \omega^2 / \omega_s^2)}{2 \cdot r^2 \cdot K} \tag{2.13}$$

where E is the spring constant of the tube in twisting oscillation or Young's modulus, ω is the driving frequency, ω_s is the natural frequency of the tube in twisting oscillation, d the width of the tube, Δt the time difference for transit of the two side of the tube or the time for each leg of the tube to cross the mid plane that corresponds to the total deflection and K a constant (allows for the fact that the twist of the tube will not form a straight integration).

The deflection angle θ is of the order of 1/100 degrees, the amplitude of the vibration is typically between 60 μm and 1 mm and the frequency is in the range 80 – 1100 Hz.

The time differential between the two legs is zero in the no-flow condition. By increasing the flow, θ increases, resulting in an augmentation of the time differential between the two transducer signals. In practice, the time differential Δt between the two transducer signals is converted to pulses of differential lengths by a digital logic circuit.

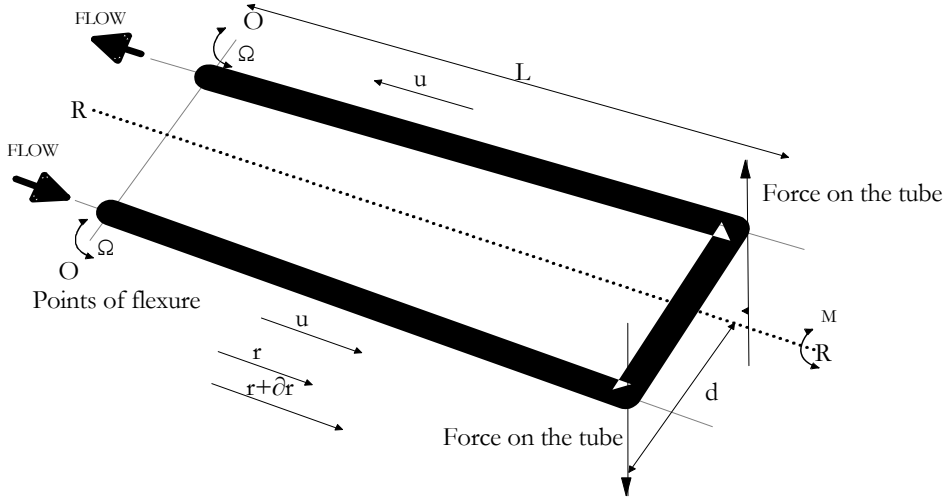

Figure 15: Oscillating U-tube schematising the Coriolis operating principle

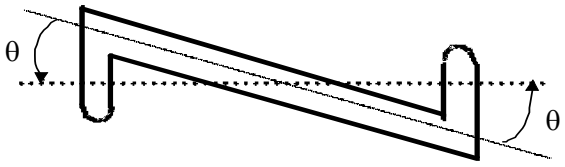

Figure 16: Twisting of fluid tube and subsequent deflection angle

The time interval is proportional to the mass flow rate with a proportionality constant represented by the Young's modulus and some geometric factor.

Consequently, the mass flow rate is proportional only to the time interval and is independent of the vibrating frequency.

2.6 Flow conditioning and installation

Even the best type of flowmeter, calibrated by a certified laboratory, can give poor results if it is not installed and operated properly.

The accuracy of many flowmeters is affected if the velocity profile of the flow is different from that under which the flowmeter was calibrated. The velocity profile will vary in smooth pipes with changes in Reynolds number. In rough pipes the velocity profile will vary depending on the level of pipe wall roughness, pipe fittings, valves and welding.

Upstream and downstream straight pipes of equal diameter, whose length is expressed as multiples of the inside pipe diameter, are often suggested by the manufacturer of the flowmeter together with the use of piping with smooth inner surfaces. Great care is needed during welding operations in order to limit welding burrs that in principle should be reamed off.

Even if a few flowmeters do not depend at all on the velocity profile (e.g. Coriolis) and some flowmeters require less attention because their construction is capable of reshaping a non uniform velocity profile (e.g. V-cone), most flowmeters can give wrong results in non uniform velocity profiles (e.g. thermal mass or turbine flowmeters). Flow conditioners should be considered in case the required pipe conditions cannot be achieved, but it must be taken into account that the pressure losses would increase and that only clean fluids would give trouble free performances.

Velocity profiles similar to those found in the CERN cryogenic applications (figure 17) have been already reported in the literature and our geometry (two

bends close to each other in a S-type arrangement in two 90 degree planes) is clearly described as one of the worst conditions to recover a normal velocity distribution because of the formation of a forced type vortex (Murakami et al, 1969; Murakami and Shimizu, 1978). The available pipe length before the flowmeter is well below the length required to recover the normal velocity distribution. This is mainly due to the closeness of the two bends. Therefore, the conditioning of flow profile seems necessary unless the flowmeter employed is independent of the velocity profile, e.g. Coriolis flowmeter. Flow conditioners such as tube bundles, perforated and honeycomb box layout can all be employed but care must be taken in the increase of pressure drop and the risk of clogging. In cryogenic installations the mass flow rate can depend on the temperature, it is therefore advisable to perform absolute temperature and pressure measurements of the metered fluid to take into account variations of the fluid characteristics that might yield errors in the measured mass flow rate (Rivetti, Martini, Birello, 1996).

2.7 Summary

This chapter has listed the most practical flow rate meters and methods for cryogenic installations found in the literature. Table 2 summarizes qualitatively the main features of the flowmeters presented and it can be used as a guide to optimize the selection procedure. The ultimate accuracy can be obtained only if the instrument is installed and maintained according to the manufacturer specifications and is individually calibrated at operating conditions.

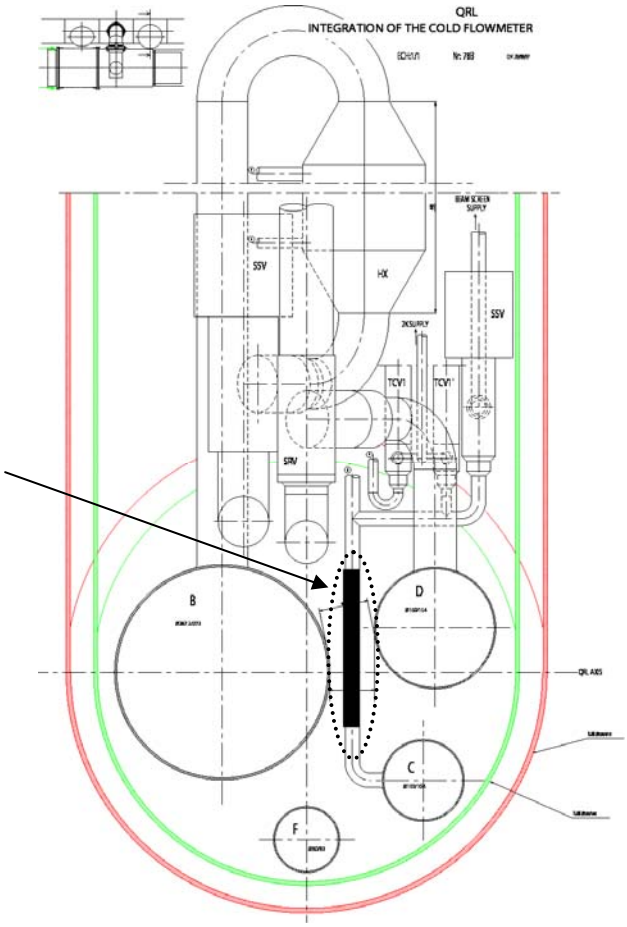

Figure 17: Flow meter position in the cryogenic distribution line insulation vacuum envelope and pipe geometry

If ultimate performance is desired, turbine is the flowmeter of choice with the drawback of higher maintenance requirements and cost. An alternative method for ultimate performance and direct mass flow measurement is given by Coriolis flowmeter but it requires some development and testing to make it compatible with cryogenic temperatures operation (materials compatibility, operating modes and low temperature assessment of Young's modulus). Otherwise for lower cost and maintenance differential flowmeters can be used with relatively lower accuracy and rangeability or thermal mass flowmeters based on rate of heat loss. For large cryogenic facilities with large helium inventory, the fluid management is

a critical issue and of course fluid rate metering devices are widely used. Most of the instruments are differential pressure flowmeters because of the requirements of industrial robustness and little maintenance. The drawbacks of such methods are medium rangeability and accuracy. The above mentioned qualities and advantages could be found in Coriolis mass flowmeters.

	Ultim. acc.	Range-ability	Pressure loss pipe requirement	Recommended applications	Cost	Cryo conditions
Coriolis	**0.1 %**	**high**	**medium/none**	**mass, acc, no maint.**	**high**	**suitable**
Orifice	**1 - 2 %**	**medium**	**high / 10-30 D**	**clean gas**	**low**	**suitable**
Venturi	**1 %**	**medium**	**low / 5-10 D**	**dirty gas**	**high**	**suitable**
V-cone	**0.5-1 %**	**medium**	**medium/3-5 D**	**short pipes**	**medium**	**suitable**
Pitot tube	**3 %**	**medium**	**low / 20-30 D**	**velocity meas.**	**low**	**suitable**
Thermal	**1 %**	**good**	**low / none**	**mass flow**	**high**	**suitable**
Turbine	**0.3 %**	**good**	**high / 10-20 D**	**accuracy**	**high**	**suitable**

Table 2: Qualitative comparison of various gas flow rate meters (Baker, 2000, (f); Spitzer, 1991, (e)).

Other types of metering devices, such as variable area, positive displacement, vortex and target flowmeters, have not been included because not suitable for cryogenic conditions.

Next chapter will introduce the physical properties of helium as a coolant and the main states and configuration employed for superconducting magnets cooling. It

will also highlight helium main properties of interest for the flowmeter selection and operation.

Chapter 3

3. PHYSICAL PROPERTIES OF HELIUM AS COOLANT

Cryogenics fluids, produced via industrial processes, are employed to obtain and maintain low temperatures. A cryogenic bath gives a cooling source at constant temperature with the liquid in equilibrium with its vapour. The cooling power is mainly given by the latent heat of vaporization of the cryogenic fluid inside the cryostat (cryogenic vessel), but the vapour between the bath and ambient temperature can also contribute to the cooling of the devices or the intercept of heat inleaks at intermediate temperatures.

The main fluids employed for cryogenic applications are:

- Liquid nitrogen – between 65 and 100 K
- Liquid hydrogen – between 15 and 30 K
- Liquid helium 4 – between 1 and 5 K

Other specific laboratory applications can also employ fluids such as methane, argon, oxygen, neon, deuterium and helium 3.

The guiding, focusing and acceleration of high-energy particles in accelerators and colliders is nowadays mainly performed by superconducting devices to achieve high performances at minimum investment and operating costs.

The choice of the cooling system is mainly determined by the level of temperature required, the heat exchange capacity, engineering and cost optimization criteria.

The temperature level must be one or two degrees below the current sharing temperature of the superconductor used. This temperature, identified as the temperature at the critical current surface of the superconductor, is a function of the operating point defined by the magnetic field B and current density Jc.

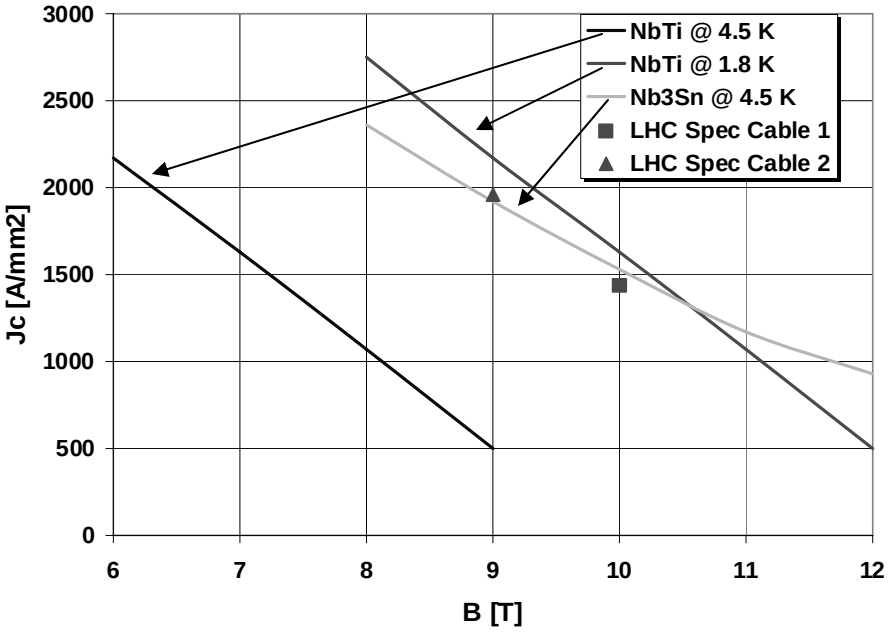

Figure 18: Critical current density of some commercially available superconductors.

Critical current density values for commercially available Nb-Ti and Nb3Sn alloys are given in figure 18 (Lebrun, 2001) together with the requirements for the LHC.

The heat transfer must allow operation under steady state conditions (mainly static heat loads through the cryostat and electrical connections) as well as transient conditions such as current ramping / de-ramping, mechanical instabilities, nuclear radiation, beam losses.

From the above, it can be concluded that the only fluid providing these temperature levels is helium.

3.1 Physical properties of helium

There are two stable isotopes of helium: helium 4 (atomic mass 4) and helium 3 (atomic mass 3). Helium 4 can be found in air (about 5.3 parts per million by volume), but the main reserves of helium 4 are natural gas deposits in the United States, North Sea, with some minor reserves in Europe and Africa. Helium 3 is practically produced artificially in nuclear reactors.

Helium 4 has some peculiar and interesting properties but differs from conventional fluids such as water and air. Small pressure and temperature ranges enclose the various fluid phases as shown in figure 19. The critical point is given by the pressure of 2.27 bar, temperature of 5.2 K and density of 69.64 kg/m3. The transposed critical line represents the maxima in the specific heat and can be viewed as an extension of the evaporation line.

The latent heat of vaporization is small, but the gas available enthalpy is remarkably high, much higher than the latent heat of vaporization.

The low critical value does not allow a high pressure saturated bath (liquid in equilibrium with its vapour).

There is no triple point for helium. To obtain solid helium, its pressure must be increased above 25 bar at low temperatures.

Reducing the liquid helium temperature by decreasing vapour pressure modifies drastically the liquid properties around 2.2 K. Liquid helium condenses into a quantum state and becomes superfluid helium (helium II). The line on the phase diagram where this change takes place is called the lambda line. The lambda point

is the triple point of equilibrium of helium I – helium II – vapour and is found at 2.172 K and 50.39 mbar. Superfluid helium has zero viscosity and extremely high thermal conductivity (Hebral et al, 1995).

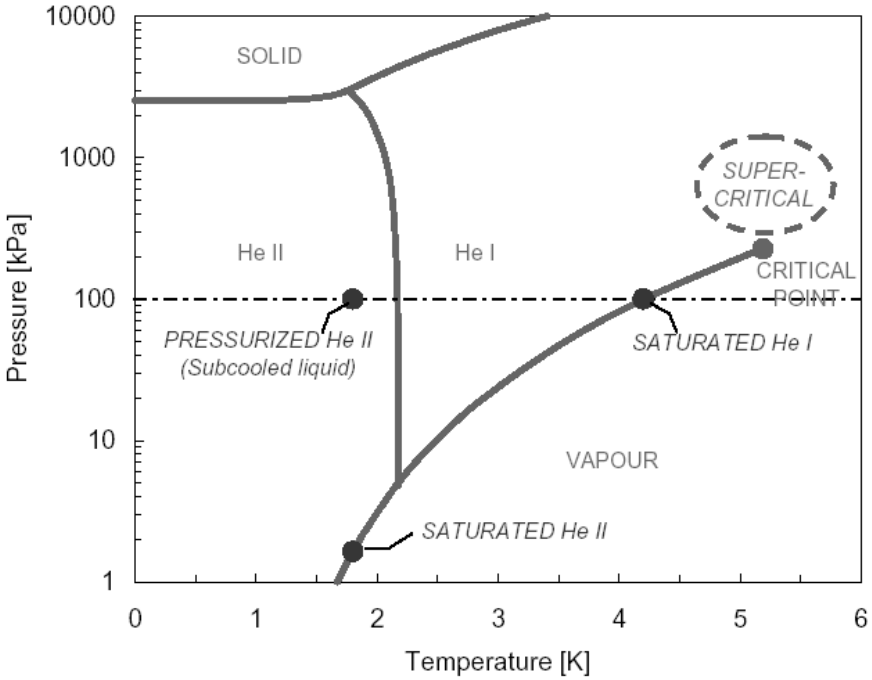

Figure 19: Helium 4 phase diagram (van Sciver, 1986 (a))

The specific heat, thermal conductivity, density and viscosity of helium near the expected pressure and temperature working points of the flowmeter are summarized in tables 3 and 4 (extracted from Hepak®[Cryodata Inc.]), h being the heat transfer coefficient for our geometry.

The use of the particular transport properties of superfluid helium, both for extracting heat and for transporting it over long distances makes it a very useful coolant for superconducting applications. Various types of cooling methods such as pool boiling or forced flow, as well as a combination of pool boiling and a pressurized bath can be and are successfully employed (Lebrun, 1997).

Helium properties at working conditions (i.e. 3 bar and 4.6 K):							
	Temp [K]	Pressure [bar]	Density [Kg/m3]	Cp [J/Kg-K]	Enthalpy [J/Kg]	Conduction [W/m-K]	h [W/m2 K]
	4.6	2.4	124.3	5441	12170	0.01984	282.514
	4.6	2.5	124.9	5337	12180	0.01992	280.445
	4.6	2.6	125.5	5241	12190	0.02001	278.644
	4.6	2.7	126	5154	12210	0.02009	276.887
	4.6	2.8	126.6	5073	12220	0.02017	275.305
	4.6	2.9	127.1	4998	12240	0.02025	273.744
	4.6	3	127.6	4928	12260	0.02033	272.391
	4.6	3.1	128.1	4862	12280	0.02041	271.051
	4.6	3.2	128.5	4801	12300	0.02048	269.7
	4.6	3.3	129	4744	12330	0.02055	268.419
	4.6	3.4	129.5	4690	12350	0.02063	267.377
	4.6	3.5	129.9	4639	12380	0.0207	266.263
	4.6	3.6	130.3	4590	12410	0.02077	265.197
% variations		**40**	**4.7133**	**-16.97**	**1.9528**	**4.58015**	**-6.3234**
% variations around working pressure +/- 100 mbar							
		6.6667	**0.7837**	**-2.759**	**0.3263**	**0.78701**	**-0.9886**

Table 3: Helium 4 properties around working pressure

Helium properties at working conditions (i.e. 3 bar and 4.6 K):							
	Pressure [bar]	Temp [K]	Density [Kg/m3]	Cp [J/Kg-K]	Enthalpy [J/Kg]	Conduction [W/m-K]	h [W/m2 K]
	3	4.6	127.6	4928	12260	0.02033	272.391
	3	4.7	125.4	5261	12770	0.02034	281.026
	3	4.8	123.1	5667	13310	0.02032	290.626
	3	4.9	120.5	6180	13900	0.0203	301.993
	3	5	117.5	6854	14550	0.02027	315.85
	3	5.1	114.1	7796	15280	0.02022	333.333
	3	5.2	110	9225	16130	0.02017	357.099
	3	5.3	104.8	11670	17160	0.02011	390.143
	3	5.4	97.63	16700	18550	0.02	450.804
	3	5.5	86.22	28120	20720	0.1968	549.333
% variations		**17.82178**	**38.7055**	**140.3534**	**51.30382**	**162.5478**	**67.40511**
% variations around working temperature +/- 50 mK							
		4	**-5.4561**	**23.12536**	**9.458533**	**-0.39487**	**9.865801**

Table 4: Helium 4 properties around working temperature

Superfluidity (van Sciver, 1986 (b)) is mainly the ability of a fluid system to flow without friction although it involves other striking effects, such as the "macroscopic quantum effects". Superfluidity occurs at suitably low temperatures in many condensate matter systems: liquid helium 4 ($T < 2.17$ K), liquid helium 3 ($T<\sim2$ mK), conventional superconducting metals, high temperature superconductors. The basic underlying mechanism of superfluidity (a form of Bose condensation) is common to all. In liquid helium this results from a symmetry-breaking transition involving Bose condensation with the formation of a coherent condensate wave function and "off diagonal long-range order".

The existence of liquid at $T=0$ must be a quantum effect arising from zero point energy; pushing the atoms sufficiently close together to allow solidification gives a too large zero point energy. The Third Law of Thermodynamics requires the entropy to go to zero as the temperatures goes to zero. Therefore liquid must become completely ordered at $T=0$. This ordering must be quantum mechanical in nature. Superfluidity is associated with an ordering process.

Taking into account the presence at a finite temperature of thermal excitations or the presence of impurities (He - 3) leads to two-fluid behaviour (high thermal conductivity; second sound; etc.). From the lambda transition (second order phase transition with no latent heat of transformation), some of the atoms are condensed to the state called superfluid, while the other atoms stay in the so-called normal state, the concentration of the superfluid atoms growing fast and approaching 1 below 0.7 K. The two fluids made of the different atoms are mixed and their proportion is well defined for a specific temperature. In this model only the normal fluid carries entropy, while the superfluid component has zero entropy being in an energy state which is the one of absolute zero. Helium II behaves as if it were composed of two fluids:

a) the superfluid with

- zero entropy; there is no transport of heat
- zero viscosity; there is no friction on the walls and between atoms
- no turbulence; there are no classical vortices

b) the normal fluid that transports all thermal excitations and has a viscosity

The connection between the phase of the condensate wave function and superflow leads to quantum restrictions on the superfluid velocity field and to topological defects in the form of quantized vortex lines. These defects play a major role in many properties of the superfluid phase (van Sciver, 1986 (c)).

3.2 Helium as a coolant

The main states of helium used for cooling superconducting systems or, more generally, cryogenic devices are:

1. boiling normal liquid helium (helium I) (usually slightly above atmospheric pressure and at about 4.2 K); main advantages are the fixed temperature and high heat transfer; main drawbacks are two-phase flow and boiling crisis (critical heat flux);

2. superfluid helium (helium II) (below 2.17 K); main advantages are the lower temperature, high conductivity and low viscosity; main drawbacks are the cost of refrigeration, the low-pressure piping and pumps required.

3. supercritical helium (above 2.27 bar and at around 5 K); main advantage is the monophase fluid flow; main drawbacks are the temperature rise accompanying the absorption of heat, the high pressure and flow rate;

3.2.1 Liquid helium I as a coolant

Liquid helium I is commonly used to cool superconducting devices where the application requires low critical current density. It is also widely used to cool the coldest end of "high temperature superconductors" (HTS) in current leads for powering superconducting magnets and superconducting RF cavities of accelerators.

Pool boiling is defined as the configuration consisting of a heater or a heated device immersed in a large bath of fluid.

Helium I has a rather small thermal conductivity and large specific heat, suggesting that conduction plays a small role in the overall heat transfer. In the steady state, the heat transport is dominated by convection. The behaviour of helium I is described in terms of models based on engineering correlations.

The heat flux per unit surface area defines the heat transfer from a solid surface to liquid helium I.

At low heat fluxes the heat transfer is dominated by conduction and convection.

When increasing the heat flux, bubbles start to appear at the interface. At first this enhances the heat transfer. It is followed by a steady increase in temperature difference between the surface and the bath temperature. The bubble formation takes place in cavities on the surface. The nucleate boiling depends on the surface roughness, material and condition. The heat flow per unit area is a function of the temperature increase in the nucleate boiling range and can be fitted, for engineering calculation, by the relation (Schmidt, 1981):

$$\dot{q} = c \cdot \Delta T^{m} \qquad (\mathrm{W/m^2}) \qquad (3.1)$$

where $\dot{q}$ is the flux per unit surface, T is in degrees Kelvin, m is equal to 2.5 and $c=10^4$.

Beyond a certain critical heat flux (called the peak nucleate boiling flux), a temperature jump occurs due to the formation of an insulating gas film on the surface. Experimental data from Cumming and Smith, 1966, for the film boiling on horizontal surfaces, fits the following relation:

$$\dot{q} = 290 \cdot \Delta T^{0.92} \qquad (\mathrm{W/m^2}) \tag{3.2}$$

In the film boiling regime the heat transfer can be improved by increasing the real surface area (using grooves or fins) and by employing surface structures that facilitate the removal of bubbles and the oxidation of the surface which helps to postpone the transition from film boiling to nucleate boiling.

A comprehensive analysis of heat transfer in pool boiling helium I can be found in van Sciver, 1986 (d).

The heat transfer in boiling helium I can be further increased by increasing the liquid helium velocity. In heated vertical channels helium flow can be induced by thermosiphon action with stagnant liquid helium. This phenomenon is preferred to the use of a pump whenever the heat loads to be extracted are limited and there is space in the cryostat for the thermosiphon.

3.2.2 Superfluid helium as a coolant

The prime reason to use superfluid helium for the cooling of magnets is the increased working range of the superconductor given by the lower operating temperature.

The transition to the superfluid phase is accompanied by a large peak in the heat capacity. There is, however, no latent heat, the transition being continuous. The

proportion of liquid that is superfluid continuously goes to zero as the transition is approached from below. Therefore superheating or subcooling cannot occur at the lambda transition.

3.2.2.1 Superleaks

A superleak (Kuper, 1958) is a channel that allows only the superfluid component to pass. It is therefore an entropy filter that does not pass energy but only fluid mass at zero entropy.

Two thermo-mechanical effects appear when two vessels with superfluid helium are linked by a superleak made of a narrow channel with nano-metric holes. On applying heat to the first vessel, the superfluid component is reduced and superfluid helium is pumped in from the other vessel. The level in the first vessel increases and the pressure difference which can give rise to the "fountain" effect is the difference of the osmotic pressure between the normal fluid and the superfluid. On the contrary, if we push the fluid to pass from one vessel to the other the first vessel will be reduced in the superfluid component and its temperature will increase, while the second vessel, enriched in superfluid component will fall in temperature (giving so-called superfluid refrigeration).

3.2.2.2 Thermal conductivity

In order to understand the phenomena of quasi-infinite thermal conductivity of superfluid helium, we have to use the two-fluid mode.

Let us consider a cylindrical channel transporting heat. A temperature gradient due to a heater element of one side of the channel will give rise to a movement of superfluid component from the cold to the warm side due to the reduction in superfluid helium on the heater (warmer) side. However, since we cannot have an accumulation of matter on only one side of the channel, it will be compensated by the opposite movement of the normal fluid component. Therefore the heat is

transported by a dynamic flow of entropy carriers (the normal fluid atoms) at a speed which is limited by the normal fluid viscosity or by the turbulences associated with the superfluid imperfections, instead of being transported via energy transfer between adjacent atoms. A typical value of thermal conductivity around 2 K is 2 kW/m K in a channel of 1 cm^2. As an example, the heat flux transported by conduction between 1.9 and 1.8 K in a 1-m long static column of helium II is about 1.2 W cm^{-2}, i.e. three orders of magnitude higher than what would be conducted along a bar of OFHC copper of the same geometry (Lebrun, Serio, Tavian and van Weelderen, 1997).

An equation to compute the thermal conductivity of pressurized superfluid helium can be found in Bon Mardion, Claudet and Seyfert, 1979.

3.2.2.3 Rollin film

Superfluid helium is capable of going up the walls of the vessel that contains it. If there is a thermal gradient, superfluid helium forms a film, called Rollin film, which moves towards warmer zones. In practice, this film gives rise to higher heat loads on the bath by vaporization. In a vessel, the film flow depends on the temperature (it disappears at 2.17 K), the wetted perimeter of the film and the status of the surface on which it flows. For T<1.5 K and 1 m of wetted perimeter, the flow is of the order of $7.5 \cdot 10^{-9} m^3/s$ (Hebral et al, 2000).

3.2.2.4 Pool boiling

Heat transfer through superfluid helium is described in terms of a two-fluid model. Only the normal component transports energy while the superfluid component flows in the opposite direction without carrying energy (zero entropy). The energy of a hot surface transforms superfluid atoms into their normal state that carries the heat. This counter flow of the two fluid components has no net mass flow. At very small heat fluxes we can neglect superfluid turbulences; therefore the only dissipative process is represented by the viscosity

of the normal component. At larger heat fluxes the superfluid component becomes turbulent and leads to a mutual friction between the two fluids. This mutual friction is the dominant source of dissipation. The turbulent heat transport equation in one dimension can be written in the form

$$\frac{dT}{dx} = f(T) \cdot \dot{q}^m \tag{3.3}$$

where $f(T) = \frac{A\rho_n}{(\rho_s^3 s^4 T^3)}$ and m is a numerical coefficient which theory indicates should be equal to 3 but experimentally has been shown to vary from below 3 to nearly 4 as the temperature approaches T lambda (van Sciver, 1986 (e)). A is the Gorter –Mellink mutual friction parameter, s is the entropy and ρ_n and ρ_s are respectively the normal and superfluid densities. Bon Mardion, Claudet and Seyfert, 1979, have shown that from experimental results, the thermal flux $\dot{q}$ (in W/cm^2) can be expressed as a function of temperature and channel length l:

$$\dot{q} = \left[\frac{X(T_{cold}) - X(T_{warm})}{l} \right]^{0.29} \tag{3.4}$$

X (T) is a tabulated function of temperature, physically analog to a conductivity integral, which values are given in Bon Mardion, Claudet and Seyfert, 1979.

The design of cooling system with superfluid helium must also take into account that when heat flows from a solid material into superfluid there is a discontinuity in the temperature across the boundary separating the two media. This additional thermal resistance, called Kapitza resistance, is usually an important component in the total resistance computation. It occurs from the transmission of phonons (sound waves) from one medium to another and it seems to be due to the mismatch between the speeds of ordinary sound in superfluid helium and in the solid (Wilks, 1967 and Khalatnikov, 1965). The theory of Khalatnikov predicts

that the Kapitza resistance is proportional with $1/T^3$. Therefore, the heat transfer coefficient goes with T^3. The resistance depends on the material and the surface finish. A typical value of Kapitza resistance at 1.8 K for standard copper is of the order of 2500 W/m^{2}K (extracted from Metalpak® [Cryodata Inc.]).

3.2.2.5 Pressurised bath

Specialised services of CEA (the French Atomic Energy Association) have developed techniques to use superfluid helium at atmospheric pressure. The advantage of using pressurized (above 1 bar) instead of saturated superfluid helium is mainly due to:

1. the maximum heat flux that can be extracted, which is higher and is independent of immersion depth
2. the absence of two-phase flow
3. the filling of all openings and cavities by liquid for optimum cooling and transfer
4. the good dielectrical properties
5. the reduced risk of air inleak

Pressurized superfluid helium can be obtained either by heat extraction from the bottom of a stratified cryostat (Roubeau bath), thus obtaining a superfluid phase on the bottom (at T lambda) and normal phase on the top or separating the two phase by a small orifice (Claudet bath) ensuring the thermal gradient between the top Roubeau bath and the bottom bath at all possible superfluid helium temperatures.

A further improvement of superfluid helium cooling techniques comes with the bayonet heat exchanger developed at CERN (Lebrun, Serio, Tavian and van Weelderen, 1997). This technique was pioneered at Tore Supra Tokamak in France, to transport heat over distances of up to a few tens of meters via a large yet finite thermal conductivity of superfluid helium but insufficient for the heat loads and geometric configuration of the LHC machine. In order to extend and enhance the cooling for the LHC magnets over the length of each individual cooling loop extending over 107 meters, the cooling system evolved into one with combined static baths of pressurized superfluid helium, single-phase, quasi-isothermal medium, with a bayonet heat exchanger providing continuous heat exchange with flowing saturated superfluid helium, the latent heat of vaporization of which provides a quasi-isothermal heat sink (see figure 20).

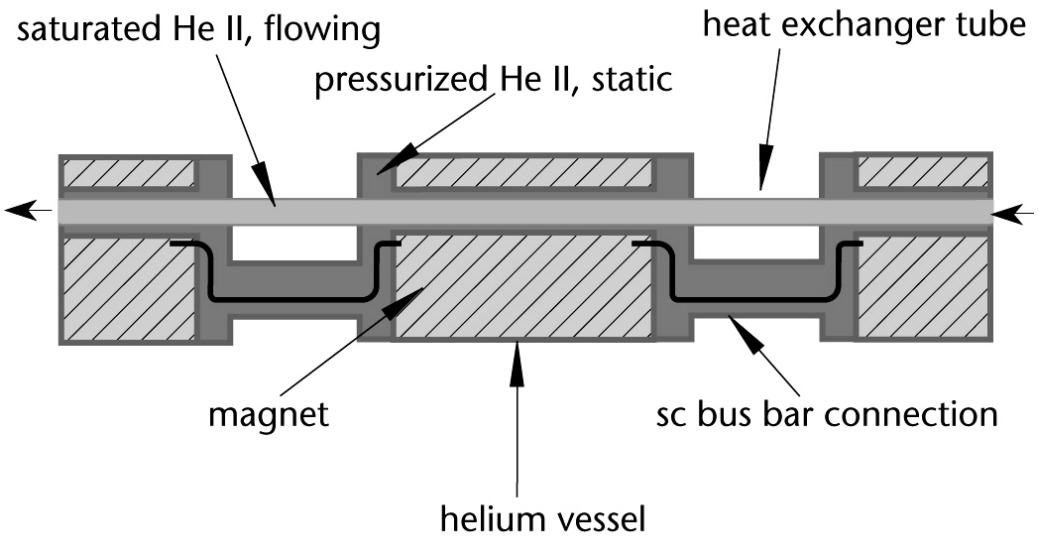

Figure 20: Principle of the LHC magnet cooling scheme

3.2.3 Supercritical helium as a coolant

The unique property of helium of having a low critical pressure (2.27 bar) and solidification pressure of no less than 100 bar at 4.2 K, makes it a suitable fluid for a cooling circulation system under pressure. Furthermore, because there is no discontinuous change in physical properties above the critical point and practically no definite distinction between the liquid and gaseous phases, the heat transfer phenomena can be referred to one phase. Therefore, especially for a long distributed system such as the LHC, the use of a monophase fluid is a significant advantage compared to the difficulties and physical phenomena occurring in two-phase flow of subcritical helium.

In general, fully developed forced flow of supercritical helium can be assumed to have a well-established engineering basis (Hebral, 1995). Since the fluid is single phase, its hydrodynamics can be evaluated in terms of the Navier-Stokes equation of motion including compressibility factors. The hydrodynamic equations appropriate for compressible fluids adequately describe the pressure drop and heat transport character. Because of the variability of physical properties with temperature and pressure, the problem is quite difficult to solve, requiring numerical integration of complicated non-linear equations. The conventional approach to predict the heat transfer coefficient between the tube or duct and the helium stream demands the development of engineering correlations appropriate to the particular configuration of interest. This will be shown in chapter 5.

Therefore, as will be shown in the next chapter, the helium flow distribution is in the supercritical helium phase while the cooling of superconducting magnets is performed with superfluid helium (via sub-cooling heat exchangers and sub-atmospheric pumping) in order to profit from the lower temperature, high conductivity and low viscosity.

Chapter 4

4. THE CRYOGENIC SYSTEM FOR THE LHC

Figure 21: The LHC machine installed in the CERN underground tunnel

The LHC cryogenic system (see figure 21), with more than 24 km of underground (100 m below ground level) cooling distribution, 80 t of superfluid helium below 2 K, 1800 main superconducting magnets and 120 kW 4.5 K equivalent refrigeration power, is of unique design.

The main superconducting magnets, dispersion suppressors and inner triplets are immersed in a pressurized bath of superfluid helium at about 0.13 MPa (1.3 bar) and a maximum temperature of 1.9 K. This allows a sufficient temperature margin for heat transfer across the electrical insulation. The low bulk viscosity enables the coolant to permeate the heart of the magnet windings, while the very large specific heat combined with very high heat conductivity have a powerful

stabilising action against thermal disturbances. This cooling requirement applies during both ramping and stored-beam operation. In the case of fast current discharge, the temperature excursion may be larger but must still remain below the helium II/helium I phase transition (lambda line). In the matching sections, superconducting magnet windings will be immersed in a saturated bath of helium at a temperature of 4.5 K.

The large cold mass of the LHC ($37 \cdot 10^6$ kg) must be filled in a maximum time of 15 days while avoiding thermal gradient in the cryo-magnet structure higher than 75 K. This also applies to the forced emptying and warm-up of the machine prior to shutdown periods.

The cryogenic system must be able to cope with the resistive transitions of the superconducting magnets, which occasionally will occur in the machine, while minimising loss of cryogen and system perturbations. It must handle the resulting heat release and its consequences including fast pressure rise and flow surges. In order to maintain a high operational availability of the LHC machine, it must limit the propagation to the neighbouring magnets and recover in a reasonable time. Therefore a resistive transition extending over one lattice cell should not result in a down time of more than a few hours.

In addition to these basic operational duties, the LHC cryogenic system should allow rapid cool-down and warm-up of limited lengths of cryo-magnet strings, e.g. for repairing or exchanging a defective unit. It should also be able to cope with the resistive transition of a full-sector - this defining the maximum credible accident - without impairing personnel or equipment safety. Finally, to ensure reliable operation, it should provide some redundancy of functions among its components and sub-systems.

Equipment will be installed above ground as much as possible in order to avoid the need for excavation of further large underground caverns. However, certain components which must be close to the cryostats or which cannot be installed on the surface because of the hydrostatic head, will have to be installed underground.

Concerning safety and operational design constraints, the use of nitrogen in underground areas is forbidden as well as helium discharge in the tunnel in large quantity. The cryogenic system is designed for a fully automatic operation during nine consecutive months followed by three months of shutdown for maintenance.

4.1 Cooling requirements and main parameters

The staging of temperature levels for the LHC cryogenic system has been essentially maintained, with some minor adaptation, in order to match the thermodynamic cycles of existing refrigerators that will be used for LHC refrigeration after suitable modification and upgrading. The thermal design of the LHC cryogenic components aims at intercepting the largest fraction of applied heat loads at higher temperatures, hence the multiple, staged temperature levels in the system. The temperature levels are:

a) 50 K to 75 K for thermal shield as a first major heat intercept, sheltering the cold mass from the bulk of heat inleaks from ambient;

b) 4.6 K to 20 K for lower temperature heat interception and for the cooling of the beam screens which protect the magnet cold-bore from beam induced loads;

c) 1.9 K quasi-isothermal superfluid helium for cooling the magnet cold-mass;

d) 4 K at very low pressure (VLP) for transporting the overheated helium flow coming from the distributed 1.8 K heat exchanger tubes across the sector length to the 1.8 K refrigeration units;

e) 4.5 K normal saturated helium cooling for special superconducting magnets in insertion regions, superconducting acceleration cavities, and the lower sections of HTS current leads;

f) 20 K to 300 K cooling for the resistive upper sections of HTS current leads.

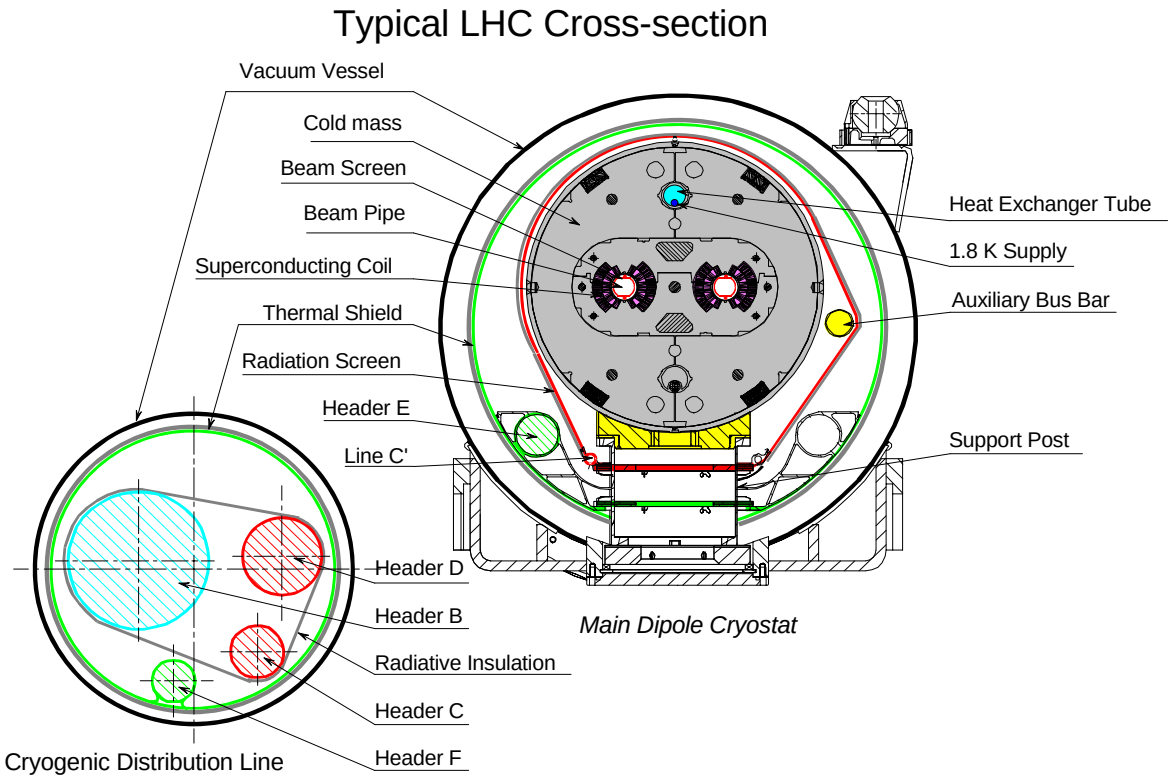

Figure 22: Cross section of magnet cryostat and cryogenic distribution line.

The cryostats and cryogenic distribution line (see figure 22) combine several low-temperature insulation and heat interception techniques, which have to be reliably implemented on an industrial scale. These include low-conduction support posts

made of non-metallic glass-fibre/epoxy composite, low-impedance thermal contacts under vacuum for heat intercepts and multi-layer reflective insulation wrapping the some 80'000 m^2 of cold surface area below 20 K.

Besides their primary function of intercepting beam-induced heat loads at a temperature well above that of the magnets, the beam screens also act as an intermediate-temperature baffle for the cryo-pump constituted by the 1.9 K surface of the magnet bores, thus sheltering the cold surface from synchrotron radiation, preventing desorption of the trapped gas molecules and avoiding breakdown of the beam vacuum. In order to limit resistive heating as well as residual heat inleaks to the magnets, the beam screens must operate below about 30 K. To match the available temperature levels in the existing refrigerators, they are cooled non-isothermally by a forced flow of weakly supercritical helium, between 4.6 K and 20 K, which reduces the entropic load by a factor of 8 with respect to 1.9 K isothermal refrigeration. The choice of mono-phase, supercritical helium aims at avoiding the potential problems of two-phase flow in long, narrow channels.

Heat inleaks result from the design of the cryostats and come from the ambient temperature environment. Thermal calculations, conducted on the basis of the detailed construction drawings, precise heat inleak measurement on critical components and global measurement performed on prototype cryo-magnets, test strings and full-scale thermal models have permitted to estimate and validate the heat inleaks and confirmed the technical feasibility of efficient compound cryostats housing long superconducting magnets operating in superfluid helium.

Resistive heating is produced in the non-superconducting sections of the magnet excitation circuits, essentially in splices of the superconducting cables and in current leads. The heat load in magnet splices has to be taken by the cold-mass helium bath.

Beam-induced loads are deposited in the cryo-magnets through several processes and by the circulating and colliding proton beams. They depend strongly on the energy and on the bunch intensity, number and length of the circulating beam bunches as well as on the luminosity of the collision. The different beam-induced loads are:

a) synchrotron radiation from the bending of the beam, mostly absorbed by the beam screens;

b) resistive dissipation of beam-image currents induced in the resistive walls and geometrical singularities of the beam channel;

c) impingement of photo-electron clouds accelerated by the beam potential, mostly adsorbed by the beam screen;

d) nuclear inelastic beam-gas scattering corresponding to a continuous distributed loss of particles from the circulating beam, mostly absorbed by the cold-mass helium bath; this value is expected to decrease with running time due to improvement of the vacuum by beam cleaning;

e) continuous random loss of particles escaping the collimation system, mostly absorbed by the cold mass helium bath over a length of a few tens of metres corresponding to the region of aperture restriction;

f) secondary beam losses, mostly absorbed in the magnet cold-mass helium bath close to the high-luminosity experimental areas (inner triplet and dispersion suppressor cold masses) at 1.9 K level;

g) RF losses in superconducting acceleration cavities.

Ramping the magnetic fields up and down will produce additional transient heat loads on the superfluid helium due to the eddy currents developed in the superconducting cables and in the mechanical structure of the magnets. Raising the current to its nominal value in 1200 s is expected to dissipate an energy of 480 J per metre length of magnet. This represents a power of approximately 0.4 W per meter. In the case of a resistive transition or other emergency, it must be possible to reduce the full current to zero in 80 s. This will result in a energy dissipation of 3000 J per meter in the magnet string which represents a power of approximately 38 W per meter.

The only practical way to absorb these transient heat loads, keeping the temperature below 1.9 K during current ramping up to nominal and below the lambda line during fast current ramp-down to zero, is to make use of the heat capacity of the liquid helium contained in the magnet cold-masses. About 26 l of liquid helium per metre length is required to cope with the loads to be buffered.

Table 5 shows the contributions of the machine distributed heat loads at various operating conditions.

Temperature	**50-75 K**	**4.5-20 K**	**1.9 K LHe**	**4 K VLP**
Heat inleaks	6.7	0.27	0.20	0.05
Resistive heating	0.006	0.01	0.13	0
Beam-induced nominal**	0	0.91	0.07	0
Beam-induced ultimate**	0	2.24	0.09	0
Total nominal	6.7	1.19	0.40	0.05
Total ultimate	6.7	2.52	0.42	0.05

** *Breakdown*		
	nominal	**ultimate**
Synchrotron radiation	0.33	0.52
Image currents	0.40	1.00
beam-gas scattering	0.06	0.06
Photoelectron	0.19	0.74

Table 5: Distributed heat loads in the machine for steady operation [W/m]

4.2 Layout

The main constraints result from the need to install the system in the existing previous accelerator (LEP) tunnel and its facilities, including the four existing LEP refrigerators (Claudet et al, 1994) and cryogenic infrastructure. The limited number of access points to the underground areas must be reflected in the architecture of the LHC cryogenic system. The cooling power required at each temperature level will be produced in eight refrigeration plants and distributed to the adjacent sectors over distances of up to 3300 km.

The LHC cryogenic system is therefore based on a five-point feed scheme (see figure 23) with one cryogenic plant dedicated to each of the eight 3.3 km-long sectors (Benda et al, 1996).

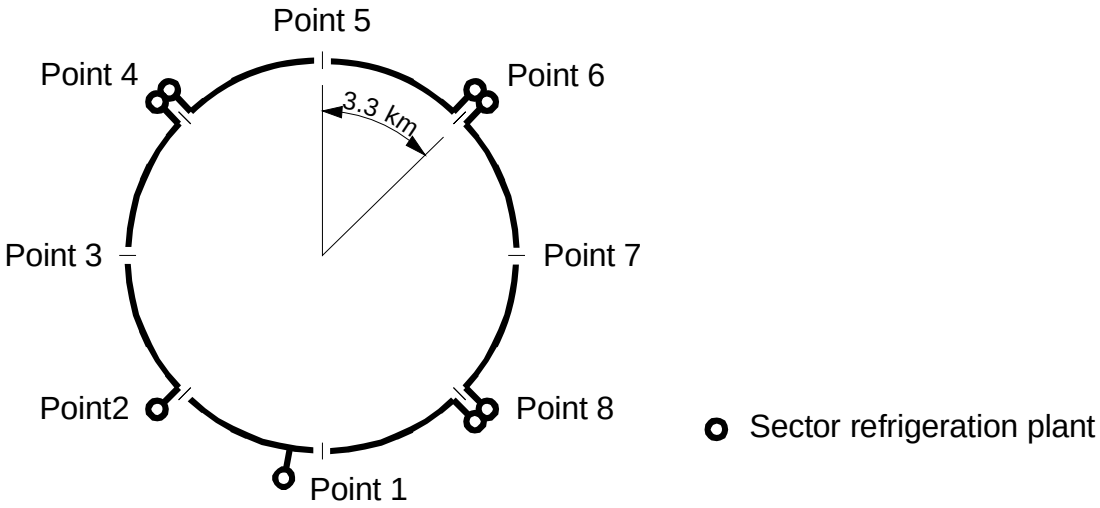

Figure 23: General layout of the cryogenic system

As shown in figure 24, all refrigeration and ancillary equipment is concentrated, both at ground level (electrical substation, warm compressor station, cryogen storage, cooling towers, cold-boxes) and underground (lower cold-boxes, 1.8 K refrigeration unit boxes, interconnecting lines, interconnection boxes). Each cryogenic point houses one or two refrigeration plants feeding one or two

adjacent tunnel sectors. This requires distributing and recovering the cooling fluids over distances of 3.3 km underground. A refrigeration plant is constituted of one 4.5 K refrigerator, which is either one of the four split-cold-box ex-LEP refrigerators or one of the four new integrated-cold-box refrigerators, and one 1.8 K refrigeration unit. At each cryogenic point, an interconnection box couples the different refrigeration equipments and the cryogenic distribution line and allows, when possible, redundancy functions in between refrigeration plants.

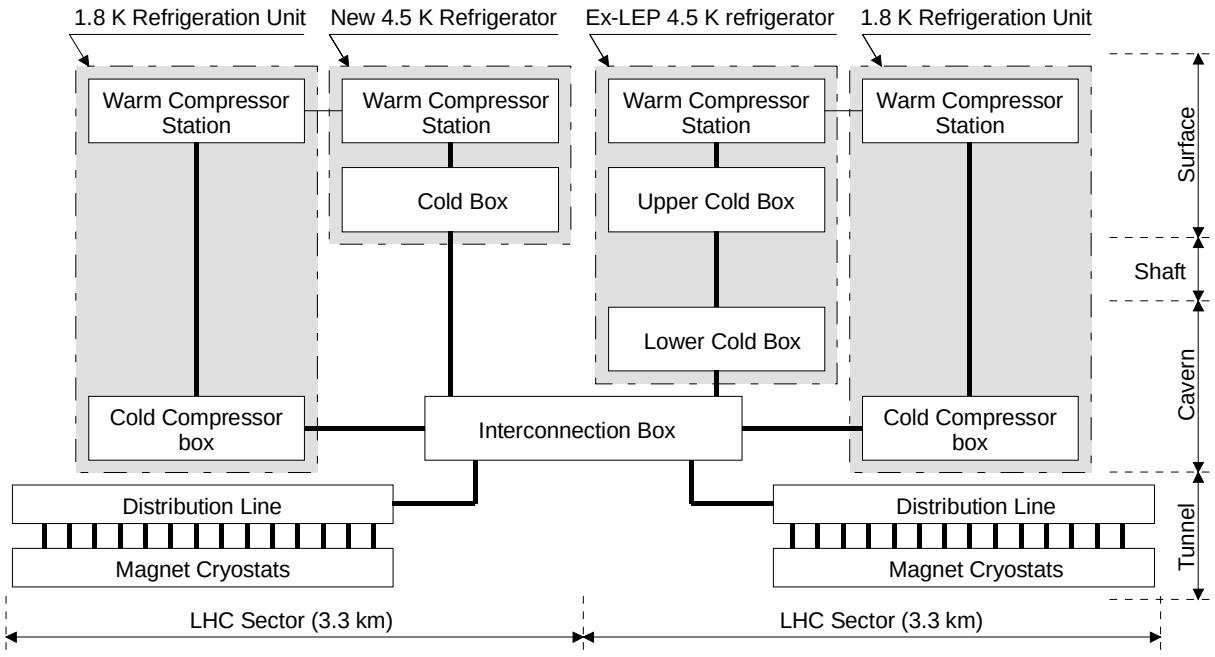

Figure 24: Layout of the cryogenic system at points 4, 6, 8

Due to the lack of space at point 2 for integration of two refrigeration plants as well as the need at point 1.8 for large refrigeration capacity for individual cryo-magnet testing, it was decided to break the architecture symmetry and to install two refrigeration plants at points 4, 6 and 8 and only one refrigeration plant at points 1.8 and 2. The drawback of this architecture concerns the sector 2-3 for which the redundancy functions are limited.

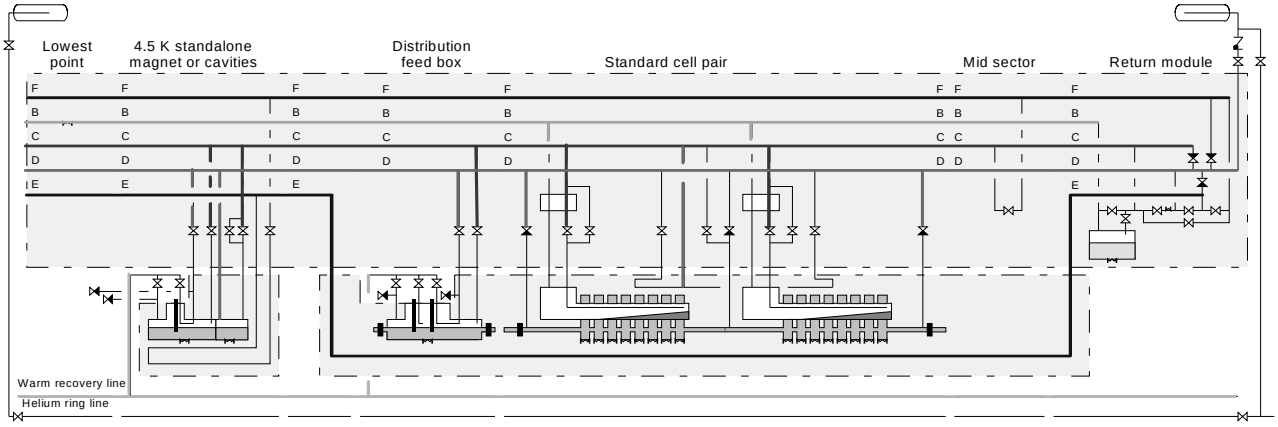

Figure 25: The tunnel cryogenic system layout for a typical sector

Due to impact study considerations as well as for limiting the pressure build-up during helium discharge of a generalized resistive transition of a magnet sector, cryogen storage infrastructure also exists at points 3, 5 and 7.

To simplify the magnet string design, the cryogenic headers distributing the cooling power along a machine sector and all active cryogenic components in the underground tunnel are contained in a compound cryogenic distribution line (QRL) which runs along the cryo-magnet strings in the tunnel and feeds via jumper connections at every 107 m-long lattice cell in parallel (figure 25).

The LHC tunnel is inclined at 1.41 % with respect to the horizontal, thus resulting in elevation differences of up to 120 m across the tunnel diameter. This can generate hydrostatic heads in the cryogenic headers as well as flow instabilities in a two-phase, liquid-vapour, flow. To avoid these harmful instabilities, all fluids should ideally be transported over large distances in a mono-phase state, i.e. in the superheated-vapour or supercritical region of the phase diagram. Local two-phase circulation of saturated liquid can be tolerated

over limited lengths, within a controlled circulation direction. Therefore cryogenic power is distributed as supercritical helium at 3 bar and 4.6 K. Gas is recovered or pumped at various temperatures. The thermal screens are separately cooled in series between 50 and 75 K to intercept radiation loads.

The cryogenic distribution line is interconnected to the cold compressor system (for very low pressure pumping), the 4.5 K refrigerator and the helium gas storage via a Cryogenic Interconnection Box situated in the underground cavern.

The Cryogenic Distribution Line (QRL) supplies the local cooling loops of:

a) the arc full-cells

b) the DFBs (electrical distribution feed boxes) for electrical powering of the sector

c) the superconducting cavities

d) the inner triplet

e) non standard cryostats

4.2.1 Large-capacity refrigeration at 4.5 K and 1.8 K

The refrigeration demands of the LHC sectors (Lebrun et al, 1997), listed in table 6, include contingency for excess capacity and uncertainty in heat load budgets for the nominal operation mode and allow for performing the ultimate operation mode according to the heat load level without contingency. These values were used for specifying the new 4.5 K refrigerators and the 1.8 K refrigeration units.

Temperature level		New refrigerator (high-load sector)	Ex-LEP refrigerator (low-load sector)
50-75 K	[W]	33000	31000
4.6-20 K	[W]	7700	7600
4.5 K	[W]	300	150
1.9 K LHe	[W]	2400	2100
4 K VLP	[W]	430	380
20-280 K	[$g.s^{-1}$]	41	27

Table 6: Installed refrigeration capacity in the LHC sectors

The refrigeration of the LHC sectors requires mixed-duty operation of the cryogenic helium refrigerators, in order to fulfil a variety of isothermal and non-isothermal cooling duties. This amounts to a total equivalent entropic capacity of 120 kW at 4.5 K, thus making the LHC the world's most powerful helium refrigeration system.

The large cryogenic helium plants delivered by European industry are based on different variants of the Claude cycle and are designed to reach efficiencies around 30 % with respect to the Carnot cycle (Claudet et al, 1999). The refrigerators are constituted of a compressor station and a cold box. Each compressor station has five to eight oil-lubricated screw compressors, water refrigerant for helium and oil as well as a final oil removal system achieving an oil content of a fraction of ppm. The installed electrical input power is about 5 MW

per refrigerator. The cold boxes are vacuum isolated and house aluminium plate-fin heat exchangers and from 8 to 10 turbo-expanders to provide the cooling capacity. Only the sector cool-down to 80 K is made using a built-in pre-cooler of 600 kW cooling capacity provided mainly by boiling-off liquid nitrogen. Switchable 80 K adsorbers remove up to 50 ppm of air and a 20 K adsorber removes remaining traces of hydrogen and neon. In addition, switchable dryers are connected at the ambient temperature cold box inlet to remove humidity.

The efficient production of 1.8 K refrigeration in the kW range (Lebrun, Tavian and Claudet, 1996) – a novel requirement set by the LHC project – may only be achieved practically through combined cycles making use of sub-atmospheric cryogenic compressors (hydrodynamic compressors, each handling 18 $g.s^{-1}$ at 1 kPa (10 mbar) suction pressure, with a pressure ratio of 3) and low-pressure heat exchangers. The overall coefficient-of-performance of these 1.8 K refrigeration units, once attached to the main 4.5 K refrigerators of the LHC, is expected to be around 900 W per W. Although being relatively simple, the cycle of these 1.8 K refrigeration units is somehow particular, as they have to be interconnected to 4.5 K refrigerators to allow production of cooling capacity at 1.8 K. A set of 3 or 4 centrifugal cold compressors delivers gas through heat exchangers to screw compressors, at a pressure between 30 and 50 kPa (300 and 500 mbar) to minimise the volumetric capacity of the latter. The cold compressors are equipped with active magnetic bearings operated at ambient temperature with rotational speeds from 200 to 800 Hz for the warmest stages. An isentropic efficiency of 75 % has been achieved reproducibly on several sets of cold compressors. As the return temperature to the 4.5 K refrigerator was imposed at 20 K as explained earlier, re-cooling after the heat exchangers with a turbo expander was necessary within the 1.8 K refrigeration units. The cooling capacity to be achieved defines the delivery pressure of the warm compressors

(typically 0.3 to 0.6 MPa). As for other refrigerators, switchable 80 K adsorbers are provided to remove up to 50 ppm of air.

4.2.2 Cryogenic cooling power distribution: the Cryogenic Distribution Line

A Cryogenic Distribution Line (QRL) is used to transport from the refrigerators cooling power to the local cryogenic clients and to recover cold gas at the required pressure and temperature levels (Erdt, Riddone, Trant, 1999).

This distribution line houses the helium supplies and recovery headers at the required pressure and temperature levels (table 7). It runs inside the machine tunnel parallel to the superconducting magnets and it interconnects to them every 107-m.

	Feed / recovery Temperature	Feed / recovery Pressure
Supply	4.5 K SHe	0.3 MPa
Recovery	20 K GHe	0.13 MPa
Supply Thermal screen	50 K GHe	1.9 MPa
Recovery Thermal screen	75 K GHe	1.8 MPa

Table 7: Supply and recovery temperatures and pressures

There are about 27 arc full-cells in a machine sector, which are fed in parallel from the QRL (figure 26). During cool-down, line C supplies helium at progressively lower temperatures to each pair of full-cells and the helium flow is discharged into line D and returned to the refrigerator (Lebrun et al, 1998). Two weeks are needed to cool the 4500 t of the magnets down to 4.5 K. Feed and

discharge valves are closed to evenly distribute the cooling flow depending on the cool-down speed of each full-cell.

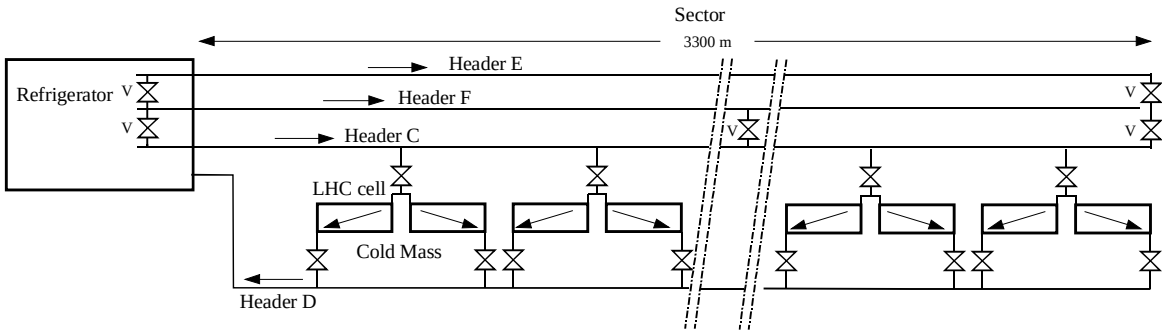

Figure 26: Cooling flow distribution of a sector

Once at 4.5 K, liquid helium is distributed to the cells to fill the magnet cold masses. Once filled to 70 % the inlet and outlet valves are closed and the cold masses filled by condensation of gas pockets and further filling via the feeding valve.

The bayonet heat exchanger inside the pressurised liquid helium bath in the cold mass (see figure 27) cools the magnets down to superfluid helium temperatures by vaporisation of a saturated liquid helium flow (Lebrun et al, 1997). The superfluid saturated helium flow comes from the subcooling in a counterflow heat exchanger and further expansion in a Joule-Thomson valve of supercritical helium at 4.5 K and 3 bar supplied via line C in the QRL.

The Electrical Distribution Feed Boxes (Hauviller et al, 2000) are several meters long liquid helium cryostats which support and cool 13 kA, 6 kA and 600 A current leads. They are used to power the LHC main dipole and quadrupole superconducting magnets, together with their correctors. The DFBs are fed, via a Joule-Thomson expansion valve, with 4.5 K liquid helium from line C to cool the bottom part of the HTS current leads and the LTS busbars. The heat exchanger

(classical) and the top part of the HTS of the current leads are cooled with 20 K gaseous helium forced flow from the return of line D. Gas recoveries from the DFB are sent to the warm recovery line.

Superconducting cavities and non-standard cryostat cooling loops are directly fed with liquid helium from the main feed line C. Cold gas at/or below 20 K is recovered via line D.

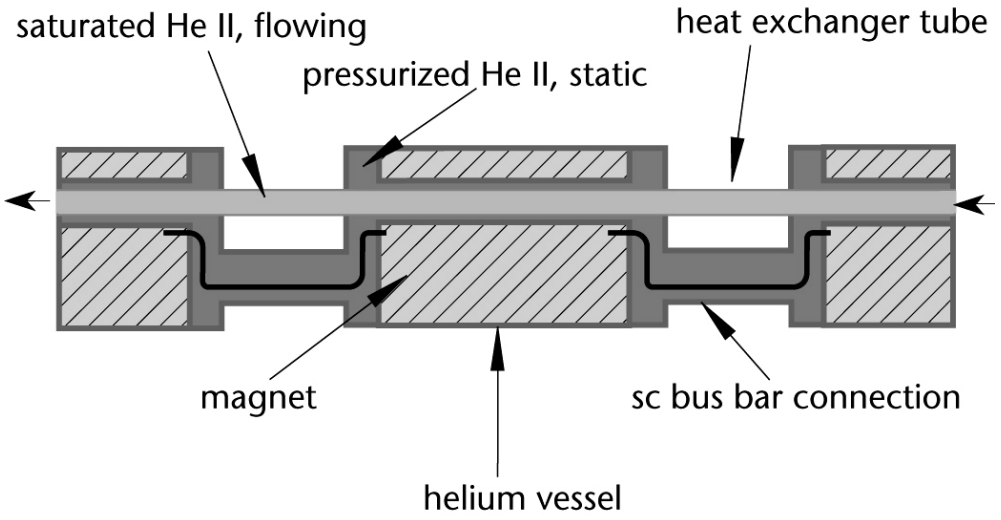

Figure 27: The superfluid helium bayonet heat exchanger

4.3 Instrumentation

The cryogenic operation of the LHC requires a large number of sensors, electronic conditioning units and actuators, most of which are located inside the machine tunnel (see figure 28) and must therefore withstand the environmental radiation. This environment imposes a strict radiation qualification procedure in order to mitigate problems related to future maintenance of the instrumentation located inside the tunnel.

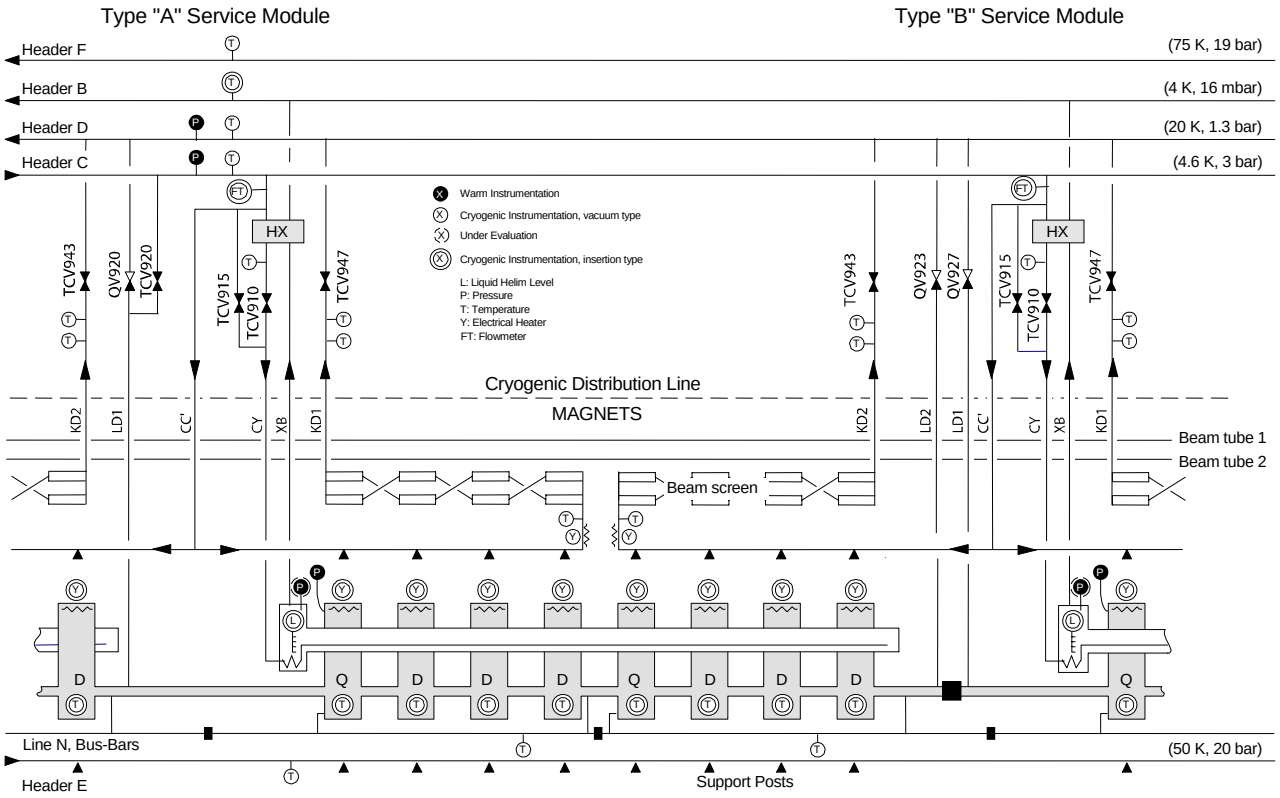

Figure 28: Cryogenic flow-scheme and instrumentation of a LHC lattice cell

While a large number of sensors and actuators are commercially available, specific development and qualification is required for others, in particular temperature, flow and pressure sensors. Furthermore, all tunnel electronics are custom designed to be radiation tolerant.

The tight temperature margins allowed along the cryo-magnet strings in the LHC require implementing precision cryogenic thermometry (overall measurement uncertainty down to $\pm$ 10 mK) on an industrial scale (several thousand channels) with long-term robustness and reliability.

During the final helium filling and normal operation of the LHC, it is very important to know when the cryo-magnet cold-mass is completely filled with pressurized superfluid helium. This information is obtained from warm pressure transducers hydraulically connected to the cold-mass enclosures via the instrumentation feedthroughs.

The requested cryogenic cooling power, unprecedented in size, is based on the stated heat loads assumed for all components. The correct sharing of cryogenic power, to assess individual cryogenic loads and for process monitoring (early diagnosis of faulty components/systems), can only be achieved via accurate flow rate metering on the superfluid helium loops. Robust flow rate metering devices, capable of assessing the cryogenic power going into each independent superfluid helium loop with medium to low accuracy, could be extremely useful for the operation of the future LHC machine and to identify characteristics and limitations of the cryogenic system.

The flowmeters (FT in figure 28) should be mounted on each tapping on line C in all service modules of the future LHC cryogenic distribution line, before the J-T valves, the beam screen supply line and the very low-pressure heat exchanger. The flowmeters will be in the insulation vacuum of the technical modules and will not be accessible from outside.

As a rule, instrumentation sensors (used for control) that are not exchangeable without breaking the vacuum, are duplicated for redundancy purposes. An exception is formed by the cold mass temperature sensors, where the redundancy is provided by the adjacent cold-mass temperature sensor.

5. MODELLING OF HEAT TRANSFER IN SUPERCRITICAL HELIUM

This chapter is a review of the theory of transient and steady state heat transfer laws as well as velocity profile characteristics in the flowmeter axi-symmetric geometry and pipe layout of our application (figure 17). The main heat transfer equations and laws employed to design, size and validate the thermal flowmeters, in steady state as well as during transients, will be reviewed and presented.

5.1 Theory of transient and steady state heat transfer and simulation in our geometry

In order to determine the behaviour of a Newtonian and incompressible fluid, such as gaseous (with velocities much lower than the isentropic sound speed) or liquid helium, we need a set of 3 equations (Bird et al., 1966).

The first equation can be derived from the classical physics concept that mass can neither be created nor destroyed (conservation of mass) and is the continuity equation:

$$\frac{\partial \rho}{\partial t} + \nabla \cdot \left(\rho \vec{u} \right) = 0 \tag{5.1}$$

$\vec{u}$ is the velocity vector and ρ the local density.

The second equation is derived from the conservation of momentum, simplified for the special case of constant viscosity μ:

$$\rho \frac{d\vec{u}}{dt} = -\nabla p + \mu \nabla^2 \vec{u} + \rho \overrightarrow{F_b} \tag{5.2}$$

where $\overrightarrow{F_b}$ is the body force per unit mass of fluid and

$$\frac{d\vec{u}}{dt} = \frac{\partial \vec{u}}{\partial t} + \vec{u} \cdot \nabla \vec{u} \tag{5.3}$$

Equation (5.2) is generally described as the Navier-Stokes equation.

The final conservation equation needed to describe Newtonian fluids is the energy equation that simply states that a fluid system must conserve energy:

$$\frac{d}{dt}\left(\frac{1}{2}\overrightarrow{u^2} + U\right) = -\frac{1}{\rho}\nabla \cdot \left(\rho \vec{u}\right) + \dot{q}_h + F_b \cdot \vec{u} \tag{5.4}$$

U is the specific internal energy, $\dot{q}_h$ is the specific rate of heat input and $F_b \cdot \vec{u}$ is the work done by external forces. This equation can be derived from the general equation for heat transfer in an incompressible fluid:

$$\frac{\partial T}{\partial t} + \vec{u} \cdot \nabla T = \alpha \nabla^2 T + \frac{\mu}{\rho C_p}\left(\frac{\partial u}{\partial y} + \frac{\partial v}{\partial x}\right)^2 \qquad (5.5)$$

with (ρ) density, (C_p) heat capacity, (k) steady-state thermal conductivity, (μ) viscosity, and α the thermal diffusivity. u and v are the velocity components.

5.1.1 Review of the Giarratano/ Dittus-Boelter equation

The convective heat transfer can be derived from equation 5.5.

If the fluid is flowing axi-symmetrically in a tube only 2 dimensions are necessary to describe it. Therefore the velocity can be subdivided in two principal components u and v, in the direction of the tube and perpendicular to the axis of the tube respectively.

If we consider the thermal boundary layer approximation, the temperature T gradient along the axis of the tube is significantly smaller than the one perpendicular to the axis:

$$\frac{\partial T}{\partial y} >> \frac{\partial T}{\partial x}$$

Assuming for simplicity constant properties (ρ) density, (C_p) heat capacity, (k) steady-state thermal conductivity and (μ) viscosity, we obtain the thermal boundary layer equation:

$$u\frac{\partial T}{\partial x} + v\frac{\partial T}{\partial y} = \alpha\frac{\partial^2 T}{\partial y^2} + \frac{\mu}{\rho C_p}\left(\frac{\partial u}{\partial y}\right)^2 \qquad (5.6)$$

where $\alpha = \frac{k}{\rho C_p}$ is the thermal diffusivity.

The first term on the right-hand side represents the thermal diffusion. Normalizing (5.6) we obtain that the average Nusselt number is a general function of Reynolds number and Prandtl number ($\mathrm{Pr} = \frac{\upsilon}{\alpha} = \frac{\mu C_p}{\kappa}$, where υ is the kinematic viscosity):

$$\overline{Nu} = f\left(\mathrm{Re}_D, \mathrm{Pr}\right) \tag{5.7}$$

where the Nusselt number is defined in terms of the average heat transfer $\bar{h}$ and thermal conductivity $\bar{k}$ of the fluid, D being the diameter of the tube:

$$\overline{Nu} = \frac{\bar{h}D}{\bar{k}}, \tag{5.8}$$

Most of the empirical heat transfer correlations are constructed in a form consistent with (5.7) provided Re>0.5 and $Gr \cdot \mathrm{Pr} < 10^{-4}$ (natural convection can be ignored) and $\Delta T < 250K$ (thermal radiation negligible). The Grashof number $Gr = \frac{gD^3 \beta \Delta T}{\nu^2}$, with g being the dimensional constant of gravity and β the coefficient of thermal expansion, is a measure of the ratio of the buoyant forces to the viscous forces and is absent if buoyancy is neglected.

Investigations of heat transfer by forced convection in supercritical helium have shown that traditional engineering correlations are best at describing the data.

Results of analysis of the thermal boundary layer indicate that the average Nusselt number should be written in a form consistent with (5.7). In the turbulent regime a number of good correlations exists for single-phase turbulent heat transfer.

The Dittus-Boelter expression (Dittus and Boelter, 1930), perhaps the most common heat transfer correlation, is written in the form:

$$\overline{Nu} = 0.023\,\mathrm{Re}_D^{4/5}\,\mathrm{Pr}^{2/5} \tag{5.9}$$

where $\overline{Nu}$ represents the average Nusselt number over the tube length.

Correct application of this expression (5.9) requires consideration of the temperature dependence of the fluid properties. The appropriate properties must be evaluated at the film temperature $T_f = \dfrac{T_s + T_m}{2}$ that is the simple average between surface and mean fluid temperature.

In the case of supercritical helium Giarratano et al, 1971 have suggested that a scaling factor 0.022 gives a better fit to the data.

A further improved fit was achieved by use of a correlation of the form:

$$Nu = 0.0259\,\mathrm{Re}_D^{4/5}\,\mathrm{Pr}^{2/5}\left(\frac{T_s}{T_m}\right)^{-0.716} \tag{5.10}$$

where the explicit temperature variation of the fluid properties is taken into account.

This relationship has been shown to correlate to a standard deviation of 8.3 % with several sources of experimental data (Giarratano et al, 1971).

5.1.2 Review of the King's equation

King's equation can be derived from the heat loss or power to be injected in a wire immersed in a fluid flow (forced convection) to maintain its temperature. A special case of equation (5.7) is that due to King for the hot-wire anemometer (King, 1914):

$$Nu = A + B\,\mathrm{Pr}^{0.5}\,\mathrm{Re}^{0.5} \tag{5.11}$$

Where A=1/π and B=$(2/\pi)^{0.5}$. The hot-wire anemometer provides a tool to measure the local fluid velocity.

King investigated the relationship between heat transfer rate and flow velocity. Using equation (5.11) the heat loss per unit length $\dot{q}_L$ of a cylinder of diameter d at a temperature ΔT above the fluid temperature in which is immersed is:

$$\dot{q}_L = \Delta T\left[k + 2\left(kC_p\rho\pi du\right)^{1/2}\right] \tag{5.12}$$

where k is the thermal conductivity of the fluid, C_p is the specific heat of the fluid at constant pressure, ρ is density, and u is the velocity assumed to be perpendicular to the cylinder (Ower and Pankhurst, 1966).

The first term is due to conduction and natural convection and it is important at very low flow rates. The second term becomes more important when velocity increases. The relationship between $\dot{q}_L$ and ΔT is usually obtained by calibration. A device designed to measure velocity with (5.12) will need a means of measuring also the temperature of the stream and the heat loss from the heated wire. This can be achieved by calibration at the fluid operating conditions.

Equation (5.12) can be further simplified introducing the heating current I and the resistance R:

$$\dot{q}_L = I^2 R = C + Du^{1/2} \tag{5.13}$$

where C and D are functions of temperature. Maintaining the resistance of the cylinder or the wire constant the temperature will also be constant and C and D are constant and given for a particular fluid. The advantage of using a constant resistance is to maintain a constant temperature and avoid thermal inertia, and that the equation is further simplified.

Using equation (5.13) and allowing for temperature variation, we can rewrite it as:

$$\dot{q}_L = k(1 + K\dot{m}^{0.5})\Delta T \tag{5.14}$$

Where K is a constant incorporating the area of the duct into which the probe is inserted and the fluid heat transfer constants, $\dot{m}$ is the mass flow rate, $\dot{q}_L$ is the heat supplied and ΔT is the temperature difference between heated and unheated sensors.

5.1.3 Transient heat transfer

Because the thermal diffusivity of helium is very small (about $5 \cdot 10^{-8}\, m^2/s$ at 4.2 K), transient heat transfer to forced flow of supercritical helium takes place in a small layer of the fluid along the wall of the tube on the millisecond time scale (Bloem, 1986, (a)). The heat penetration is of the order of tens of micrometers. Further radial heat transport in the fluid from the outer layer to the core of the flow is governed by the turbulence of the fluid. With a constant heat flux the heat transfer becomes stationary after 0.1 sec.

Therefore the heat transfer during a heat pulse can be divided in three different regimes:

1. up to 2 ms

2. from 2 to 100 ms

3. after 0.1 s

In the first regime the heat transfer is qualitatively represented by the absorption coefficient

$$\varepsilon = \lambda \cdot \rho \cdot C_p \tag{5.15}$$

Where λ is the thermal conductivity, ρ is the density and C_p is the specific heat of supercritical helium.

During the first milliseconds of the heating process the heat transfer takes place in a thin layer of helium along the heated wall. The heat transfer phenomenon is ruled by simple heat penetration. The heat transfer mechanism based on penetration is after a few milliseconds taken over by convection caused by turbulence of the supercritical helium flow.

In this second regime, after 2 ms and before 0.1 s, the heat transfer is determined by the heat conduction in the boundary layer of supercritical helium because of the small thermal diffusivity of helium at our working temperatures and pressure.

After 0.1 sec the heat transfer becomes stationary and the Dittus-Boelter equation applies.

The process of heat transfer for our applications are mainly governed by steady heat transfer as the heat pulses and measurements take place over several hundred ms.

5.2 Velocity flow profile

The piping in the LHC cryogenic system present a certain number of bends that would make the flow profile not uniform thus requiring further analysis to understand or mitigate possible flow measurement problems.

It has been experimentally shown (Murakami et al, 1969; Murakami and Shimizu, 1978) that recovery of a disturbance on the flow profile is dependent on the number of elbows, their development in different planes or not, and the distance between them. A fully developed flow is recovered from a flow profile disturbance after:

1. 3 tube diameters after a single elbow or after two elbows if the distance between the elbows is more than 4.7 times the tube diameter (3 diameters in Spitzer, 1991, (f))

2. up to 135 times the tube diameter if the distance between two elbows in different planes is smaller than 4.7 times the tube diameter

In a pipe line like that of the present application, the fluid flowing through a curved pipe acquires a secondary component not present in a straight pipe flow. This secondary flow produces additional hydraulic loss and in some particular case (two curve pipes located in different planes) a strong spiral motion. This deformed velocity profile can considerably alter the accuracy and performance of most flowmeters. The effect of a double elbow in two anti-parallel planes (90°) is significant when the distance between the two elbows is less than 4.7 diameters and when the flow profile of interest is at less than 160 times the tube diameter downstream of the second elbow (in our case the flow profile of interest is at a distance of 1 tube diameter). The disturbance is the highest when the angle between the two planes is 135° (in our case 90°) and it can take up to 135 diameters downstream the second elbow to recover.

Flow meters with no dependence on the flow profile should be chosen because of the complexity of the piping and the difficulty to verify that the meter measures on a fully developed flow. Otherwise flow conditioners such as tube bundle, honeycomb box or perforated plates, must be employed to guarantee the flowmeter accuracy or the chosen instrument should be calibrated with the upstream pipework.

6. DESIGN AND CONSTRUCTION OF THE PROPOSED FLOWMETERS

In chapter 4 it has been shown how the cryogenic power produced by the eight 18 kW refrigerators is distributed around the 27 km-long LHC machine. In order to know the exact cooling power distribution along the cryogenic distribution line, cryogenic flowmeters should be installed at each cryogenic user tapping to measure the flow rate and infer the individual heat loads for the system and the required cooling power under static and dynamic conditions.

6.1 Flowmeter specification

The required cooling power per individual cooling loop of each standard full-cell at the 1.9 K and 4.5 K temperature levels, respectively for the magnets and beam screen cooling loops, can be derived from table 5 and is summarized in table 8.

mode	static [W]	dynamic [W]	beam screen [W]	collimation [W]	total [W]	Installed [W]
Standby	28.8	0	40	0	28.8	114
Injection nominal	28.8	11.4	160	12	172.2	329.1
Injection ultimate	28.8	11.4	270	19	289.2	336.4
Nominal	28.8	17.6	160	3.4	169.8	325.5
Ultimate	28.8	16.2	270	5.4	280.4	327.6

Table 8: Standard cell required cooling power

Five steady-state operating modes and their corresponding requirements for the cryogenic operation of the machine are considered:

'standby operation' when no beam is circulating, with no current in the magnets, characterized by no resistive dissipation nor beam-induced heat loads in the magnets, but only static heat loads;

'nominal operation' at 7 TeV beam energy, 2 x 0.582 A beam current and 10^{34} cm^{-2} s^{-1} luminosity, excitation current in the magnets characterized by high resistive dissipation and beam-induced heat loads in the magnets;

'ultimate operation' at 7 TeV beam energy, 2 x 0.86 A beam current and $2.5 \cdot 10^{34}$ $cm^{-2}.s^{-1}$ luminosity, excitation current in the magnets characterized by high resistive dissipation and beam-induced heat loads in the magnets (assuming a two-fold reduction of residual pressure in the beam channel over long term operation);

'injection standby' (nominal and ultimate depending on beam current and intensity) when the beam is injected in the machine at its minimum energy of less than 1 TeV, excitation current in the magnets characterized by negligible resistive dissipation and beam-induced heat loads in the magnets.

The cooling power required for collimation is given by the amount of particles that are lost or not intercepted by the collimation system and therefore impinge on the magnets thus requiring additional cooling power to extract the heat load.

For efficient operation, a large turndown capability is required for the refrigeration plants as well as for the cryogenic flow measuring system.

The installed refrigeration cooling power includes contingency (50 %) for excess capacity and uncertainty (25 %) in heat load budgets for the nominal operation mode and allowance for the ultimate operation mode without contingency:

- Q_c installed = 1.5*[1.25*(Q_c static+ Q_c dynamic+ Q_c beamscreen)] in nominal

- Q_c installed = [1.25*(Q_c static+ Q_c dynamic+ Q_c beamscreen)] in ultimate

These values were used for specifying the new 4.5 K refrigerators and the 1.8 K refrigeration units. The full-scale flow can therefore be defined as:

- F.S. flow = f(MAX{MAX(Q_c installed$_i$) AND [1.5*MAX(Q_c nominal$_i$)]})

  where [i] defines the 5 modes of operation as for table 8.

Since the flow rate in g/s is equal to:

- Flow [g/s] = { Q_c [W]/L[J/g]}*flash OR Q_c [W]/DH [J/g]

table 8 can be expressed in terms of required cooling flow rates and gives table 9.

The required cooling flow has been calculated for the nominal cryogenic operating conditions of the machine and therefore for the following values (extracted from Hepak®[Cryodata Inc.]) of latent heat of vaporization for the 1.9 K magnets cooling flow, the enthalpy difference (inlet / outlet) to calculate the beam screens cooling flow and flash or unused cooling flow (amount of gas present in the liquid after Joule-Thomson expansion):

1. L @ 1.9 K = 23 J/g – superconducting magnets cooling flow at 1.9 K

2. DH @ 4.5 – 20 K, 0.3 MPa = 106 J/g – beam screen cooling flow between 4.5 and 20 K (inlet / outlet)

3. Flash = 15 % gas fraction in the liquid after Joule-Thomson expansion not available for superconducting magnets cooling (2.2 K and 0.3 MPa expansion to 1.9 K and 2.1 kPa)

Mode	static [g/s]	dynamic [g/s]	beam screen [g/s]	collimation [g/s]	total [g/s]	installed [g/s]
Standby	1.4	0	0.4	0	1.8	3.4
Inj. nominal	1.4	0.6	1.5	0.6	4.1	6.6
Inj. ultimate	1.4	0.6	2.5	1	5.5	6.9
Nominal	1.4	0.9	1.5	0.2	4	7.1
Ultimate	1.4	0.8	2.5	0.3	5	6.3

Table 9: Standard cell required cooling flow

Therefore, the flowmeter full-scale flow based on table 9 is given by the Nominal conditions and is equal to 7.1 g/s

The minimum required flow is given by the standby conditions and is equal to 1.4 g/s.

The minimum required accuracy can be arbitrarily defined as the flow change due to the minimum variations of heat loads, e.g. beam screen flow in standby over static, and is therefore equal to 0.4 g/s, or +/- 0.2 g/s (i.e. +/- 2.5 % of F.S.).

The maximum withstanding flow of 36 g/s is given by the cool-down flow that can physically traverse the control valve in series with the flowmeter.

In order not to reduce the maximum flow that can be distributed, the pressure drop over the flowmeter must be lower than 5 kPa at full scale flow in nominal conditions (7.1 g/s) and below 20 kPa during the cooldown phases where up to 36 g/s are flowing through. Because of the ranges of flow (7 g/s to 36 g/s), Reynolds number (120000 and 260000 at 7 g/s and between 16000 and 35000 at 1 g/s) and helium density (130 kg/m^3 at 4.5 K and 0.3 MPa, down to 1.6 kg/m^3 at 300 K and 1 MPa) in nominal and cooldown conditions, and in order not to oversize the flow channels of the flowmeter with the risk of reducing accuracy and creating flow instabilities or cavitation, a cold spring pressure actuated valve can be inserted in parallel with the flowmeter in order to by-pass it during cooldown sequences when the pressure drop across it is larger than 20 kPa.

We can therefore summarize below the functional specification for the flowmeter based on the analysis of the operating conditions of the accelerator, the thermodynamic state of the process fluid in various points of the LHC machine and the environment conditions (tunnel and cryostat):

1. Fluid: supercritical helium nominally at 5 K, 0.3 MPa
2. Measuring range: 1 to 7.1 g/s (F.S. linear)
3. Flow withstanding range: 36 g/s
4. Precision in the measuring range: better than +/- 2.5 % F.S.
5. Sampling and measuring rates: at least 0.5 Hz
6. Pressure drop: less than 5 kPa at F.S. and less than 20 kPa at 36 g/s

7. Heat inleak: target 0.1 W but in any case less than 0.5 W

8. Output signal: 4 - 20 mA or 0 - 10 V - linear or linearized

9. Pressure withstanding range: 0 – 2 MPa

10. Materials: suitable for cryogenic and radiation environment

11. Pipe connections: butt weld ends of 20 mm nominal diameter

12. Leak tightness to insulation vacuum with a helium process line pressure of 2 MPa:

    less than 10^{-10} Pa m^3/s (less than 10^{-12} bar l/s)

13. Leak tightness to atmosphere with a helium process line pressure of 2 MPa:

    less than 10^{-7} Pa m^3 / s (less than 10^{-9} bar l / s)

14. Environment: the flowmeter made up of the sensor located along the pipe and the conditioning electronics located outside the vessel should be able to operate under the following conditions at the specified accuracy and reliability:

    Conditioning electronics:

    Ambient pressure: 0.1 ± 0.01 MPa

    Ambient temperature: 5 to 35 C

    Humidity: 30 to 80 %

Radiation dose over the lifetime of the flowmeter:

120 Gy, neutron flux of 6 10^{12} n/cm^2

Sensors:

Insulation vacuum pressure: 10^{-8} to 10^{-11} MPa

Process line pressure: 0.0001 to 2 MPa

Working pressure between 0.24 to 0.36 MPa

Variation at working pressure: ± 0.02 MPa

Process line temperature: 4.5 to 300 K

Working temperature between 4.6 and 5.5 K

Variation at working temperature: ± 0.1 K

Radiation dose over the lifetime of the flowmeter:

120 Gy, neutron flux of 6 10^{12} n/cm^2

15. Flowmeter reliability: when the flowmeter is integrated in the LHC, inside the Cryogenic Distribution Line insulation vacuum, it must function according to specification for 15 years continuous operation and for a number of at least 30 thermal cycles between 4.5 K and room temperature. It should not, in any possible condition, increase the pressure drop or obstruct the fluid flow.

16. Dimension and layout (figure 17):

it must fit inside a volume of 300 x 200 x 50 mm^3

17. Flow: vertical upwards (along the 300 mm length).

Due to variation in temperature (because of heat loads along the machine) and pressure (because of frictional and hydrostatic pressure drops along the machine), the flowmeters installed at each line C tapping to the magnet cell will see a fluid of different and varying thermal characteristics. Furthermore, there will be local variation of temperature and pressure due to stability in the supply.

The temperature is expected to vary between 4.6 and 5.5 K along the sector (worst sector), with a local stability of about +/- 50 mK.

The pressure is expected to vary between 0.24 and 0.36 MPa along the sector (worst sector), with a local stability of +/- 10 kPa.

The mass flow measurement should be ideally insensitive to these variations thus avoiding individual calibration of the required 300 flowmeters with a sensible reduction in cost. Flow measurement with dependence on temperature and pressure provoking measurements errors comparable with the expected precision should not be considered unless a continuous feedback of the temperature and pressure readings (available at each tapping) is used to calculate the actual flow.

Variations in pressure, even if relatively larger, give rise to smaller changes in important helium properties and to relatively small measurement errors.

Local variation in temperature can give errors up to 11.5 % in heat capacity (thus excluding the use of a thermal mass flowmeter), up to 5 % in heat transfer

coefficient, up to 2.7 % in density, 2.5 % in viscosity and 1 % in heat capacity at constant volume (values extracted from Hepak®[Cryodata Inc.]).

6.2 Selection of working principles

Taking into account the flowmeter specification and the analysis of the physical properties of the metered fluid, the choice is oriented to instruments based on a differential pressure measurement (e.g. V-cone, Venturi, orifice – output a function of density and viscosity), on a heat loss measurement (e.g. rate of heat loss flowmeter – output a function of heat capacity at constant volume, conductivity and heat transfer) and a thermal time-of-flight flowmeter (output a function of density). Another promising candidate, because of high accuracy and direct measurement of mass flow (independent of temperature and pressure), is a Coriolis flowmeter adapted for cryogenic operation. The higher cost of this type of flowmeter is partially mitigated by the fact that it does not require calibration at operating conditions to fulfill the precision requirements. An alternative solution, if cost is a major issue, would be to infer the mass flow from the valve opening.

Other possible devices not retained are:

ultrasonic flowmeters that have not been considered because of the low acoustic impedance of helium and their intrinsic high cost;

thermal mass-flowmeters that have not been considered because of the supercritical helium properties ;

target flowmeters (the output of which is a function of density) might be interesting (low cost), but accuracy will be limited by the requirements of maximum flow impedance and robustness of the device and measuring instruments working at cryogenic temperatures.

.

For most of the instruments whose measurements depends or have non negligible dependence from the fluid properties, a continuous monitoring of feedback on the temperature and pressure of the fluid stream is required to improve performance.

Because of the high Reynolds number in this geometry and working conditions we should always be in a turbulent flow regime. These high Reynolds numbers make the use of differential pressure flowmeters preferable as they will show little variations from the theoretical performance (i.e. the viscous effects are relatively low).

The length of the straight pipe upstream and downstream of the flowmeter must be sufficient to ensure a reasonably well developed flow profile for flowmeters dependent on flow profile.

6.3 Flowmeter design strategy

After having introduced the flowmeter specifications and the selection of working principles, the following sections will described the design, construction and operating mode of the selected flowmeters. All selected meters will be tested in order to verify the design criteria and modifications, manufacturing capability, operating conditions, calibration and overall performances against flowmeter specification. Final selection will therefore be made amongst the flowmeters that fulfill the specification. The choice, based on the operating performance, will also take into account other parameters such as cost, robustness and industrialization potential.

All flowmeters based on the rate of heat loss and thermal time-of-flight were designed and built by the author. Section 6.4 introduces the design criteria used

for these flowmeters. The following sections then describe the choice of material and manufacturing of the different type of proposed flowmeters (thermal probe, thermal pulse and time-of-flight flowmeters).

The characteristics and main design parameters of flowmeters manufactured by industry or other laboratories for our application (Venturi, turbine and Coriolis flowmeters) are then described together with the main design modifications (mechanical, electrical, electronics) introduced by the author for low temperature applications. Finally the operating conditions and calibration data for low temperature operation of the Coriolis meters will be discussed.

6.4 The thermal heat loss flowmeters

The thermal heat loss flowmeter is based on the measurement of the convective heat transfer from heating and sensing elements (can be the same) inserted in the flowing stream. The sensing and heating elements can be a Rh-Fe wire or wire grid or temperature probes. The flowmeters design can be performed by estimating some dimensional and thermal characteristics for the given situation and fixing some simple criteria.

A first criterion to be taken into account is the fluid speed in the flow duct that should be subsonic in order to limit the pressure drop. The mass flow rate can be expressed as:

$$\dot{m}=\rho \cdot A_t \cdot \tilde{u} \tag{6.1}$$

where ρ is the density of the fluid, A_t the duct cross-sectional area and $\tilde{u}$ the average velocity. The sonic velocity in supercritical helium at 5 K and 3 bar is of the order of 180 m/s. For the maximum flow of 36 g/s and having to be in average lower than about 1/10 of the sonic velocity we have a minimal duct diameter of 4.6 mm.

A second criterion is the homogeneity of the fluid temperature after the heater and best heat transfer from the heating element to ensure the homogeneity. To achieve it, it is best to install a unique heating and sensing element in the middle of the conduit or to have parallel wires running inside the tube where the parallel wires grids inside the tube are used as a sensor and heating element. Measurements performed by the author and Hebral (1999) have shown that a good homogeneity is achieved after about 50 times the wire mesh spacing. Therefore, for a wire mesh with 1 mm spacing, the homogeneity should be achieved after about 5 cm.

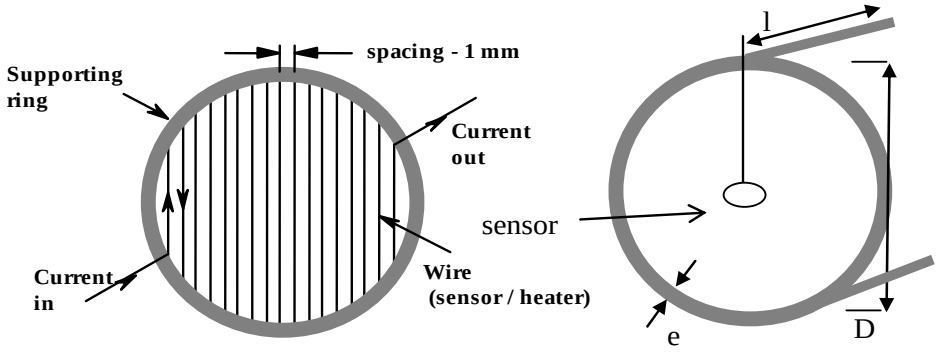

Figure 29: Wire grid spacing and unique sensing element

The third criterion concerns the thermal insulation of the flowmeter sensor(s). The minimal thermal leakage flowing longitudinally through the wall material can be fixed to about 1 % of the applied power in order to minimise the thermal leakage from external sources or between sensors. To limit the thermal loads on the system the maximal applied power should be less than 0.1 W, the target was chosen to be 1 mW. If the temperature increase ΔT due to the heater is of the order of 10 K and the wall temperature at a fixed distance (e.g. another sensor) is equal to the fluid inlet temperature, the thermal losses in Watts along the cylindrical walls can be expressed as:

$$Q_h = k \cdot \Delta T \cdot A_c / l \qquad (6.2)$$

where k is the thermal conductivity in W/m K, $A_c = \pi \cdot D \cdot e$ is the conduction surface area of the tube corona, e is the wall thickness equal to 1 mm, D is the average diameter of the wall equal to 31.4 mm (in a 10 mm tube – prototype tested in CERN test station at reduced flowrate), l is the thermal conduction length of 5 cm. Therefore for a target of 1 mW power transferred along the walls, the thermal conductivity of the material should be of the order of 0.16 W/m K. This requires low conducting materials at 5 K (fibre glass for the wire grid support) or a longer heat transfer length and reduced conduction surface (e.g. a finger insertion support for the thermal sensor).

At low flow rates the speed of thermal diffusion might be thought to be comparable to the speed of the fluid thus giving an error in the measurement. However, because the thermal diffusivity of helium is very small (about $5 \cdot 10^{-8}\, m^2/s$ at 4.2 K, giving about 2 $\mu m/s$ in our geometry) compared to the velocity of the lowest fluid flow rate (about 27 mm/s for 1 g/s at 5 K and 3 bar in a 2 cm tube), the error in the measurement at low flow rates because of thermal diffusivity would be negligible.

In the following sections two types of thermal heat loss flowmeters will be presented together with the main design characteristics. The thermal probe flowmeters based on various types of sensors and wire as sensing elements and the thermal pulse flowmeter.

6.4.1 The thermal probe flowmeters

The first two prototype thermal probe flowmeters are based on the measurement of the heat transferred from a temperature sensor: either a miniature thin film resistance CERNOX™ thermometer or a resistive grid made with a Rh-Fe wire.

Correlations and equations introduced in 5.1 are used to infer the mass flow rate from the injected power, fluid and sensor physical parameters (mainly sensor resistivity and temperature and fluid temperature and pressure).

The sensor and wire temperature has been chosen to be 15 K in order to have a sufficient ΔT to transfer heat, minimize the heat transfer to the helium and operate in a region of good sensitivity to temperature variations for the sensor and the wire but away from the transposed critical line where the physical properties of helium vary most.

A control loop maintains the sensor or wire temperature constant by varying the injected power depending on the heat transferred to the helium at changing flow rates, thus avoiding overheating or allowing only a small temperature increase of the fluid.

The calculations for a prototype have been performed on a scaled model between 0 and 1 g/s to simplify the test rig. The prototypes are scaled in order to achieve the same Reynolds number in the pipe.

To infer the mass flow rate with a temperature sensor we use the equation of heat transfer

$$Q_h = h\ A\ \Delta T \tag{6.3}$$

where Q_h is the transferred heat power, A is the sensor surface area, ΔT is the temperature difference between the fluid and the sensor and h is deduced from equations 5.8 and 5.10. Knowing the resistivity of the sensor, the required sensing current and voltage readout can be derived as shown in table 10.

Flow [g/s]	Sensing current [mA]	Read-out voltage [mV]	Dissipated power [mW]	Resistance @ 15 K [Ohm]
0.1	1	550	0.6	550
1	2.5	1370	3.4	550

Table 10: CERNOX™ sensor (2 mm) operating parameters for the 0.1 to 1 g/s range

To infer the mass flow rate with a wire grid we use equation 5.15. Knowing the resistivity of the sensor and the wire at 15 K the required sensing current and voltage readout can be derived, together with the necessary wire length as shown in table 11.

Flow [g/s]	Sensing current [mA]	Read-out voltage [mV]	Dissipated power [mW]	Resistance @ 15 K [Ohm]
0.1	441	163	72	0.37
1	750	280	208	0.37

Table 11: Rh-Fe wire grid sensor operating parameters for the 0.1 to 1 g/s range

For both types, the pressure drop due to their presence in the flow stream is within the value required in the functional specification. Furthermore, the required flowmeter accuracy can be achieved using industrially available current sources and digital voltmeters.

The flowmeter based on a wire grid thermal probe (figure 30) is constructed with a Rh-Fe wire grid meshed in a section of the 10 mm tube perpendicular to the flow. The length of wire is 10 cm. The support of the wire is a low thermal conductivity and insulating material (fibre-glass) with holes around the diameter

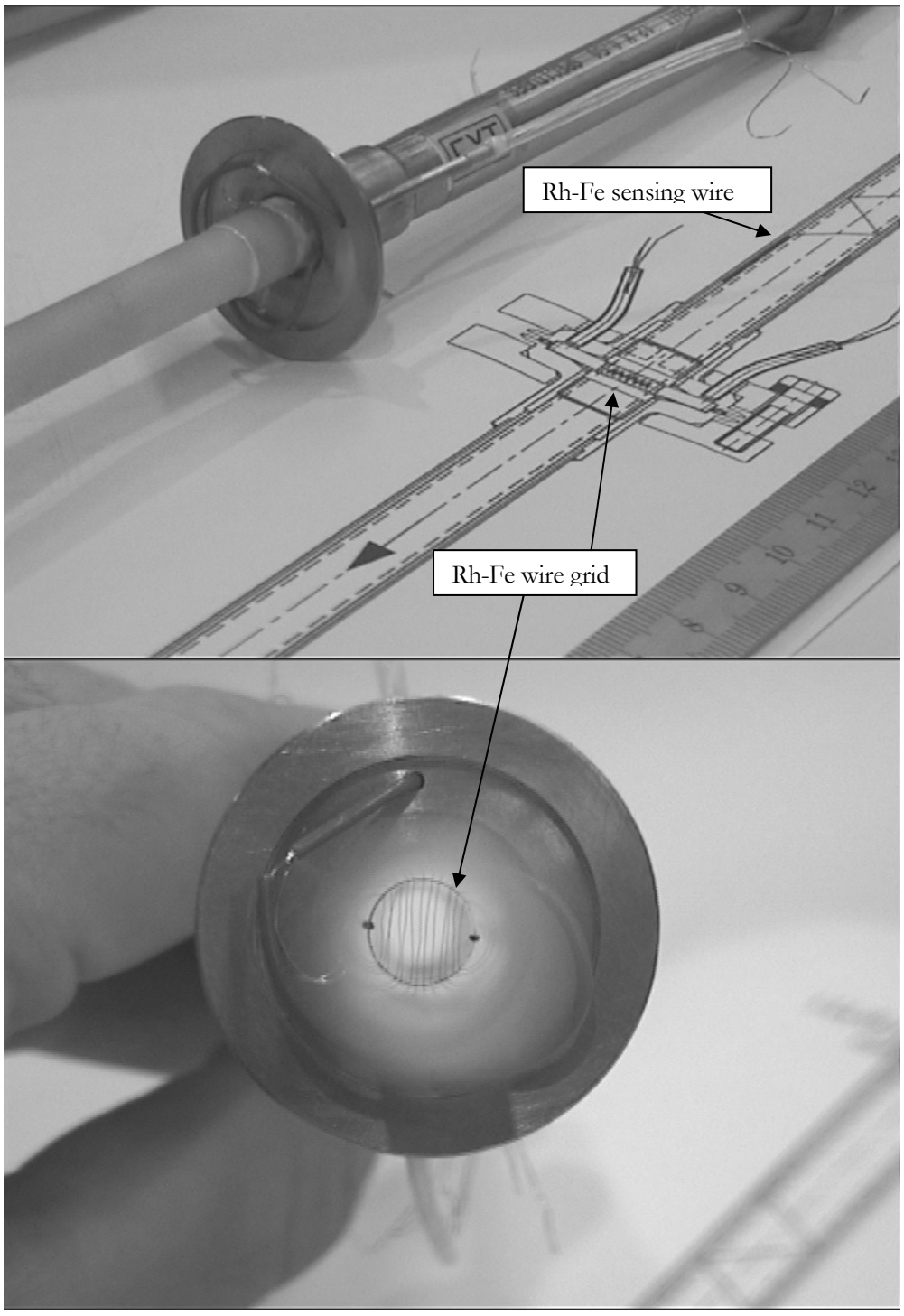

Figure 30: Rh-Fe wire grid prototype flowmeter

on which the wire is woven. A second wire of 10 cm is placed on the external part of the wire support to sense the static temperature of the fluid. The measurement can be therefore corrected at any time using the static temperature of the wire (fluid). The measuring wires come out of the tube via a leak tight passage made with an epoxy resin resistant at cold temperatures. The flowmeter can be opened and the Rh-Fe wire replaced by a leak tight Helicoflex® joint.

The flowmeter based on a CERNOX™ thermal probe (figure 31) is constructed with a fine support inside a 10 mm diameter tube on which a CERNOX™ sensor (2 mm) is glued. The measuring wires (four-wire measurement) are thermalized on the support behind the sensor in the direction of the flow and come out of the tube via a leak tight passage made with an epoxy resin resistant at cold temperatures.

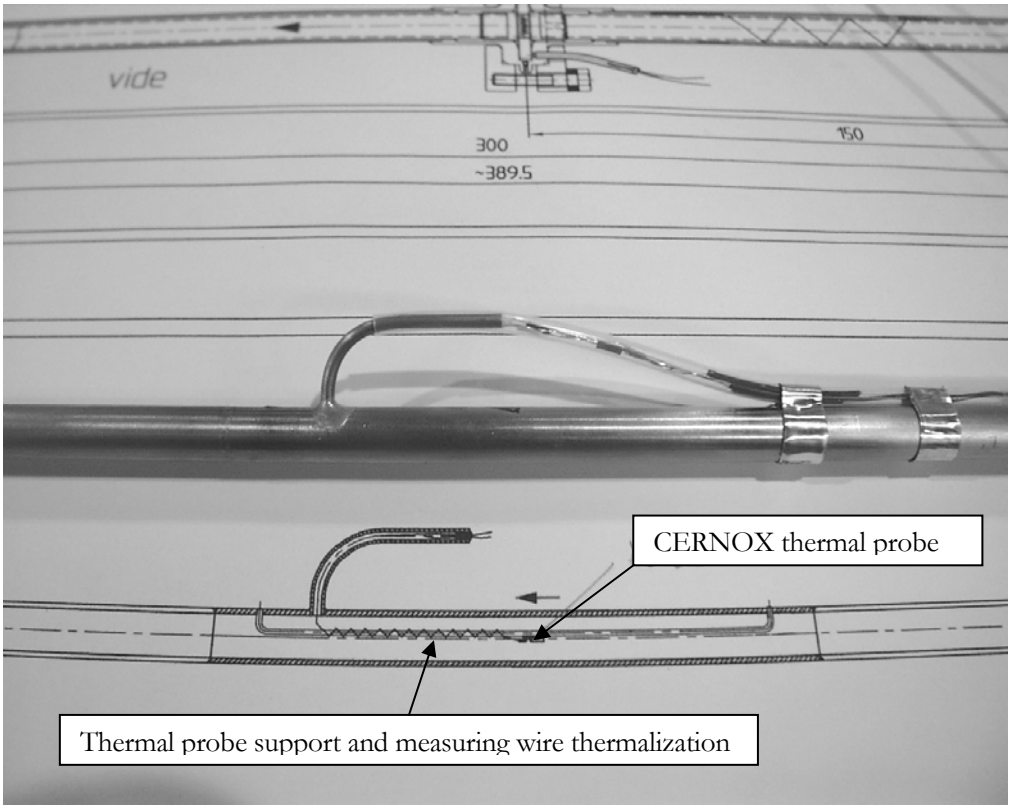

Figure 31: Thermal probe prototype flowmeter based on a CERNOX™ temperature sensor

6.4.2 The thermal pulse flowmeter

The flowmeter shown in figure 32 is comparable to a hot wire anemometer but with a pulsed power injection and a measurement of the speed of cooling. The sensor used is a cable with mineral insulator industrially available for space cryogenics application. The sensing part is made of a Rh-Fe wire. The electrical insulation is made with magnesium and compacted alumina. It is immersed in the conduit from one side to the other and has double leak tight connections.

A similar prototype (Barre, 1999) is under development to meter LOX and LH2 for cryogenics space application (i.e. fuelling of Ariane 5 rocket cryogenic boosters).

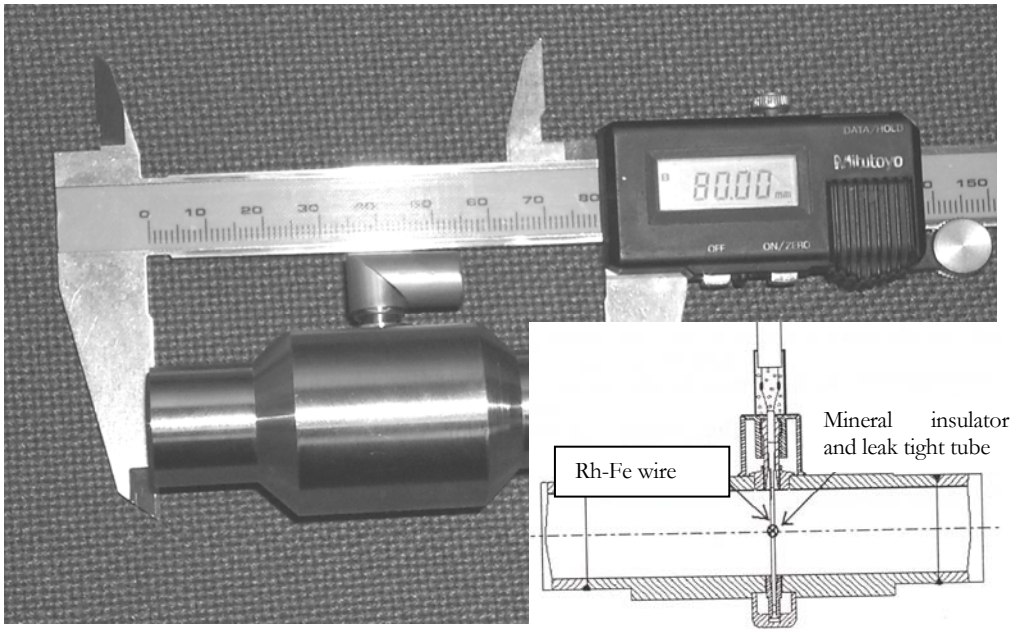

Figure 32: Thermal pulse prototype flowmeter based on Rh-Fe wire probe

The wire is excited by a series of cyclical current pulses of up to 1 A (depending on the resistivity at operating conditions) and for up to 100 msec, and it is therefore heated by the Joule effect. Each pulse is followed by a cooling period of up to 0.5 sec during which a sensing current of less than 100 mA is injected to

measure the slope of the cooldown over a fixed period (i.e. the derivative) that is proportional to the flow rate. The exciting and sensing current intensities are optimized to have the required sensitivity with minimum heat load (Joule heating) to the system as well as minimize perturbation to the fluid motion.

A model can be established on the basis of an energy balance between the heated element and the heat transfer to the fluid as main component, neglecting heat dissipated by radiation and conduction. As shown in chapter 5, the heat transfer coefficient is a function of the mass flow rate and some correlation for supercritical helium can be found in the literature. Nevertheless, due to errors, reproducibility (materials, insulation, sensor length and resistivity) of the sensors and geometry (dimensions, position) and fluid flow conditions, a calibration at working temperature and pressure is required to obtain accuracy better than 10 %. Furthermore, continuous feedback of the fluid temperature variations is necessary.

6.5 Time-of-flight flowmeter

This flowmeter is based on the measurement of the time-of-flight of an injected heat pulse. Two thermal sensors at a known distance apart detect the heat pulse injected by an upstream heater. The heat pulse should heat up a small volume of fluid in the vicinity of the heater. This heated volume travels with the speed of the fluid and passes in front of each thermal sensor. The velocity of the fluid stream is given by the measurement of the difference in time when the increase in temperature has been detected by the sensors, divided by the distance between them.

The parameters of interest for the temperature sensors are fast response time and high sensitivity, while absolute accuracy, repeatability and linearity are not required.

Rivetti, Martini and Birello, 1996, have already successfully employed this technique in single-phase helium, using semiconductors as temperature sensors.

The basic guideline for the design and construction of this flowmeter is to avoid feedthroughs to the process fluid to decrease the risk of leaks. The coils (heater and sensors) sizing and the separation distances were determined by simulating the heat transfer using the equations presented in chapter 5 and experimental validation.

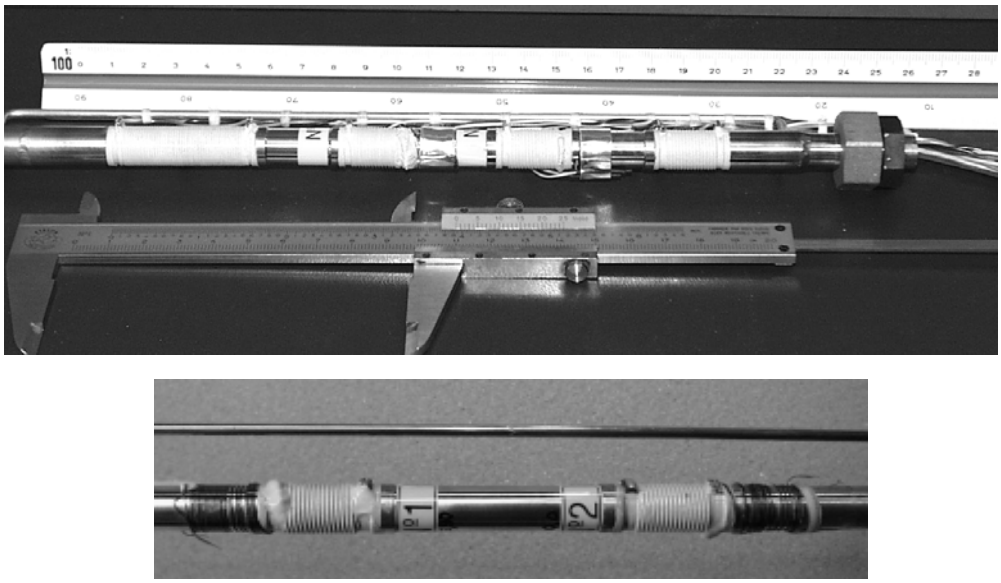

Figure 33: Pictures of a prototype time-of-flight flowmeter showing the heater and three measuring coils

For a flow of 1 g/s heat pulses of 100 J/s for about 0.4 s were simulated as sufficient to increase the temperature of the superconducting gauges above their critical value (i.e. about 9 K).

The heater is made of a copper-constantan uncoated wire and the thermometers are replaced by superconducting wire (Nb-Ti; the same that is used in commercially available liquid helium level gauges). The heater and

superconducting wires are glued to the outer surface with a thermally conductive but electrically insulating medium (epoxy with 45 % Alumina and Borum Nitride from Epotecny) to sections made of a thin copper tube with grooves to accommodate the wire and reduce the local thickness (figure 33 and 34). These copper sections are spaced apart with 5-cm-long sections made of stainless steel to reduce the conduction via the tube. Leak tight connection between stainless steel and copper section is achieved by electron beam welding.

A power of between 20 and 50 W is injected with a pulse duration of a few hundred ms; this energy increases the flowing helium temperature at nominal working conditions (0.3 MPa, 5 K) above the quenching temperature of the superconductors (i.e. 9 K). The sudden resistive transition of the superconductor allows clear detection of the passage of the warm front. Simulations have shown that thermal diffusion is negligible and therefore no cross-correlation techniques need to be employed.

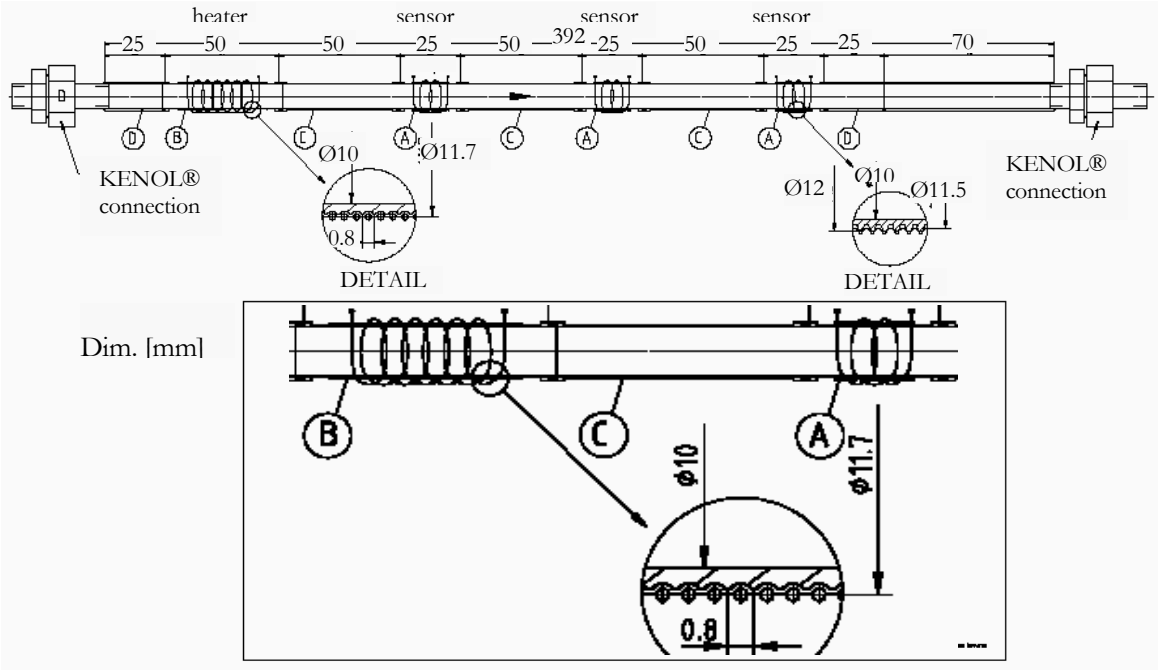

Figure 34: The prototype time-of-flight flowmeter construction drawing

6.6 Differential pressure flowmeters

Differential pressure flow rate meters are the most common measuring devices employed in cryogenics for ambient temperature flows, because of the large number of different types industrially available (Orifice, Venturi, V-Cone, Pitot tube, etc.), the reasonable cost and good accuracy, and the intrinsic robustness (simple construction, no moving parts, external instrumentation and low maintenance). Unfortunately, these considerations do not apply when the temperatures are lowered down to the cryogenic range where thermo-mechanical stresses reduce robustness, reliability and impose low temperature calibration.

Orifice flowmeters are probably the most commonly used devices in cryogenic industrial applications because of their robustness, low cost and relatively good accuracy. They consist of a plate with a concentric opening over which a pressure difference is measured. Their accuracy is of the order of 5 %.

V-cone flowmeters have the advantage of being more accurate and need less straight length of piping, and the disadvantage of being more expensive, but have never been employed at cryogenic temperatures.

Venturi flowmeters, the only cryogenic (low temperature) flowmeters known, are even more expensive, but have a lower reliability due to the cold differential pressure sensor under thermo-mechanical stress and do require low temperature calibration.

For this category of flowmeters the only disadvantage seems to be the cost and the fact that they are not linear, thus drastically reducing the accuracy in the lower part of their measuring range.

6.6.1 Venturi flowmeter

A Venturi flowmeter was designed and constructed at IMGC following the ISO 5167 specifications (Rivetti et al, 1994, (b)) scaled down to operate in the 0.5 to 6 g/s flow range for 4.2 K liquid helium.

As shown in chapter 2, Venturi flowmeters are based on Bernoulli's law (conservation of mechanical energy in a closed pipe). Therefore the mass flow rate is inferred by measuring the difference of pressure between the upstream and throat sections, according to:

$$\dot{m}=C_d A_t \sqrt{\frac{2\rho\Delta p}{\left(1-\beta^4\right)}} \tag{6.4}$$

where $\beta=\frac{d}{D}$ is the dimensionless throat-to-upstream diameter ratio, A_t the throat section in m^2, Δp the pressure difference in Pa, C_d the dimensionless discharge coefficient, ρ the fluid density in kg/m^3.

The inner profile dimensions are shown in table 12 and figure 35. The differential pressure range is 1.8 kPa for 0 to 6 g/s. The C_d discharge coefficient is in the order of 0.985 +/- 0.005 .

The differential pressure ports are made of Swagelock® connectors welded to the two annular chambers communicating to the upstream and throat sections through 6 radial small-diameter holes. The chamber is also welded to the meter body and is therefore not dismountable.

A DP-10 type Valydine cold pressure sensor of 3.5 kPa full scale range, suitable for cryogenic service (no active electronic components on the transducer and welded diaphragm), is connected to the two ports via two 3.175 mm diameter stainless steel tubes. The leak tightness of the connection is ensured by copper

gaskets. The diaphragm is made of magnetically permeable stainless steel between two identical coils excited by 5 KHz sinusoidal current. When pressure is applied, the diaphragm deflects and changes in an opposite sense the coil inductances whose variations are detected by an external (at ambient temperature, outside the cryostat) lock-in amplifier providing a 0-10 V d.c. signal proportional to the applied pressure.

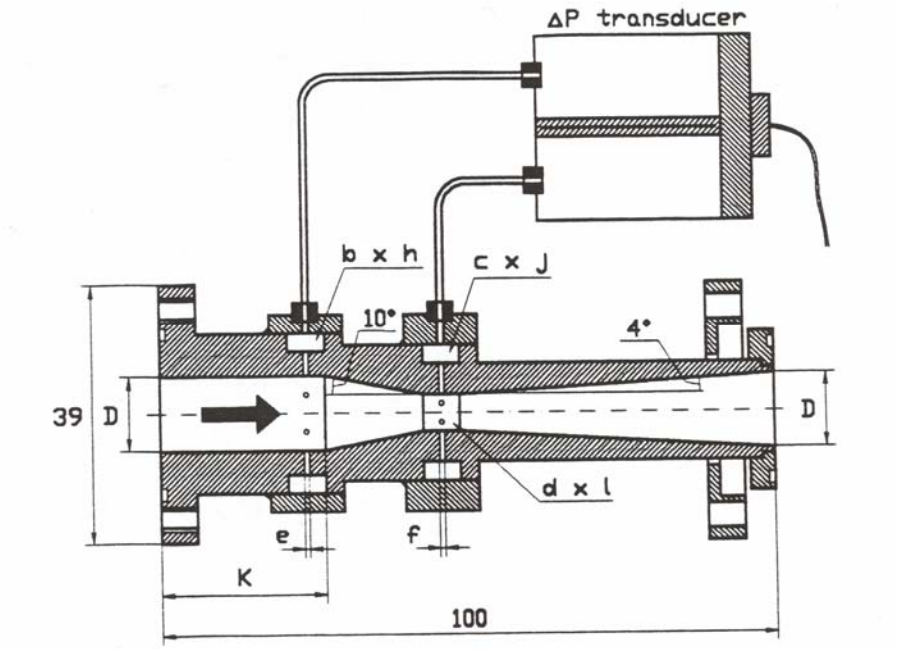

Figure 35: Venturi flowmeter construction drawing

Inlet and outlet diameter [D]	10
Throat dimensions [d x l]	3.2 x 3.2
Upstream straight length [K]	29
Upstream ann. chamber dimensions [b x h]	7.5 x 2
Throat ann. chamber dimensions [c x j]	6 x 3
Upstream pressure holes diameter [e]	1
Throat pressure holes diameter [f]	0.5

Table 12: Venturi flowmeter dimension in mm

At the inlet of the Venturi flowmeter there is a flow straightener made of 50-mm long straight pipe of the same flowmeter inlet diameter and filled with 7 low-thickness stainless steel tubes of 3.4 mm external diameter, retained at the two ends by stainless steel nets.

In order to improve the robustness of the flowmeter the cold pressure transducer chosen is designed for a flow of 30 g/s, thus reducing its precision, but avoiding risk of breaking it under high flow rates and cooldown. To further improve robustness and reliability an external pressure sensor, connected via 1 m long capillaries outside the cryostat, was added to measure in parallel to the cold transducer. Three layers of Mumetal® were wrapped around the sensor to shield it from possible magnetic interference coming from the superconducting magnet coils generating fields estimated to be up to 0.1 T.

Particular care was taken during the mechanical construction to respect the dimensioning ratios and to well polish the surfaces in order to have the coefficients of discharge and beta ratios as close as possible to those predicted by theory.

Accuracies of the order of 2 to 3 % were achieved after calibration of the flowmeter in the IMGC calibrator at operating conditions. Prior to the calibration at working conditions the accuracy was of the order of 10 % because of the uncertainty of the differential pressure measurements (zero drift and gain change) and discharge coefficient at low temperatures and possibility of flashing and cavitations phenomena.

6.7 Turbine flowmeter

Turbine flowmeters are traditionally considered to be the most repeatable instruments to measure liquid or gases flow rates provided that the bearing

friction factor is constant. If calibrated at working conditions they can achieve accuracies as low as 0.1 % of the full scale but in a limited flow range of 1:10.

Unfortunately, when used at cryogenic temperature, the wear and tear, and thermal stresses induced by thermal cycling can damage the contact surface of the bearing causing changes of the calibration factor. For laboratory applications two turbines in series are installed in order to detect calibration factor variations.

The principles of operation and governing equation have already been presented in chapter 2 and are applicable also for cryogenics use. The K factor is dependent on the type of flow and therefore on the Reynolds number. Three different flow regimes can be identified:

1. laminar flow, where the K factor rapidly increases with the flow rate because mechanical and viscous drag forces are comparable with kinetic forces exerted by the flow against the rotor blades;

2. transitional flow, where the K factor decreases because the boundary layer thickness suddenly decreases thus enlarging the free passage area and reducing the flow speed on the rotor blades;

3. turbulent flow, where the K factor stays essentially constant or increases slightly with the flow rate because the kinetic forces prevail over the drag forces.

6.7.1 Classical turbine

To test the feasibility and performances of classical turbines at liquid helium temperatures an industrially available flowmeter for liquid nitrogen temperatures was bought.

This flowmeter is a standard turbine used also at ambient temperature. All parts are made in stainless steel. The rotor is made of 17.4 Ph. SS and the self lubricating ball bearings are made of 440 SS. The pick up is by magnet/coil. The flowmeter is calibrated in water and then a scaling factor (using equation 2.11) is used for 5 K operating temperatures.

6.7.2 Magnetically levitated turbine

This flowmeter is like a standard turbine for which the rotor (made of YBCO) is magnetically levitated below 100 K because of the Meissner effect. It has been developed and calibrated at LHe temperatures at IMGC (Rivetti et al, 2004, (a)).

At each end of the rotor a niobium conical cap is repelled and centred by the magnetic flux lines generated by two superconducting windings supplied with opposite direction currents. Therefore, much stronger forces are obtained permitting high angular speed with no current flowing in the superconducting rotor during operation. Unfortunately, a highly axi-symmetric magnet is required together with an accurate positioning system.

The angular speed measurement is based on the passive distortion of the originally toroidal shape of the magnetic field generated by the magnet on board of the rotor. Twenty ferromagnetic pins inserted in the outer aluminium ring provide 20 pulses per revolution to the external pick off coil.

A positioning system is necessary to hold the rotor in the right position until the superconductive transition takes place (below 100 K). Two independent rods, operated through electromagnetic devices, ensure repeatable rotor positioning.

By eliminating contact and therefore friction, the K factor of the turbine should be much more stable, thus ensuring much higher repeatability and accuracy.

6.8 Coriolis mass flowmeter

The meters built for liquid and supercritical helium applications at CERN were standard meters (MicroMotion, 1999) with minor modifications (Serio et al, 2002, (b)) for low temperature applications. They were successfully employed down to superfluid helium temperatures.

The principles of operation and governing equations have already been described in general in chapter 2, the characteristics, modifications and peculiarities for cryogenic use will be outlined below.

6.8.1 Coriolis flowmeter design for cryogenic temperatures

A Coriolis meter makes a temperature measurement for compensation of the vibration characteristics of the sensing element. The measurement is usually made with a PT100 (RTD) thin-film element. For reliability reasons the PT100 was eliminated from the cryogenic helium meter design, and for reasons discussed in the coming paragraphs the temperature measurement is not required.

The meter sensitivity variations resulting from changing the temperature occur because the modulus of elasticity of the sensor tubes (made with stainless steel) varies with temperature; the temperature correction is simply the ratio of the modulus of elasticity between the operating and calibration temperature. The change in modulus of elasticity is well characterized over the temperature range of interest with 1 % accuracy (Ledbetter, 1980) and is therefore easily compensated. The challenge for cryogenic applications is that the effect on modulus of elasticity is non-linear to approximately 30 K. Fortunately, for liquid helium temperatures below 20 K the change of modulus is very small.

Normally during calibration of a Coriolis meter the effect of temperature is incorporated directly into the calibration constants. Since the temperature measurement is not used in this case, an alternative method is required for the

compensation. The modulus of elasticity for stainless steel 316 L is approximately constant with a value of 207.5 GPa below 20 K (figure 36); by recording the calibration temperature (usually water at approximately 20 °C where the modulus is 194.6 GPa) the correction factor is easily calculated: 207.5/194.6 = 1.066.

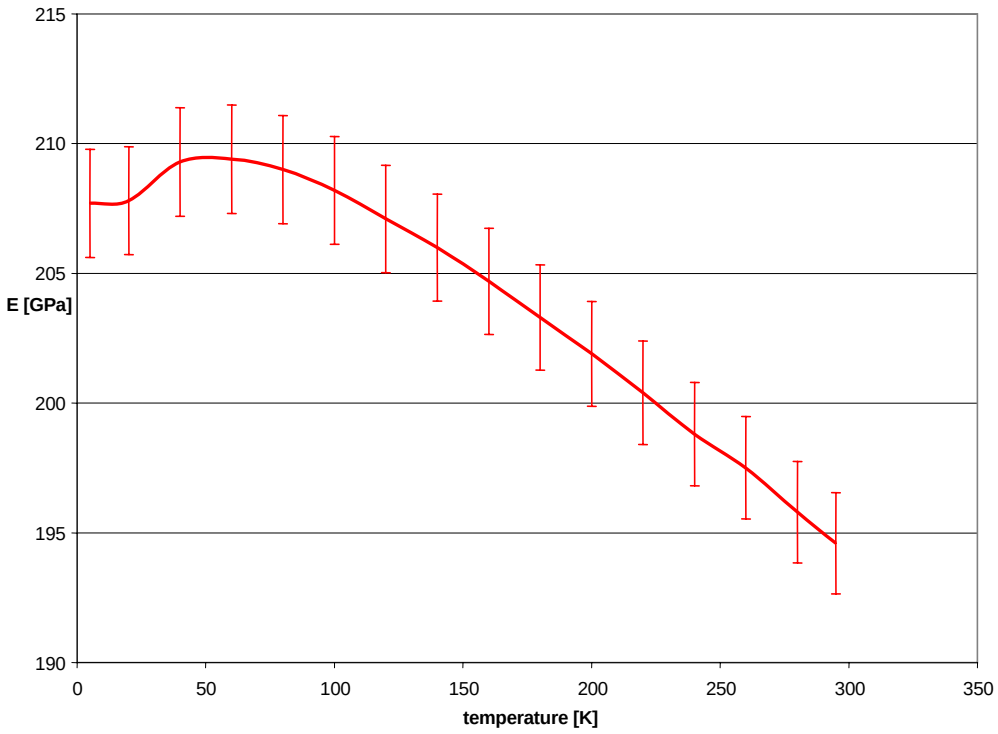

Figure 36: Temperature dependence of Young's modulus for stainless steel 316 L (Ledbetter, 1980)

One important requirement for CERN is component robustness and reliability. The specific requirement for the flowmeter was the ability to cycle at least 30 times between ambient and operating temperature (4 K). Thermal cycling was conducted on prototype meters over the temperature range to prove robustness and there was no indication of any pressure-containing component issues. However, it was found that small gauge wire internal to the sensor sometimes broke resulting in electrically open circuits, therefore causing meter failures. The

wire gauge was increased, and meters were found to survive at least 60 thermal cycles over the same temperature range.

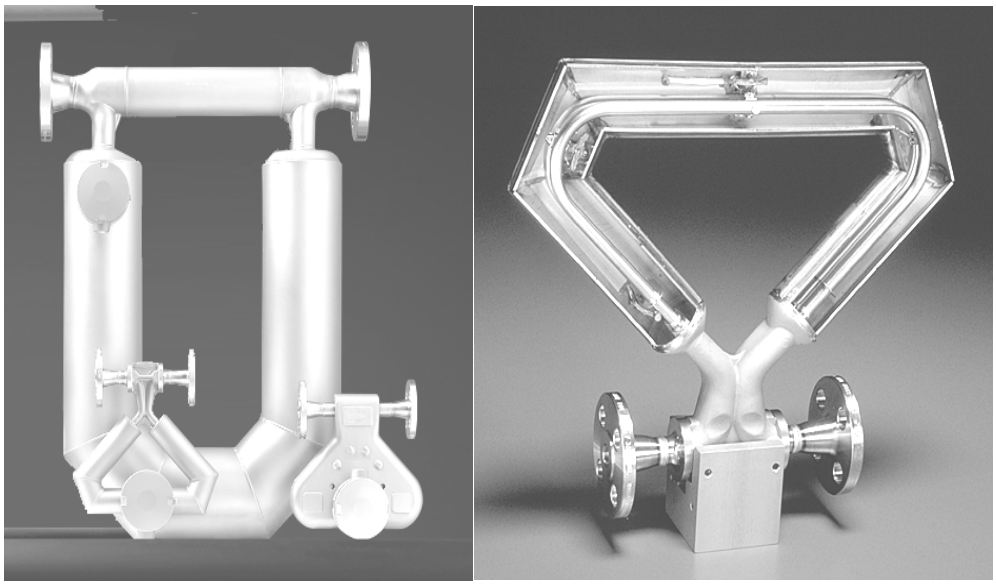

Figure 37: Coriolis flowmeters employed at CERN and a cross section showing oscillating tubes, measuring and drive coils (courtesy of MicroMotion Inc.)

The last change was rather simple and obvious. All meters are purged with an inert gas to ensure a good hermetic dry seal for the electronic components. Nitrogen or argon is typical, but these freeze at 4 K. The meter was therefore purged with helium to eliminate this issue. This makes necessary also a secondary containment for the process fluid. Alternatively the meter can be purged by leaving it open to the cryostat insulation vacuum.

6.8.2 Coriolis flowmeter operation at cryogenic temperatures

The electronics of Coriolis meters for cryogenic use needed modification in order to take into account the variation in wires and coils (drive) resistance at low temperature. During cool-down down to 4.5 K and beyond, the resistance of the

wires and coils reduces and therefore the drive power to excite the natural oscillation of the tubes increases up to a point to which it saturates. This makes the meter unstable, oscillatory and makes it difficult to obtain a proper zero at low temperatures. Therefore a resistor in the drive circuit of about 200 ohm was added and the saturation of the drive coil power was avoided. The resistor is needed to stabilize the drive circuit when coil resistance is almost zero (i.e. below 20 K). Several tests at different operating conditions were required to find the right balance between stability and required drive power.

6.9 Proposed alternative solutions to meter a cryogenic flow

The flow from line C to the 1.9 K cooling loop and the beam screen cooling loop (ref. to chapter 4 and in particular figure 28) can also be assessed via the measurement of cryogenic pneumatic valve openings together with pressure and temperature measurements. The inferred mass flow rate would however be less accurate and would require the implementation of calculation routines to calculate the mass flow rate from the valve opening and the pressure and temperature signals.

The temperature sensor accuracy on the 1.9 K loop is +/- 10 mK; while on the beam screen loop at 20 K is +/- 50 mK.

The pressure sensor accuracy on the 1.9 K and beam screen loops is +/- 5 kPa.

The standard cryogenic pneumatic valve Kv (flow coefficient) value accuracy as given by the manufacturer is 2 % at full opening (VELAN Inc.). The accuracy over the full opening range depends on the valve rangeability and, for a standard cryogenic valve is below 2 % down to openings of few %. The opening resolution given by an angular encoder is 1 %.

Therefore, the overall accuracy that can be expected in mass flow is given in a first approximation by the pressure drop, the Kv value accuracy and valve opening resolution to determine the volumetric flow rate and by the temperature and pressure accuracy to determine the density to infer the mass flow rate.

The measurement (temperature and pressure to calculate the density, pressure to calculate the flow and Kv value) errors add up to a normalised mass flow error of 12 %.

Chapter 7

7. THE TEST FACILITIES

Several test facilities at CERN and a calibration test rig at Turin Metrological Institute were employed in order to select, improve and optimize the best suitable methods.

The investigated instruments underwent an extensive test program comprising: warm pressure and leak testing, thermal cycling and cryogenic testing (flow measurement accuracy within ± 1.5 %) at CERN (flowmeters tested: all), described in section 7.1; cryogenic testing at an independent metrological laboratory (IMGC – Italy) with a calibration module of the absolute type accurate within ± 0.5 % (flowmeters tested: Coriolis, turbine levitated, Venturi), described in section 7.2; long term reliability studies and zero stability/drift measurements at CERN full-scale accelerator model (flowmeter tested: Coriolis), described in section 7.3; radiation tests, described in section 7.4 (flowmeter tested: Coriolis). The flowmeters were tested at various flow rates between 0.5 g/s and 30 g/s, temperatures between 1.7 K and 10 K and pressures between 1 kPa and 0.5 MPa, using boiling as well as sub-cooled, supercritical and superfluid helium.

The flowmeters had not been previously calibrated nor tested elsewhere. The Coriolis flowmeters were the only exception. They were tested and calibrated in water at the manufacturer premises as standard units despite having been modified for cryogenics use and operation.

The flowmeters successfully tested (fulfilling the technical specifications listed in section 6.1) and chosen for installation in the LHC machine were finally validated

in the full-scale model of the machine accelerator for long term testing, reliability assessment in real operating conditions and were also used as diagnostic tools for heat load measurements on the machine main components.

7.1 CERN test set-up

7.1.1 Test set-up description

In order to test the prototype flowmeters in supercritical helium the author designed and supervised the construction of a test cryostat (figure 38).

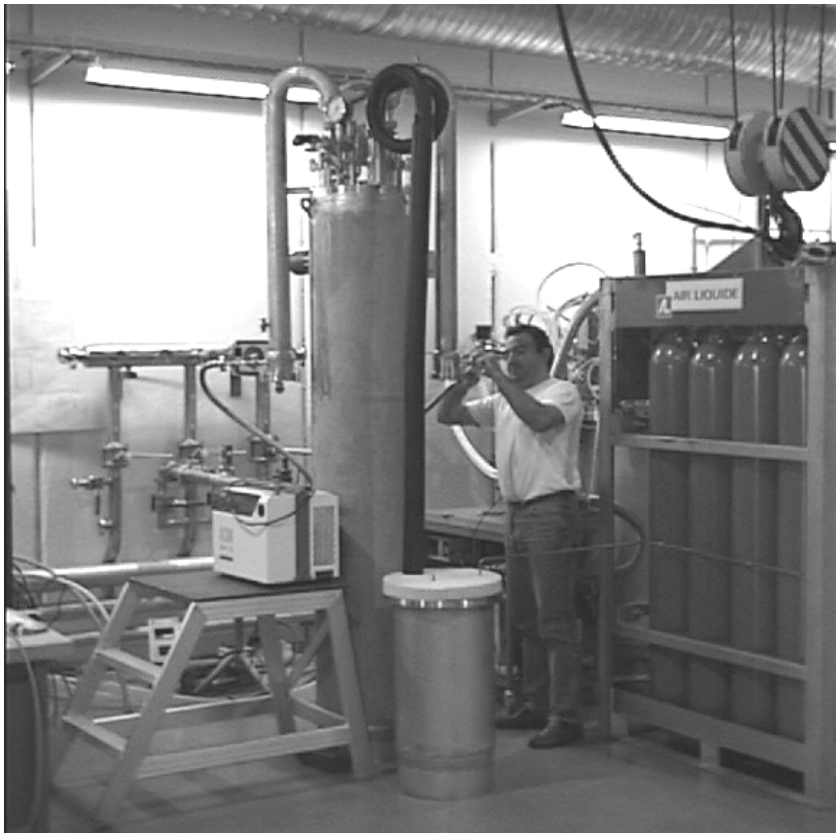

Figure 38: CERN's flowmeter test station

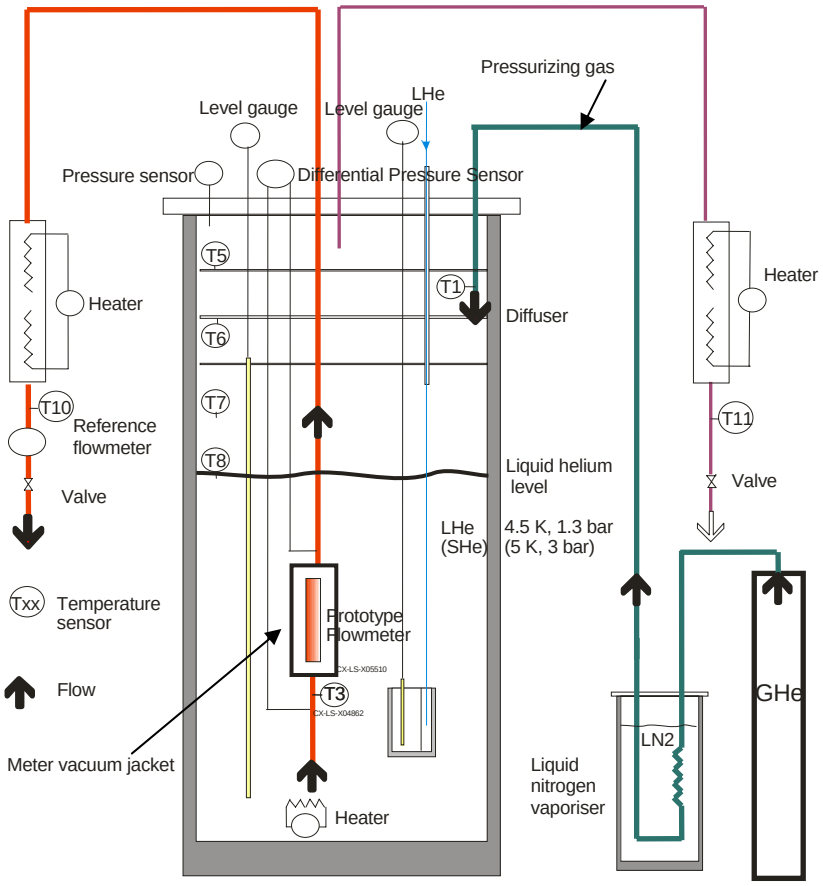

Figure 39: CERN's flowmeter test station process and instrumentation diagram

The cryostat elongated construction (about 2.2 m height and 0.4 m diameter) permits to obtain a large temperature gradient between the top and bottom part. The cryostat can be filled with up to 200 litres of liquid helium. Warm gas flow is then injected from the top flange of the cryostat to pressurise liquid helium above its critical point. In order to reduce the temperature difference, the high pressure helium gas at 300 K is cooled down via a liquid nitrogen vaporiser to about 120 K before entering the cryostat. A diffuser at the warm gas inlet has been added to reduce turbulence. Thermal baffles at the neck entry avoid mixing of the

cold helium with the warm incoming gas. At the end of the pressurisation we obtain supercritical helium at a temperature between 5 and 120 K. Cold supercritical helium is then extracted from the bottom part of the cryostat through a vacuum insulated line running up to the top flange. The flowmeters are housed in the bottom part of the vacuum insulated line.

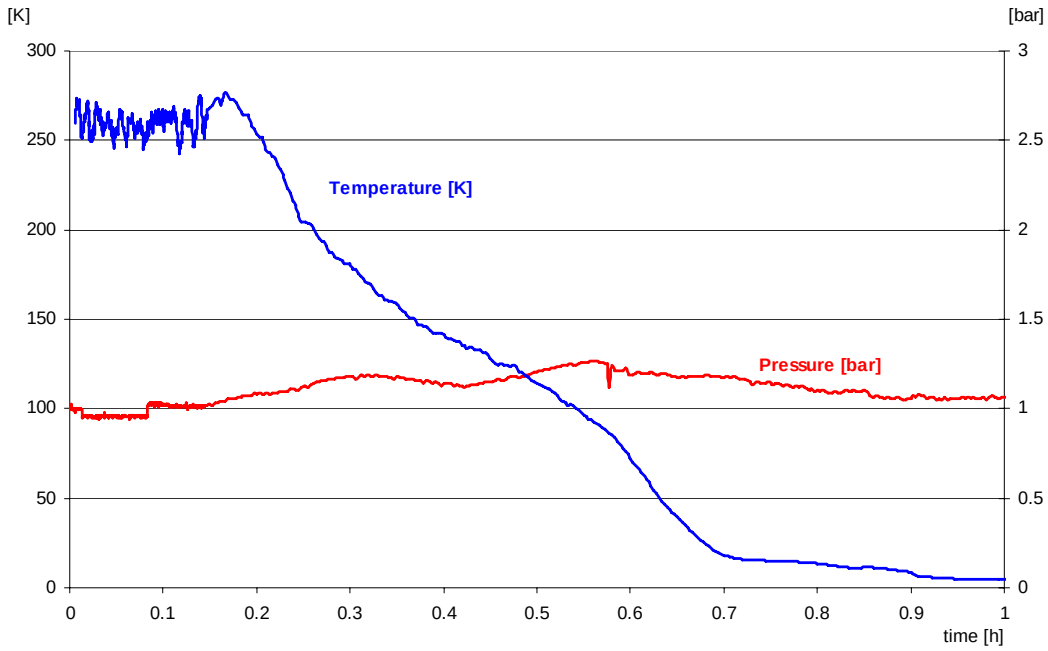

Figure 40: Typical cool-down of the flowmeter test station

The test station permits to cool-down in about 1 hour (figure 40) and test flowmeters (figure 41) for up to ½ hour at nominal conditions (i.e. around 5 K and 0.3 MPa) or with saturated liquid helium at 4.2 K. The maximum flow rate is limited by the pressure drop and high pressure feeding capacity to about 4 g/s at nominal conditions. In non steady transients the maximum flow rate obtained was in the order of 8 g/s.

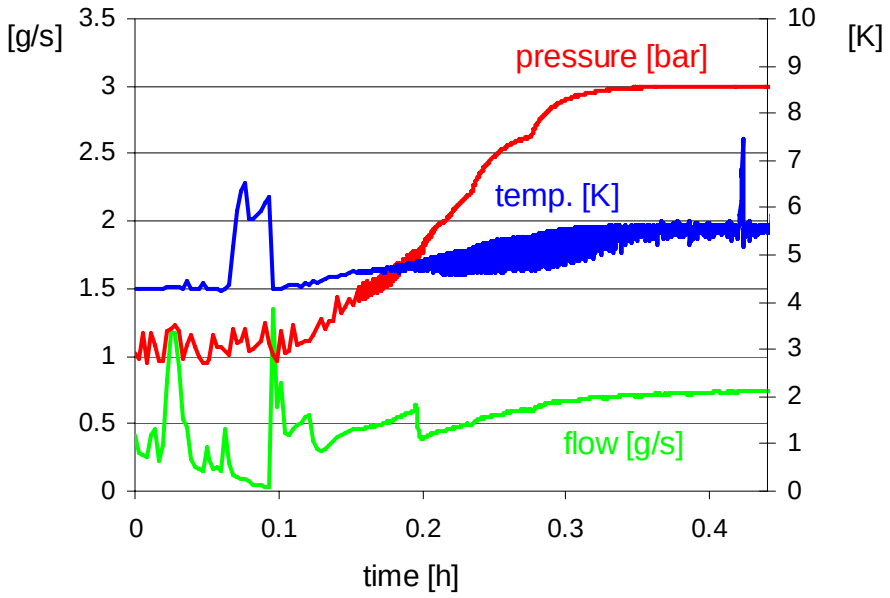

Figure 41: Flowmeter test station pressurization to supercritical helium (above 2.3 bar)

A set of Pt 100 sensors distributed vertically at the neck entry has shown that a warm front slowly progresses towards the bottom part of the cryostat without mixing.

The test station is equipped with the necessary instrumentation to operate it and to analyse the performance of the flowmeter (flow, pressure drop, temperature and pressure). The reference flow rate is measured at ambient temperature with a Hastings™ thermal mass flowmeter with 1.5 % F.S. accuracy (10 g/s F.S.).

7.1.2 Traceability and uncertainty analysis

The uncertainty of the CERN calibration process can be traced to national standards through a chain of successive measurements. The calibration of all temperature, pressure and warm flow measurement equipment is verified with traceable standards through successive measurements in calibration laboratories.

The uncertainty of the test station is due to uncertainty contributions of the measurement devices employed, the warm flowmeter at the outlet and the calibration process. The total uncertainty is calculated as the root of the sum of the squares of each of the individual contributions to the uncertainty.

The calibration method is based on steady state flow. There is also an uncertainty due to the stability and repeatability of measurements of the reference warm flowmeter and the number of points taken during each measurement.

Neglecting the uncertainties due to the pressure and temperature measurements which contribute to the variation of the calibration factor for the warm flowmeter, the main contributions are as follows:

1. uncertainty of the reference warm flowmeter - $U_{ref-flo} = 1.5\%$

2. uncertainty due to the repeatability of the reference flowmeter and the number of points taken - $U_{meas} = \left(\frac{0.5}{\sqrt{10}} \right) = 0.16\%$

Therefore the CERN test station overall uncertainty is:

$$U_{CERN\_test\_station} = \sqrt{(U_{ref-flo})^2 + (U_{meas})^2} = 1.51\%$$

7.2 IMGC Metrological Institute test rig

7.2.1 Test rig description

A calibration module of the absolute type (figure 42 and 43), designed and built at IMGC (Rivetti et al, 1994, (a)) allows testing and calibrating of flowmeters in cryogenic helium to an estimated accuracy of 0.5 %. The system is based on the axial displacement of a membrane bellows completely immersed in a liquid

helium bath by mean of a motor operated from outside the cryostat. The working bath itself is surrounded by a cooling bath. The absolute pressures inside the two baths can be independently set at different values between 100 Pa and 0.6 MPa, so that, inside the working bath, helium can be steadily kept under different thermodynamic conditions, as summarized here below:

i. *saturated normal liquid*: at any temperature between λ-point and 5.2 K;

ii. *saturated superfluid*: at any temperature between 1.5 K and λ-point;

iii. *supercritical*: at any temperature between λ-point and 5.2 K;

iv. measurements above 5.2 K are still possible, with a temperature no longer stable but with a slow tendency to increase.

The volume of the bellows was originally calibrated in water at room temperature with an application of the gravimetrical method. This was corrected for thermal contraction at the working temperature. A new calibration, recently performed in gas using the new standard gas meter of IMGC, substantially confirmed the results of the previous one.

The closed-loop brush-less motor, formerly used to produce the movement of the bellows, was recently replaced by an open-loop stepping motor which guarantees a higher speed stability and makes it possible to easily execute repeated calibration cycles with the same flow rate value. Flows of up to 320 cm^3/s (40 g/s of boiling liquid helium) can be achieved with an allowed maximum pressure drop of 50 mbar.

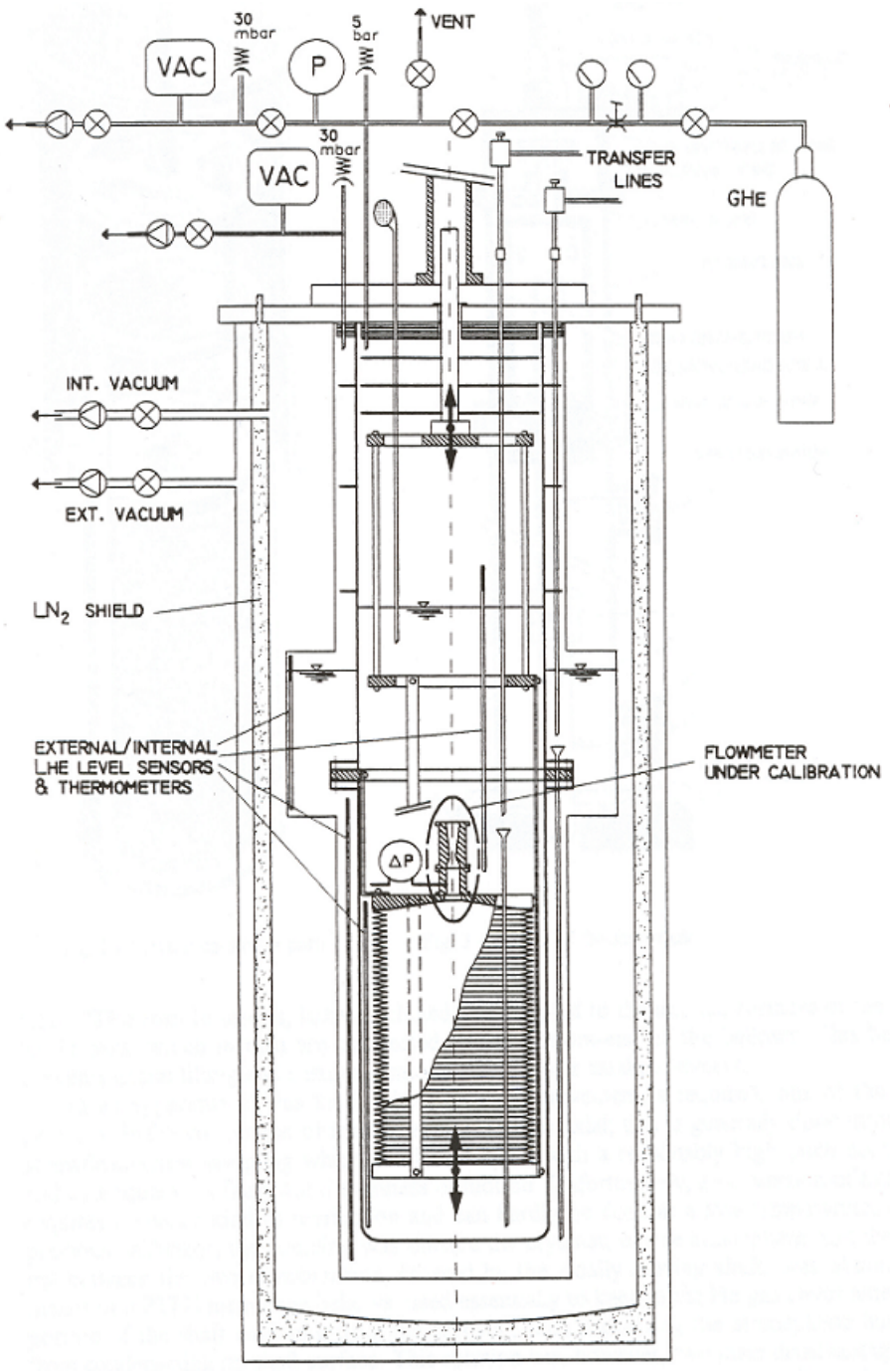

Figure 42: Scheme of IMGC calibration test rig

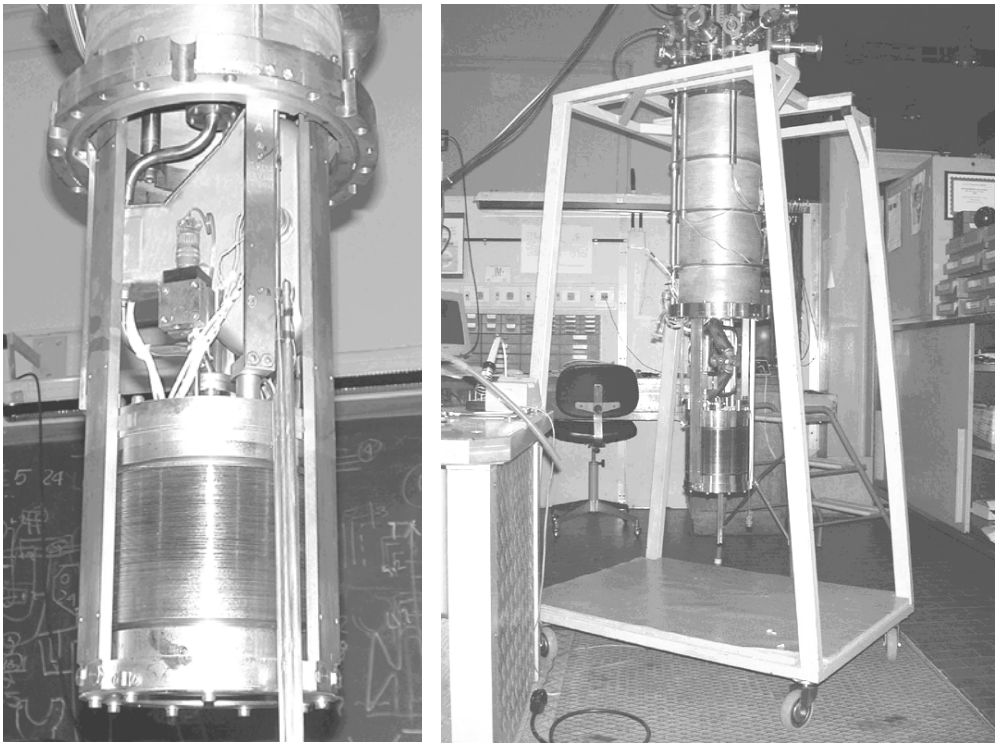

Figure 43: IMGC flowmeter test station with a Coriolis flowmeter installed

7.2.2 Traceability and uncertainty analysis

The uncertainty of the IMGC calibration process is traced to national standards through a chain of successive measurements. The calibration of every temperature and pressure measurement equipment is verified with traceable standards available at IMGC.

The uncertainty of the test station is due to uncertainty contributions of the bellow volume, the time, the linearity of the bellow movement, the pressure and temperature measurements (to infer the density) and the calibration method. The total uncertainty is calculated as the root of the sum of the squares of each of the individual contributions to the uncertainty.

The calibration method is based on steady state flow.

The claimed overall uncertainty of the IMGC test station is (Rivetti et al, 1994, (a)):

$$U_{IMGC\_test\_station} = 0.5\%$$

7.3 Full-scale model of the LHC accelerator

The design and construction of accelerator systems unprecedented in size and complexity requires careful selection and testing of components. Furthermore, operational and full-scale models, where all components can be operated altogether, become even more necessary tools to verify and improve the overall performances and limitations.

For this purpose a first version of the LHC Test String, representing a half-cell of the machine lattice, was assembled, operated and extensively tested by the author for more than 4 years (Casas-Cubillos et al, 1998). Various cryogenic components, such as the cryogenic helium flowmeters, as well as the overall cryogenic distribution scheme were not only validated but also improved and/or simplified to increase the reliability of the system and decrease investment and operational costs (Chorowski et al, 1997).

Following the first half-cell operational model a new full-cell operational model (figure 44) was designed and assembled to become operational during 2001 (Bordry et al, 1998). It incorporates all modifications following the testing of its predecessor and it represents a full-scale model of the tunnel cryogenic system for the LHC as well as other accelerator systems. It has been used to finally check all systems altogether and in particular to verify and improve the process and operation of the cryogenic system as well as to train the operation crew in view of the full sector tests in 2006 and subsequent full machine operation later in 2008.

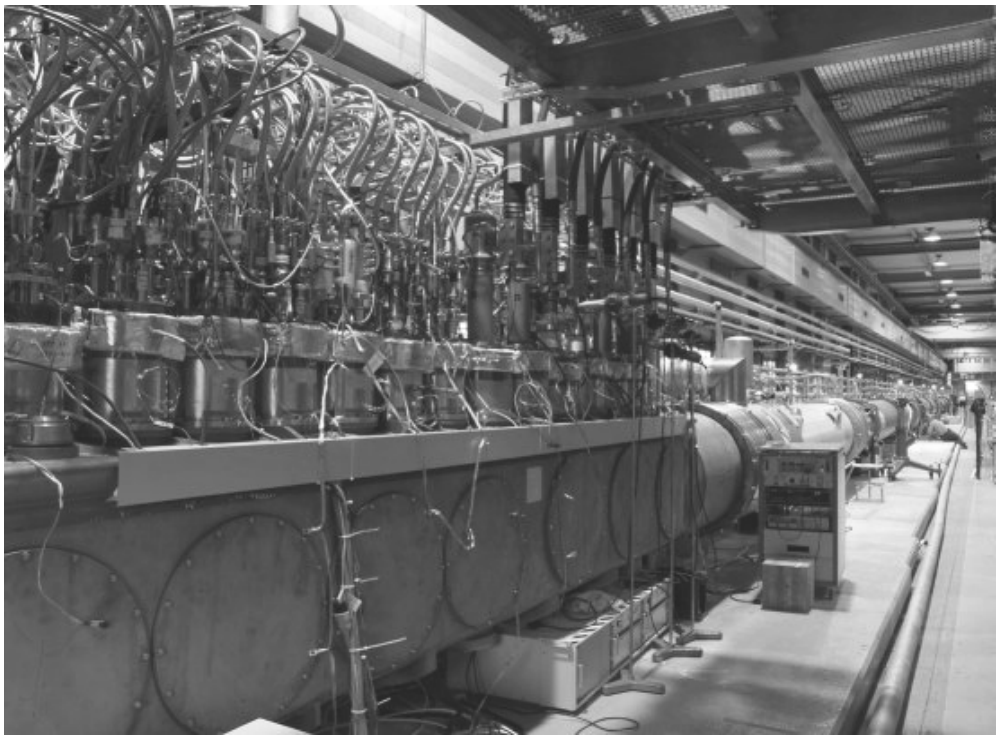

Figure 44: The LHC Test String

The cryogenic system of the Test String shown in figure 45 (Serio et al, 2002, (c)), is composed of: the superconducting magnets string with the superfluid helium bayonet heat exchanger, the cryogenic distribution line (QRL) and the electrical feed box (DFB) to allow powering. Other components such as the feed and return boxes, the quench buffer vessel (QBV), the refrigerator and ancillary systems are peculiar to the Test String although components with similar functions will be installed in each sector of the LHC machine. An existing 6 kW refrigerator provides the cooling power needed for the Test String components. It is boosted with a liquid nitrogen precooler unit to reduce the cool-down time and ensure sufficient liquefaction capacity. The helium supply and recovery are performed via three vacuum insulated and thermally shielded transfer lines, extending over a length of about 35 m between the Test String, the refrigerator and the low pressure pumping group.

The cryogenic feed box (CFB) is an interconnection module between the transfer lines coming from the refrigerator and the QRL. It includes a jumper connection to provide and recover helium at 4.5 K and 20 K from the DFB. It consists of instrumentation and valves to distribute cooling power to the various circuits and retrieve gaseous helium back to the refrigerator and the low pressure pumping group. The CFB houses safety relief devices for all circuits of the QRL and the transfer lines. It is connected to the servicing manifold for conditioning of circuits prior to cool-down.

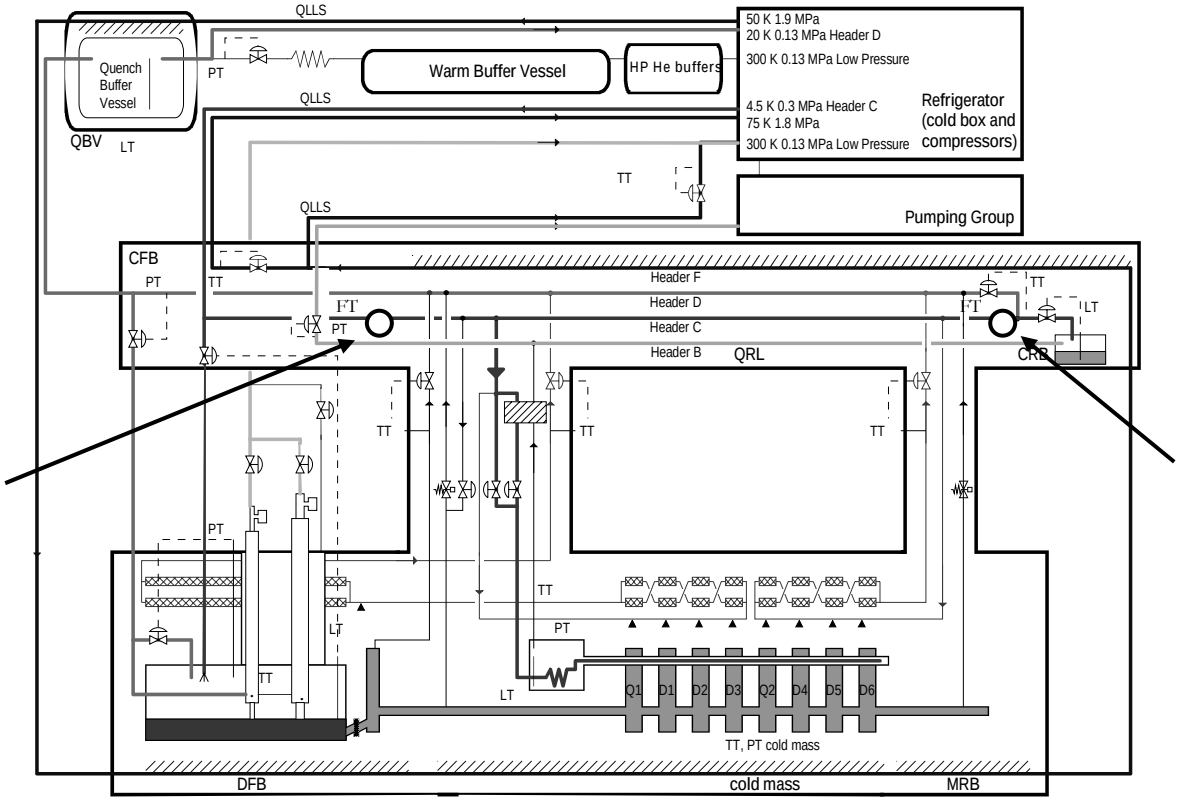

Figure 45: Simplified flow-scheme of the LHC Test String with indicated location of the flowmeters

The cryogenic distribution line is the first test cell extensively tested at CERN. As for its final configuration in the LHC machine it contains all cryogenic headers to distribute cooling power along the Test String. It consists of two service modules

and, in between, straight pipe elements of transportable length with inner and outer bellows systems.

The first service module feeds the superfluid helium loop (via a very low pressure heat exchanger and two J-T valves), the beam screen cooling loop, the DFB shuffling module and the magnet cold mass. The second service module feeds the second half-cell beam screen cooling loop and recovers helium from the cold mass during cool-down. Two prototype quench relief valves, one at each end of the magnet string in their respective service modules, protect the cold mass from overpressure by opening (as pressure actuated safety relief devices) at a set pressure of 1.8 MPa.

The electrical distribution feed box houses the HTS current leads to power the Test String magnets. The DFB mechanically supports the current leads, distributes the power via the bus-bars and provides the necessary cooling (4.5 K liquid helium and 20 K gaseous helium flow) to maintain the current leads in the superconducting state. It is connected to the magnet string via a lambda plate followed by a shuffling box where the bus-bars are re-positioned to feed the magnets. Liquid helium vaporized in the DFB helium vessel is collected, via a pressure control valve, into the 20 K supply for cooling the resistive part of the leads. This cooling flow exits the current leads at ambient temperature and is controlled by warm valves to maintain the HTS of each lead at its operating conditions (i.e. between 4.5 K liquid helium and 50 K). Six 13 kA leads supply the three main magnets circuits and twenty-eight 600 A leads feed twelve circuits for magnet correctors and auxiliary bus bars.

The superconducting magnets operate in a bath of pressurized superfluid helium at 1.9 K and 0.1 MPa. A total inventory of 2200 litres of superfluid helium is contained in the cold mass. It is employed both as a conductive medium for heat

extraction via a bayonet heat exchanger and as a thermal buffer during transient phases.

The bayonet heat exchanger is a 54-mm inner diameter, 2 mm thick wall, cylindrical tube made of cold-worked OFHC copper and running inside the cold mass. It is fed via an inner tube that deposits saturated superfluid helium at the far extremity of the magnet string. The flowing superfluid helium is evaporated along the heat exchanger length. Because of the high thermal conductivity of the pressurized bath, the wetting length of the heat exchanger depends on the heat loads and the cold mass temperature set point. The temperature of the saturated helium is maintained below the magnet temperature by continuous pumping via the very low pressure heat exchanger. Two supercritical helium loops (5 K and 0.3 MPa) provide cooling for the cold support post and the beam screens.

There are two different control systems for the Test String: an existing ABB control system for the refrigerator and the feed and return boxes, and two Programmable Logic Controllers (PLC) for the magnet string and the jumper modules of the QRL. The two control systems are independent but essential information is exchanged to synchronize and safely operate the overall cryogenic system. The magnet string process automation (Bager et al, 2001) is driven by PLCs connected to the field via four Profibus© DP and three Profibus© PA segments. The process management runs in the PLCs, controlling 126 closed control loops, 110 interlocks and 50 alarms. The operator interface is based on industrial software running on PC's and developed in collaboration with an external institute, while the programming of the PLCs has been performed at CERN. About 700 cryogenic sensors and actuators are monitored and controlled via the field buses and the PLC.

The instrumentation includes resistive temperature sensors (Platinum, CERNOX™, Carbon), warm and cryogenic pressure sensors, superconducting

liquid helium level gauges, warm (Hastings™ thermal mass)and cryogenic flowmeters (Coriolis), heaters and warm and cryogenic valves. Two Coriolis flowmeters have been installed in the Feed and Return Boxes of the Cryogenic Distribution Line that supply and recover helium at various temperatures for magnet string cooling. The meters underwent a test program to verify the long-term reliability in real-life conditions, ease of operation, zero stability, relative accuracy (all meters are in series), robustness and thermal cycling.

The instrumentation and control system, while being increased in number and complexity for diagnostic reasons, is representative of a LHC machine sector because of its relatively large size.

At the end of the Test String assembly, commissioning started with instrumentation and electrical tests, leak testing of all process lines (with the magnets interconnects open), evacuation of the vacuum envelope. It was then followed by leak testing of the external vacuum envelope and the process lines in vacuum. After circuit conditioning, leak and pressure testing, the final closure followed by pumping the insulation vacuum. When the pressure was below 10^{-2} mbar the cool-down from 300 K to 4.5 K was performed with a flow of about 80 g/s and a maximum differential temperature between the inlet and outlet of the string of 150 K (figure 46), which is representative for an accelerated cool-down of the LHC machine. During the cool-down phase all circuits and control loops were progressively commissioned, tuned and then put into operation. At 4.5 K the magnet cold mass was filled with 2200 l of liquid helium and the final part of the cool-down to 1.9 K started by pumping on the bayonet heat exchanger. Once at nominal operating conditions, i.e. 1.9 K on the magnet string and 4.5 K with liquid helium reaching the bottom of the HTS leads in the DFB, additional systems and instrumentation checks took place, followed by fine tuning of all control loops to be ready for magnet powering (figure 47).

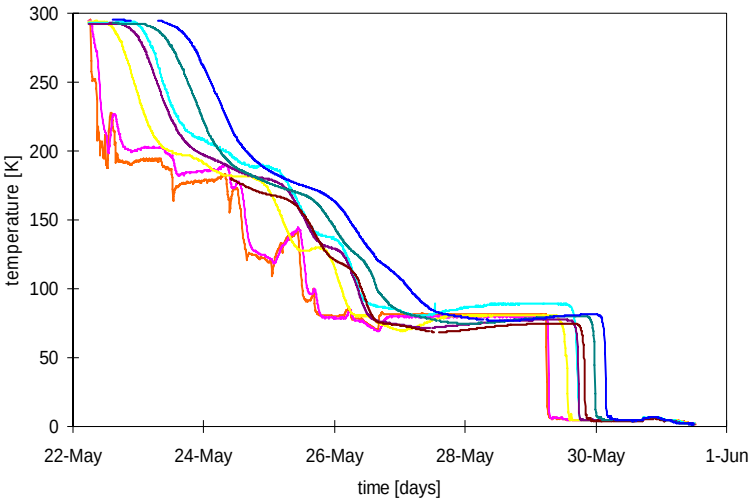

Figure 46: Cool-down from 300 K to 1.9 K: each curve represents a superconducting magnet

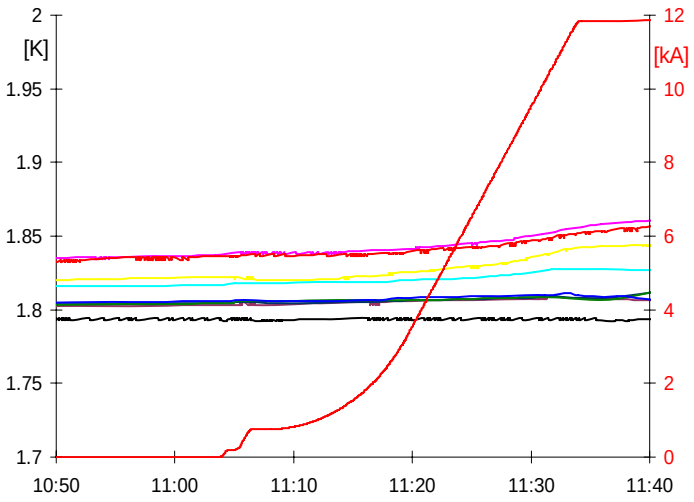

Figure 47: Magnets temperature during powering at nominal current (i.e. 11860 A)

The experimental program was defined to verify the collective behaviour of the LHC systems and components, as well as to optimise future operational performance. The main experiments for the cryogenic system were: final validation of supercritical and superfluid helium loops, evaluation of the process

control and the instrumentation under machine-like conditions, investigation of advance control techniques, optimisation of quench recovery procedures, quench propagation, quench relief valves evaluation, long term behaviour of components under electrical and thermal cycling.

String 2 has accumulated more than 8000 hours of operation at 1.9 K, comprising a 24-hour run at nominal current, more than 50 provoked and recovered quenches and an overall availability of nominal cryogenic conditions of 98 %.

The superfluid helium loop parameters and characteristics have been validated for the first time in the full test cell final configuration and a limitation of a simple PID controller to control a highly non-linear superfluid helium control loop was observed. The magnet quench tests on a full cell of the machine lattice have shown the propagation of a magnet quench to neighbouring magnets of the same half cell and, depending on the quench relief valve opened, to the adjacent cell. Continuous measurements of main component heat loads via prototype cryogenic flowmeters, in steady-state as well as in transient conditions, have confirmed the order of magnitude of global heat inleaks in the cryogenic system (0.2 W/m at 1.9 K) but have not been conclusive because of the amount of non-standard components and instrumentation peculiar to String 2.

7.4 Radiation test area

The tolerance of components and instrumentation to the LHC radiation levels of the order of several hundred Gy is tested in a dedicated test facility at CERN (Rausch and Tavlet, 1999).

At radiation doses above a few Gy per year, as for the LHC case, the possibility of installing commercial off-the shelf (COTS) electronic equipment is questionable as radiation damage can occur despite the low level of radiation. To

this purpose, industrial electronic equipment and circuits, as well as materials, have to be qualified and tested against radiation to ensure their long term stability and reliability.

In order to perform all necessary radiation tests to qualify all electronic equipment to be installed in the LHC machine tunnel, CERN has created a radiation test zone in one of the Super Proton Synchrotron (SPS) experimental areas. The 400 GeV proton beam from SPS hits in this area a metallic target to produce muons for physics experiments. The radiation field around the target is typical of a proton accelerator such as the LHC. Main radiation is gammas and neutrons, plus some high-energy particles. The gamma spectrum extends from a few hundred keV to several hundred MeV. The neutron spectrum is similar but it also includes a large quantity of low-energy neutrons thermalized by concrete shielding. Other particles such as some hadrons and muons of high energy cannot be excluded and can create particular effects in digital electronics. Instantaneous dose rates and accumulated radiation doses are continuously monitored by means of ionization chambers (3 litres of air), passive solid-state dosimeters (polymer-alanine, radio-photo-luminescent glasses and MOS dosimeters) and active semi-conductor dosimeters respectively (Tavlet and Leon Florian, 1994). The measurement of neutron flux employs the activation technique and silicon PIN diodes. The radiation field, despite not being homogeneous either in intensity or in nature, provides irradiation conditions similar to those that will exist in the tunnel of the future LHC. The weekly absorbed doses vary between 10 to more than 50 Gy, while the neutron fluencies (1 MeV equivalent) vary from 10^{11} to 2 x 10^{12} $n.cm^{-2}$.

Chapter 8

8. EXPERIMENTAL RESULTS

8.1 Testing procedure

All flowmeters described in chapter 6 were extensively tested, in the test facilities presented in chapter 7, for performance and reliability as well as for confirmation of theoretical physical parameters (heat exchange, Young's modulus, etc.) used during the design phase.

The overall test program consisted of the following steps:

1. Warm acceptance tests: visual inspection, pressure and leak tightness tests

2. Cryogenic acceptance tests: mounting on CERN test facility for test/calibration in SHe conditions (flow rate, pressure drop, zeroing)

3. Mechanical and thermal stress analysis during cooldown and temperature cycling

Only the prototype flowmeters that passed all the above tests with better than 10 % F.S. accuracy in the flow rate measurement, were considered as candidates for the following tests and for installation in the prototype LHC Test String for long term assessment.

Further and more accurate testing involved calibration at the IMGC Turin test facility at liquid, superfluid and supercritical helium conditions.

Successful prototypes were then installed in the CERN prototype LHC Test String facility for machine like operation and reliability tests. These tests consisted in thermal cycling, long term continuous operation, operation and zeroing, relative accuracy with respect to other methods of heat loads measurements (e.g. global system internal energy increase with time without cooling via temperature measurements, liquid helium boil-off measuring the loss of level without cooling), repeatability and zero drift monitoring. Finally, the devices were employed as diagnostic tools for machine experiments.

The compatibility of these flowmeters with the expected radiation field of the future LHC machine was investigated using other prototypes of the exact same design working at ambient temperature in CERN radiation test facilities.

8.2 The thermal probe flowmeter

The thermal probe or rate of heat loss flowmeter is based on a heated temperature sensor of CERNOX™ type or on a Rh-Fe wire grid, as described in chapter 6.

Using the predicted heat transferred from the sensor at different flow rates, the resistance of the sensor around the working temperature and the requirements of maximum heat loads and accuracy it is possible to select, for the range of flow variations that are required to be measured, a power input that can be measured using industrially available ammeter and voltmeter. Two main modes of operation can been employed: constant power injected in the sensor with measurement of the temperature variations with flow and control of the power injected to obtain a constant temperature at various flow rates. The latter was chosen in order to improve the response time that would have been slow due to the thermal inertia of the sensor.

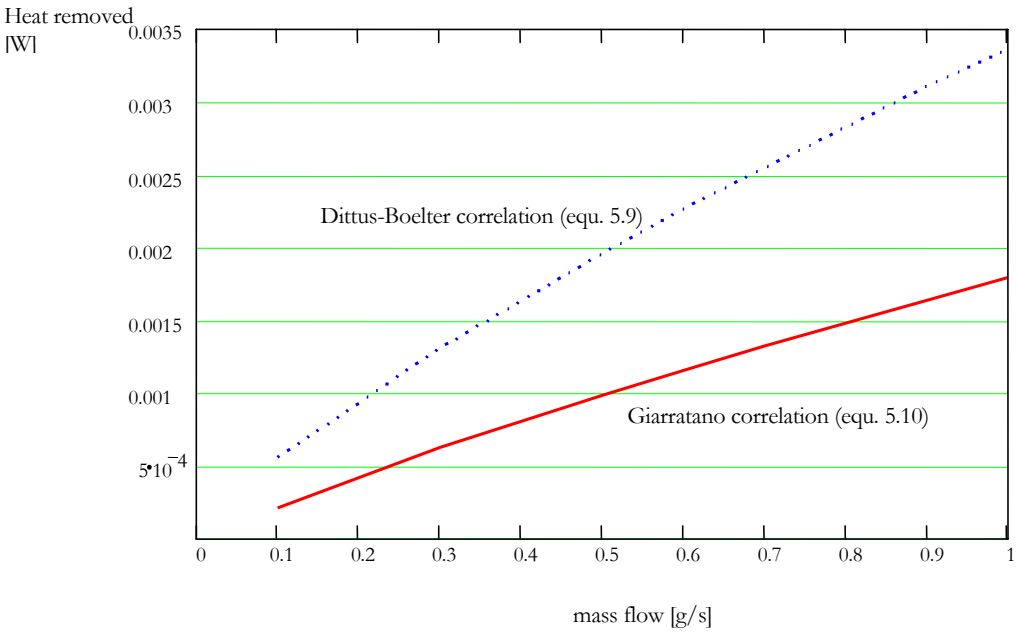

Figure 48: Prediction of heat removed from the CERNOX™ sensor type flowmeter at 15 K with a 5 K supercritical helium flow

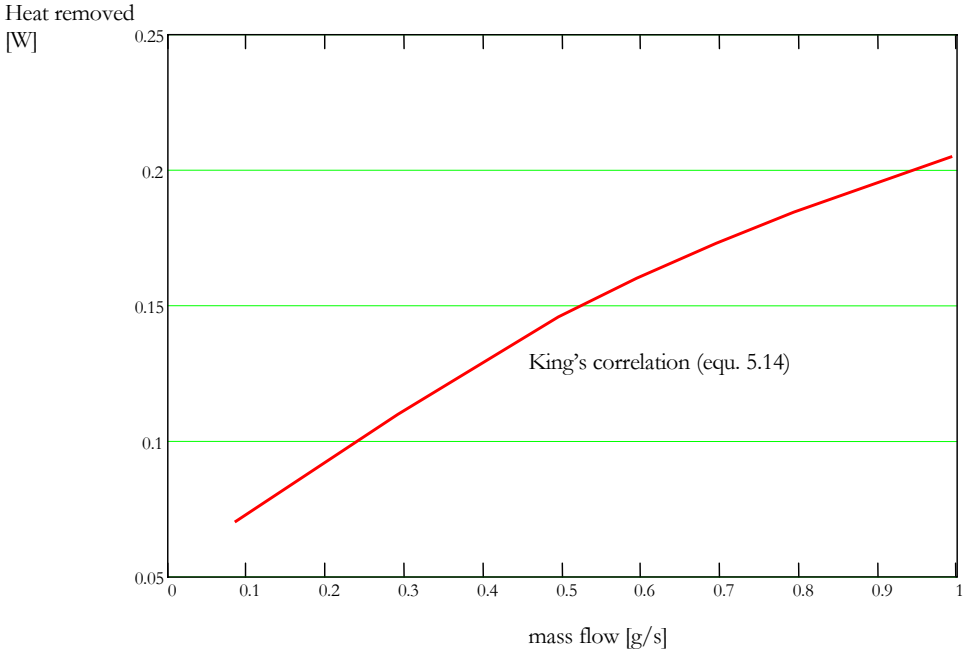

Figure 49: Prediction of heat removed from the Rh-Fe wire grid flowmeter at 15 K temperature in a 5 K supercritical helium flow

Figure 48 shows the prediction of heat transferred from a CERNOX™ sensor at 15 K; the continuous line represents the results obtained using the Giarratano correlation (5.10) and the dotted line using the Dittus-Boelter correlation (5.9). The difference between the two correlations is mainly due to the fact that 5.9 overestimates the heat transfer not taking into account the temperature variation of the fluid properties and in particular the film temperature between fluid and surface. This effect increases with the increase of the temperature difference between sensor and fluid. Figure 49 shows the prediction of heat transferred from 10 cm of Rh-Fe wire at 15 K at various flow rates using King's equation (5.14). To improve the measurement accuracy especially in presence of fluid temperature fluctuations, a second unheated sensor can be used. In the test station and the LHC machine additional temperature sensor would be available to verify the fluid temperature fluctuations. The risk of fouling and erosion can be neglected because of the high purity and inert gas properties of helium.

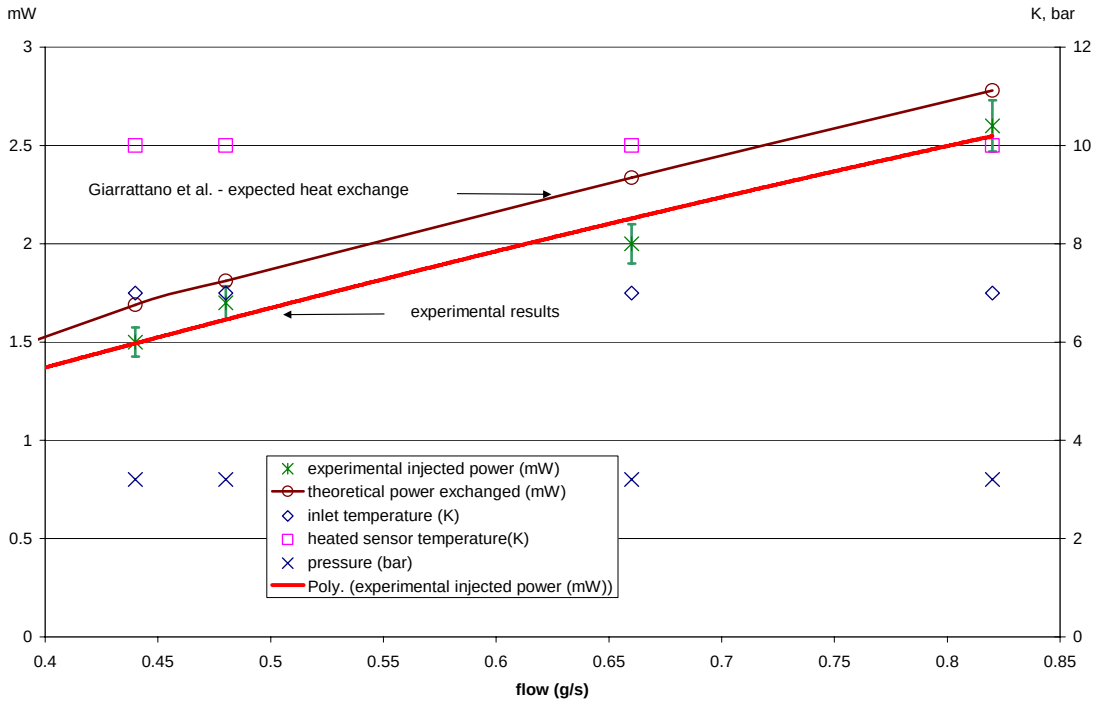

Figure 50: Comparison of the CERNOX™ sensor experimental and predicted rate of heat loss

Several runs have been performed using three different types of sensor (AllenBradley carbon resistance thermometers, CERNOX™ calibrated temperature sensors and Rh-Fe wire grid).

The data collected have been compared with the theoretical heat transfer law (Giarratano and Dittus-Boelter correlation for AllenBradley and CERNOX™ sensors and King's equation for the Rh-Fe grid).

The results, shown in figure 50, are obtained with the AllenBradley sensor heated with up to 3 mW and maintained at a constant temperature of 10 K. The measured difference when comparing the results with the theoretical law of heat transfer is within 15 % in the 0 to 1 g/s range, while the standard deviation of Giarratano's correlation is 8.3 % and the measurement errors (reference flowmeter, current, voltage, pressure and temperature) have been estimated to be +/- 5 % (normalised to a power reading error).
The Rh-Fe wire grid has shown larger errors (up to 25 %) when compared with King's equation. These errors are probably larger because of lower measurement accuracy of the low resistance values of the Rh-Fe wire at low temperatures, the neglect of end effects in the equation and the temperature instabilities of supercritical helium.

The precision of these types of flowmeters was further improved by determining the empirical correlation for our devices and therefore identifying the best fit of our data in the form of correlation 5.10 with a scaling factor of 0.023 taking into account the dependence of the fluid properties evaluated at the film temperature. Other tested prototypes showed the validity of correlation 5.10 with the scaling factor of 0.023. With the heat transfer law coefficients for this geometry and for these fluid properties found experimentally, the remaining error is due to the precision of the instrumentation (reference flowmeter, current, voltage, pressure and temperature, i.e. +/- 5 % as from sensors technical specifications) depending

mainly on the precision of the temperature measurements and on the number of experimental points taken during calibration or the overall standard deviation of the heat transfer correlation used. Therefore accuracies better than 10 % can be achieved with individual calibration.

The experimental results obtained previously between 0.4 and 0.9 g/s showed a deviation of about 15 % in the heat exchange coefficient from the empirical correlations. In order to verify the results a series of additional tests at the same operating conditions (i.e. supercritical helium at 5 K and 3 bar, with the sensor at about 10 K) have been performed up to 2 g/s.

The results obtained (h exp II – filled triangles) together with the data previously collected (h exp I - empty triangles) are plotted in figure 51 against the flow rate and compared with the empirical correlation value (h th pref = 0.0259 – squares) and the best fit that can be obtained by modifying the correlation scaling factor (h th pref = 0.023 – circles) of equation 5.10. The departure of the experimental data from the theoretical correlation at high flow rates is due to neglecting the end effects (i.e. heat exchange with the surrounding wall via heat conduction through the sensor supports as well as radiative heat transfer) which can be taken into account in the empirical correlations.

The thermal probe flowmeters do not fulfill the requirements set in 6.1 unless individual calibration at working conditions is performed on all the manufactured flowmeters. Nevertheless it is a small-size and low-cost instrument suitable as coarse diagnostic or to verify other instruments. Section 8.2.1 describes some improvements necessary for industrial and long-term operation.

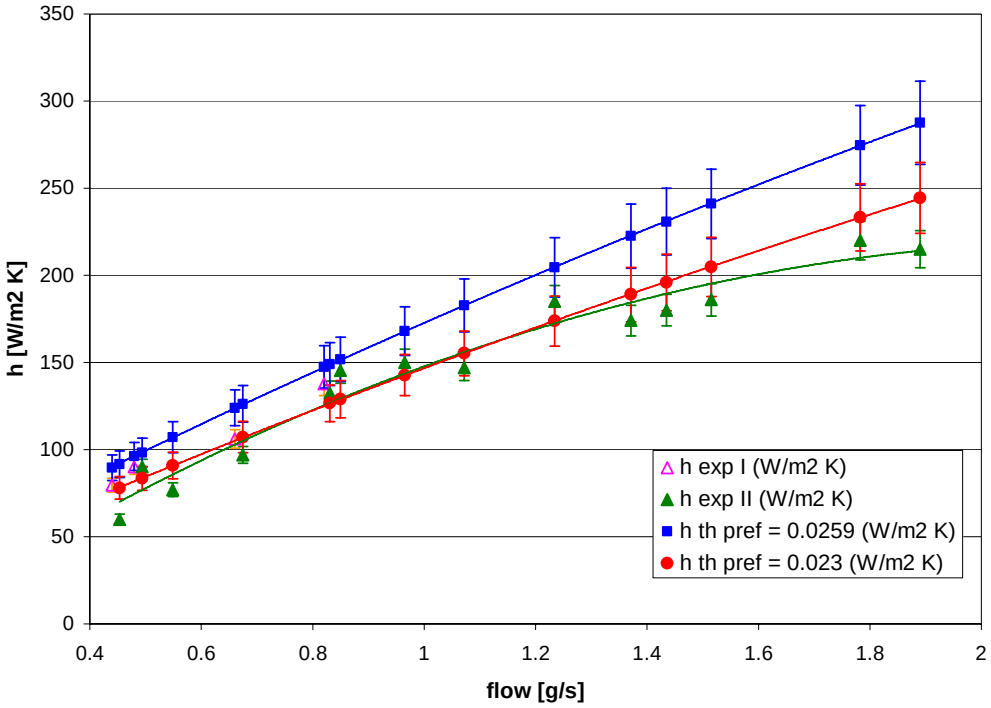

Figure 51: Theoretical and experimental comparison of the heat exchange coefficient for the CERNOX™ sensor

8.2.1 Thermal probe flowmeter improvements

After the successful testing of the thermal probe type heat transfer flowmeter based on heated temperature sensor (AllenBradley or CERNOX™ sensor) a few modifications have been introduced in order to improve the reliability and in particular the leak tightness of the device. As shown in figure 52, the temperature probe is now encapsulated in an "insertion finger" which, together with the wiring, is separated from the fluid. Thermal contact of the sensor with the fluid is improved by using a thermally conductive but electrically insulated medium (epoxy with 45 % Alumina and Borum Nitride from Epotecny). The wiring is thermalized on the tube and inside the "insertion finger" before connecting it to the sensor to minimise external temperature influences.

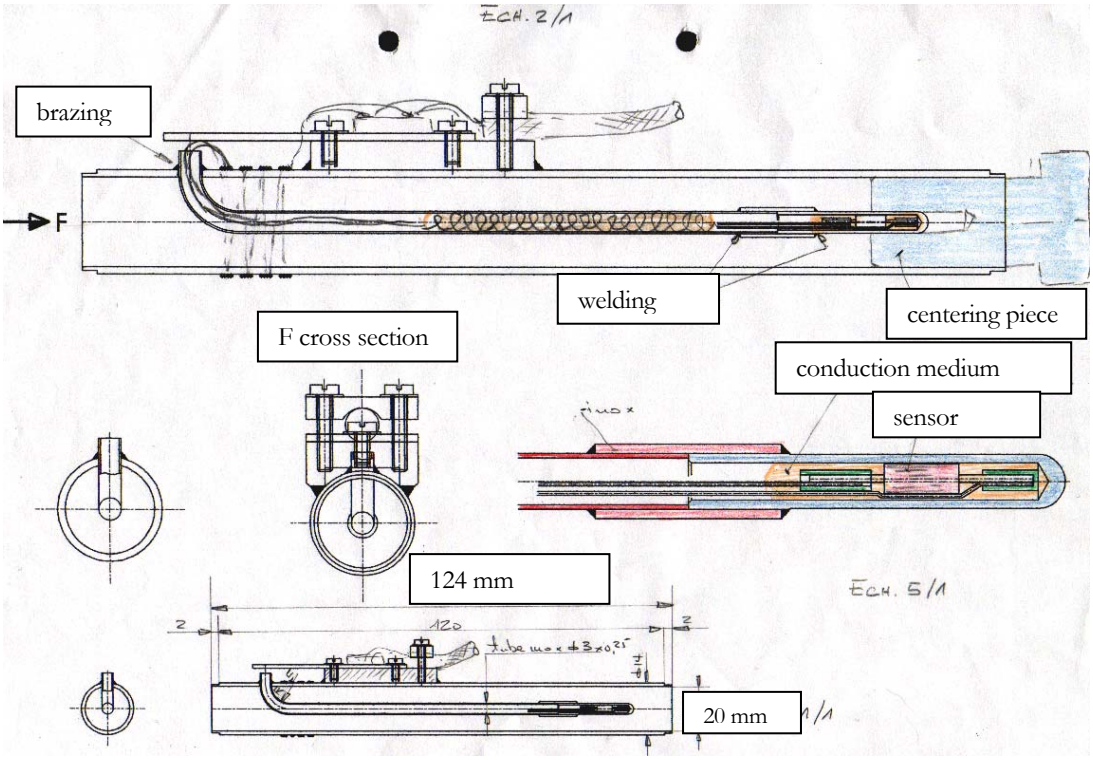

Figure 52: Proposed detailed design drawing of a rate of heat loss flowmeter

8.3 The thermal pulse flowmeter

The flowmeter is comparable to a hot wire anemometer but with a pulsed power injection and a measurement of the speed of cooling. This type of flowmeter requires a more complex electronic system for the control of the powering cycles and the acquisition and analysis of the data to compute the flow. Temperature and pressure oscillations of supercritical helium flow have highlighted that this different mode of operation is impractical and not accurate as it requires continuous adjustment of the injected power and the injection / measurement periods lengths. Testing has shown no real advantage in terms of improved

performance of this technique with respect to the thermal probe and this type of flowmeter has therefore been quickly dismissed.

8.4 Time-of-flight flowmeter

Tests on the prototype time-of-flight flowmeter have revealed a difficulty in operating the superconducting sensors. Table 13 shows the results obtained and the comparison with the expected transit time between heater and first sensor calculated using the fluid density value at operating temperatures. The delay necessary to heat the fluid and the sensor has been experimentally measured in varying conditions) and subtracted from the measured time delay.

Mass Flow	Temperature	Pressure	Experimental	Expected	error	error
[g/s]	[K]	[Mpa]	[s]	[s]	[s]	[%]
1.1	5.9	0.305	0.288	0.284	0.004	1.17
1.5	5.8	0.305	0.242	0.234	0.008	2.98
1.4	5.7	0.296	0.286	0.271	0.015	5.17
1.13	5.83	0.297	0.328	0.286	0.042	12.6
1.23	6	0.247	0.164	0.162	0.002	0.89
1.06	5.65	0.3	0.407	0.407	-0.0009	-0.23

Table 13: Calculated and measured transit time between heater and first sensor

Once the first superconductor has quenched (detecting the heat pulse) and become resistive, further heat is added to the helium. Furthermore, the transient heat transfer is within the thin helium layer called the effective layer. Because of radial transport - governed by the turbulence of the fluid - from the outer layer to the core of the flow, the bulk helium temperature therefore increases after a few diameter lengths and the fluid velocity increases to fulfill the conservation of mass criteria. Therefore the first transit time is defined by the velocity of the fluid at 5 K and the second transit time (sensor 1 – sensor 2) is defined by the velocity

of helium at a higher temperature (lower density), and is subsequently much shorter at the same mass flow rate (figure 53). Put another way, the addition of a heat pulse sufficient to quench the Nb-Ti superconductors induces acceleration in the fluid that can cause the dominant local velocity under transient conditions.

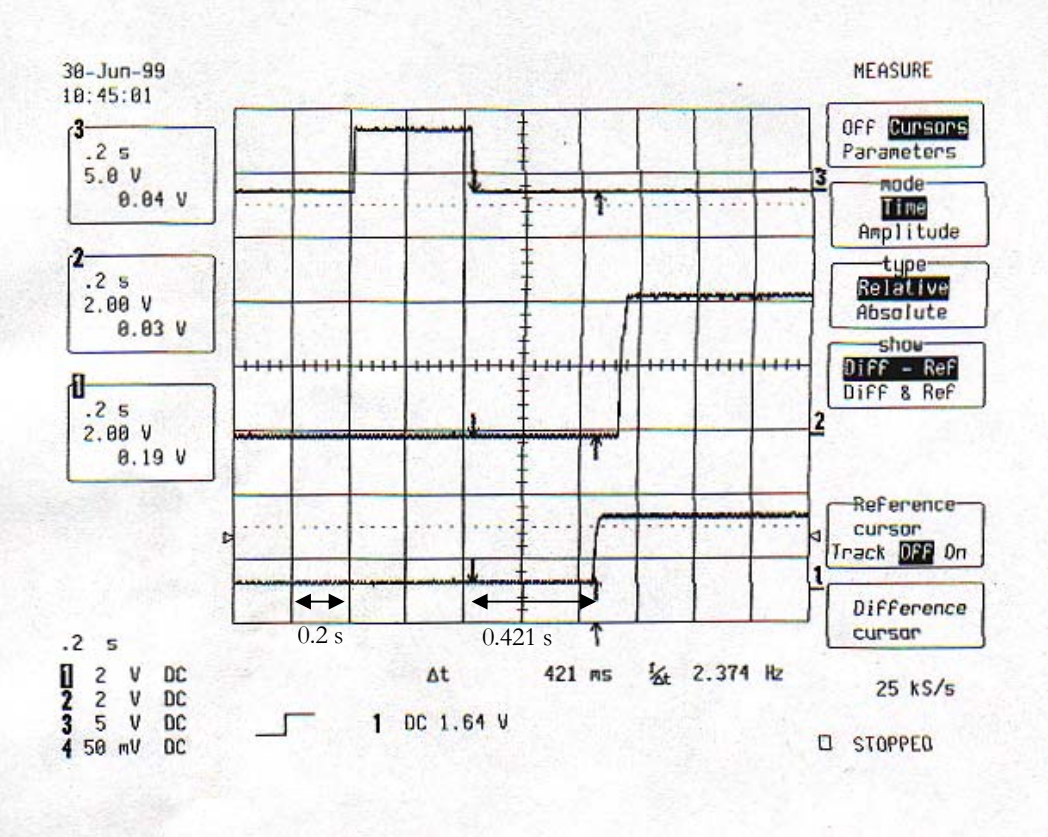

Figure 53: Typical response of the time-of-flight flowmeter at 1 g/s (signal 1 is the first sensor, signal 2 is the second sensor and signal 3 is the heater

Experimental values have confirmed that the velocity measured between sensor 1 and sensor 2 is within 20 % of the velocity of supercritical helium at 11 K (see table 14). The temperature of 11 K is derived from the amount of heat injected in the flow stream and confirmed by the resistance measurement of the superconducting gauge.

Mass Flow	Temperature	Pressure	Experimental	Expected	error	error
[g/s]	[K]	[Mpa]	[s]	[s]	[s]	[%]
0.9	11	0.27	0.043	0.052	0.009	17
1.6	11	0.29	0.035	0.033	0.002	6
2.8	11	0.23	0.016	0.015	0.001	7

Table 14: Calculated and measured transit time between first and second sensor

In order to have a reliable, industrial and easy-to-use flowmeter the detection of the heat pulse should be performed using an accurate cryogenic thermometer with which it would only be necessary to increase the helium temperature by a few tens of mK, thus not modifying the fluid properties. Unfortunately the other requirement of having a fast response can not be achieved with our standard cryogenic instrumentation. Therefore it would be preferable to investigate the use of a superconducting sensor with a critical temperature nearer to the fluid temperature making this type of flowmeter presently not suitable for our application.

8.5 Venturi flowmeter

A Venturi flowmeter was assembled, calibrated and tested at IMGC at cryogenic temperatures (Rivetti et al, 1994, (b)). The flowmeter, once calibrated (i.e. the discharge coefficient value found experimentally), performed well with accuracies of the order of few % and similar repeatability. The main errors seemed to be due to non-negligible zero drift, mechanical variations of the pressure sensor diaphragm and of the body due to thermal stresses during cooldown, dependence of the electrical resistance of the sensing coils on temperature and the presence of cavitation. It was confirmed that this type of flowmeter requires calibration at working conditions to obtain accuracies better than 10 %.

A similar meter designed, assembled and calibrated at IMGC was directly installed in the LHC Test String and extensively tested in real machine conditions. When compared with the other flowmeters in series the Venturi calibrated at cryogenic operating temperatures showed a larger spread of results giving rise to an overall accuracy of approximately 2 %. By repeating the tests and the thermal cycling it was found that the main errors were due to the difficulty of performing in-situ zeroing (pressure and temperature oscillations during the zeroing phase) of the Validyne differential pressure sensor and the decreased rangeability due to the choice of a higher than required pressure drop sensor to decrease the risk of mechanical failure of its membrane. An important factor in the errors could be due to the temperature measurements. These were taken several diameter lengths from the flowmeter, and possibly gave inaccurate information on the exact density and therefore mass flow rate.

The readings of the warm and cold pressure sensors were compared and found to agree after correction of the introduced delay and integration due to the length of connecting tubes.

The tests clearly showed that this flowmeter would be difficult to operate in an industrial-like environment. Furthermore, the use of a cold and delicate pressure sensor, in order not to have any delayed signal and integration effect, would make the instruments vulnerable to pressure rises and unexpected thermal shocks.

8.6 Classical turbine

Industrially available turbine flowmeters should in principle work at cryogenic temperatures as long as one takes into account the modification of material properties, uses the appropriate materials and performs a calibration at working conditions.

To verify the possibility of using such a device for our application, a technical specification was prepared and a flowmeter was ordered in industry (Hoffer Flow Controls, model H01/2X1/4-.25-4.5-CB-1M-SW-SP) following extensive discussion on the design to make it compatible with cryogenic fluids.

The turbine flowmeter was calibrated at room temperature with water at the factory premises. It did work after preliminary testing at 5 K, but a completely new K factor needed to be introduced to take into account material and fluid properties at 5 K.

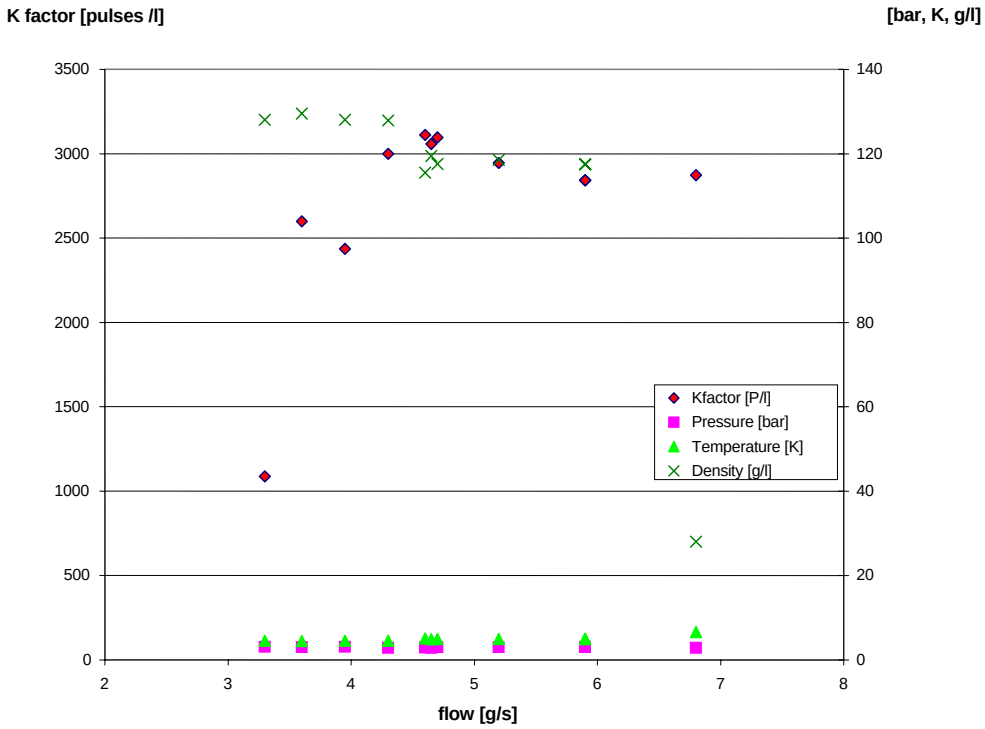

Figure 54: Test results of the classic turbine flowmeter with 5 K helium and modified K factor values

Testing at 5 K between 3 and 8 g/s in the CERN test station against the reference flowmeter, allowed the establishment of the new calibration curve

(figure 54). The curve has the typical characteristic of dependence with the Reynolds number in the 2 to 5 g/s range and shows that the boundary layer flows of interest are around the transitional status between laminar and turbulent flow. This makes the precision of the turbine lower and even more dependent on a calibration at working conditions. The new calibration curve was found to be lower than the original made by the manufacturer at ambient temperature with water. An increase in friction due to differential shrinking of rotor/stator was ruled out because of the use of identical materials for these components. Nevertheless, with time and thermal cycles the turbine flowmeter did show a variation of about 10 % in K factor. The most probable cause was determined to be an increase of mechanical friction.

8.7 Magnetically levitated turbine

The magnetically levitated turbine (IGCM, unique model) was calibrated and extensively tested in liquid and supercritical helium at around 4.2 K in the IMGC calibration test facility before being shipped to CERN to be tested in the flowmeter test station and the LHC Test String facilities.

Testing at IMGC showed very promising results with measurement uncertainties of 0.8 % and independence of the K factor from the thermodynamic conditions of helium (supercritical or liquid) and repeated thermal cycling. Unfortunately, the tests performed at CERN did not confirm these good performances. In conditions that were not the same as those of the calibration laboratory, the turbine proved to be very difficult to operate and the mechanism to centre the rotor before the superconducting transition proved unreliable. Because of temperature and pressure oscillations the rotor was often passing out of its superconducting state thus requiring restarting of the positioning procedure. When installed in the LHC Test String the turbine did not work at all, due to the unstable conditions of an industrial-like environment.

The use of a magnetically levitated rotor for a turbine flowmeter has demonstrated that the most critical parameter for its accuracy and long-term performance and reliability, namely the mechanical friction in the bearings, can be successfully eliminated. Unfortunately, this instrument remains a laboratory device to be treated with care and requires specialized attention for its correct operation. It can nevertheless be considered as a reliable secondary standard for cryogenic calibration of flowmeters.

8.8 Coriolis mass flowmeter

The Coriolis flowmeters tested were manufactured and prepared for cryogenic operation as described in 6.8.1 and 6.8.2 by Micro Motion Inc., models CMF010 and CMF025, with respectively single 2 mm size internal tube and double 6 mm size internal tube, both made of SS 316 L. The performances (accuracy, reproducibility, pressure drop, zero stability) at nominal working conditions (supercritical helium at 5 K and 0.3 MPa) were first assessed in the CERN test cryostat. The Young's modulus of the flow tubes remains constant (as measured with 0.5 % accuracy in the test facility) below 20 K and the ratio of the value at ambient temperature and at 5 K has been used as a constant temperature compensation coefficient.

Figure 55 shows preliminary measurements performed on the Coriolis flowmeter during variation of the reference flow (as measured at the ambient temperature outlet by the Hastings™ thermal mass flowmeter) between 1.5 and 2.5 g/s. At first, due to the temperature (within few hundred mK) and density (100 mK change at 5.3 K gives 7 % variation in density) oscillations of supercritical helium around the critical point the Coriolis meter had some difficulty in measuring correctly (right-hand side of figure 55 without any averaging) because of varying fluid density and differently distributed densities in the two measuring tubes. To improve the measurement, averaging over 6 to 12 s was employed (left-hand side

of figure 55) and the meter measurements and stability improved considerably without any previous calibration at cold conditions (not considering offset errors due to the difficulty of zeroing the instrument at cold conditions). The differences between the reference flowmeter and the Coriolis meter were mainly due to offset and zeroing errors as well as oscillations of the drive coil power not yet modified for low temperature operation.

At lower temperatures the decreased resistance of the drive coil was increasing the power injected making the system unstable. Even with averaging over several seconds the measurements were not accurate. An additional resistance was therefore added in series and the oscillations disappeared. Smaller amplitude oscillations would nevertheless appear in some particular conditions because of density variations and mass flow pulsations, but would not affect the averaged measurements. Further tests were performed at IMGC to verify the zero stability and need of an additional resistance to lower the drive power and therefore damp the onset of oscillations (figure 56).

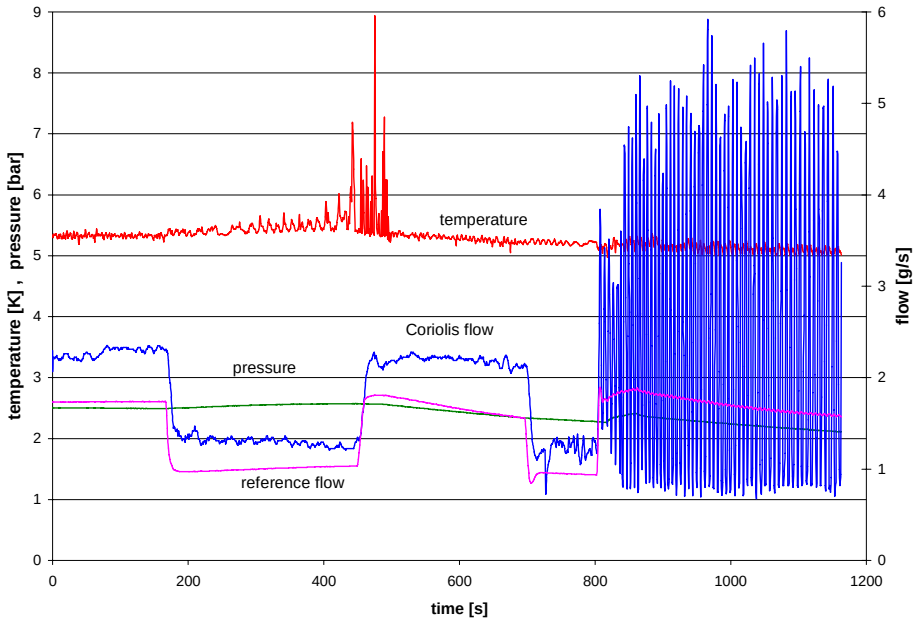

Figure 55: First measurements and oscillation of a Coriolis meter signal

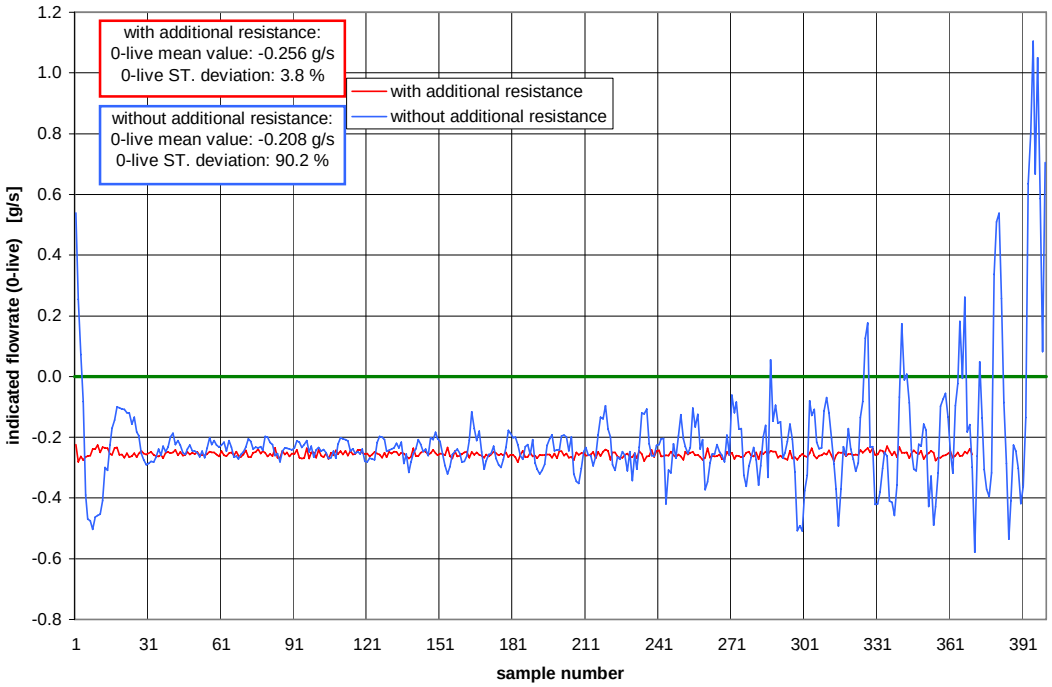

Figure 56: Coriolis meter zero stability tests performed at IMGC with and without additional resistance on the drive coil

To achieve optimal performance great care needed to be taken during the zeroing process to avoid initializing the flowmeter electronics during thermal transients or density variations in the piping.

Figure 57 summarizes most of the tests performed at CERN and IMGC on two different sizes of Coriolis meter. The least squares linear best fits results are also plotted on the graph. The CMF010 flowmeter is manufactured with a 2 mm tube diameter for 60 g/s full scale range. The CMF025 flowmeter is manufactured with two 6 mm tube diameter for a 140 g/s full scale range.

Both flowmeters were oversized in terms of maximum flow rate but this was necessary in order to fulfill the maximum pressure drop requirements. Because of their large rangeability it did not compromise their performances.

Figure 58 shows the independence, within the measuring accuracy and repeatability of the test station, of the higher range flowmeter from the

thermodynamic conditions of the measured flow. The data plotted in figure 58 were corrected with the new calibration value (taking into account the ratio of Young's modulus value at ambient temperature and below 5 K) experimentally determined during the tests at IMGC.

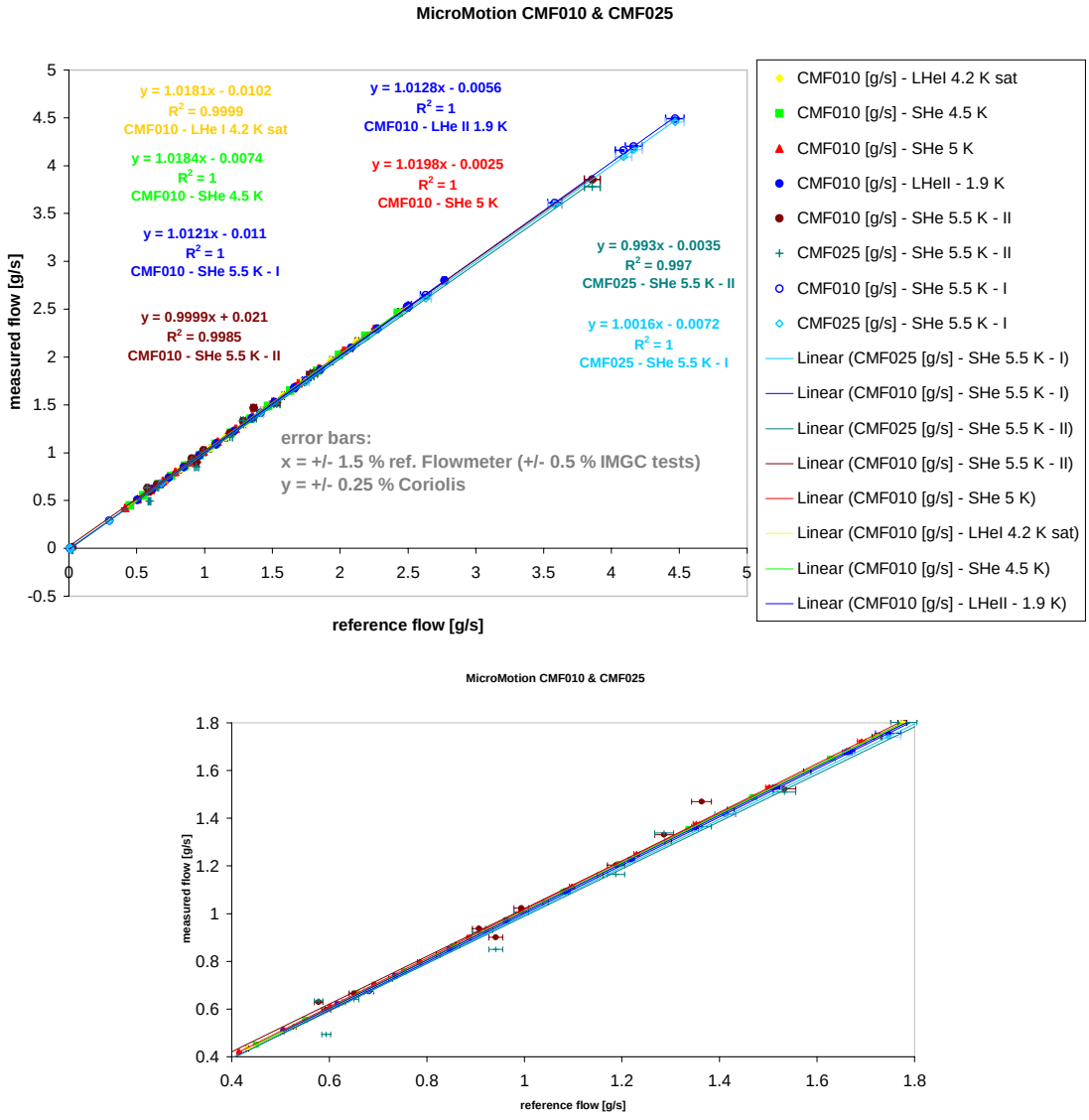

Figure 57: Overall test results from two different sizes Coriolis meter tested at CERN and IMGC at different operating temperatures (calculated least square best fits for each individual data set are also plotted)

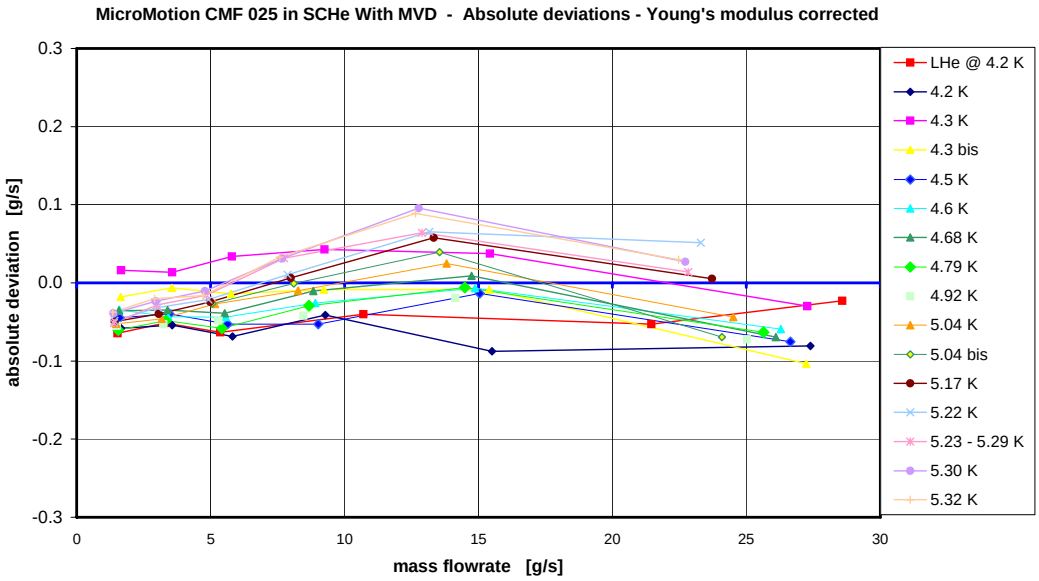

Figure 58: Coriolis meter absolute deviations at different temperatures

Finally figures 59 and 60 summarize the tests performed on the two meters at various temperatures and helium fluid states (liquid, supercritical and superfluid) in the IMGC calibration test facility. The most stable results are obtained with superfluid helium taking advantage of the intrinsic very uniform and stable temperature and flow conditions. Apart from the systematic error of about 1 %, the superfluid helium measurements are within 0.25 % accuracy for most of the CMF010 range, thus confirming the possibility of improving the accuracy of the flowmeter below 1 % with better calibration.

The final accuracy of the meters depends on the zeroing procedure in the lower range and on the accuracy of the measurement of the Young's modulus. The systematic offset of about 1.2 % for both meters seems to be due to systematic errors in the measurements. The IMGC test station is traced to national standards and has been successfully operated for low temperature calibrations with 0.5 % accuracy. The acoustic method measurements performed on stainless steel

samples at low temperatures which are used to obtain the Young's modulus have lower accuracy (1 %) and might not have been as accurate below 20 K because they were performed in a non-isothermal and stable regime (gas) while the measurement in the IMGC test station were mainly performed in pool boiling regime (Ledbetter, 2000). Therefore the calibration of the flowmeter with an accuracy of 0.5 % in the IMGC test station would better if the Young's modulus for SS 316 L at 5 K to be taken to be 205 +/- 1 GPa.

It appears that the absolute accuracy of the Coriolis meters is presently limited by the accuracy of the Young's modulus measurements (1 %) or the IMGC calibration test station (0.5 %). Nevertheless the impressive reproducibility (better than 0.2 %) over a large turn down ratio (1:100) seems to be maintained at low temperatures. Accurate measurements (to within a few %) can also be obtained up to a 1:1000 turn down ratio, allowing precise measurements with a reasonable pressure drop (figures 59 and 60).

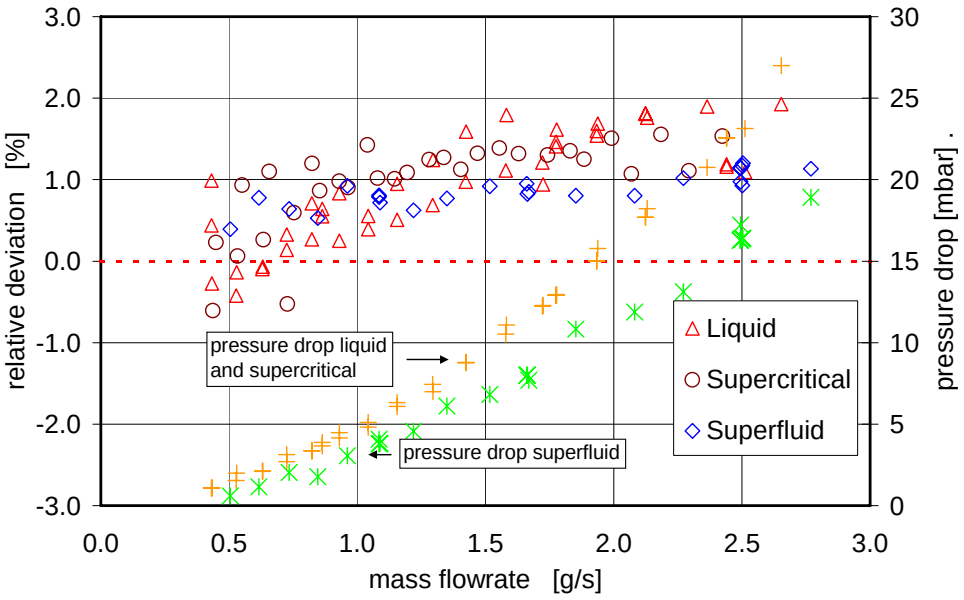

Figure 59: CMF010 (2 mm size, 60 g/s f.s.) Coriolis flowmeter: relative deviation and pressure drop vs. mass flow

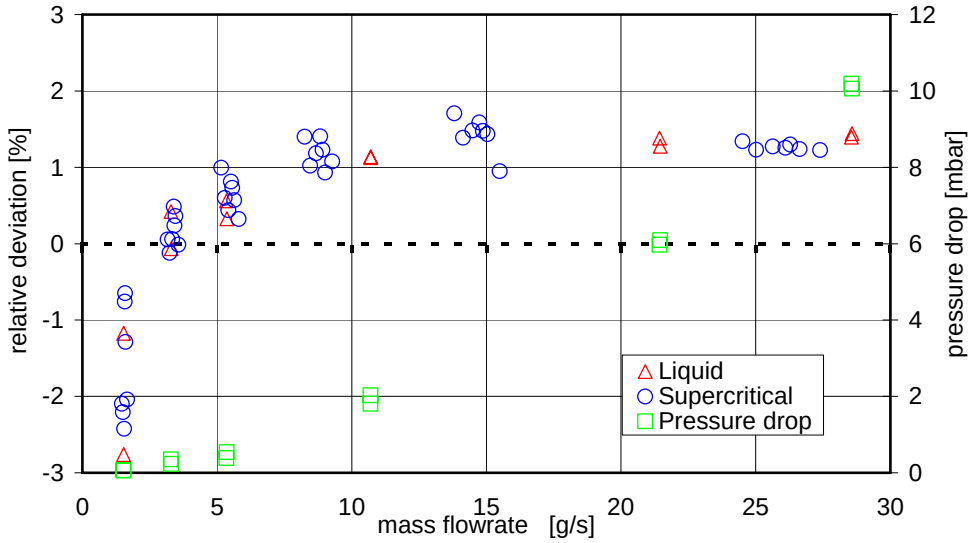

Figure 60: CMF025 (6 mm size, 140 g/s f.s.) Coriolis flowmeter: relative deviation and pressure drop

8.8.1 Traceability and uncertainty analysis

Coriolis flowmeters are calibrated at the manufacturer's premises at ambient temperature before being checked and calibrated at the CERN cryogenic test facilities and at the IMGC calibration stand.

The working mass standards in the MMI (Micro Motion, Inc.) primary stand laboratory are traceable to Japanese and the United States national standards. These working mass standards are used to calibrate and verify the weigh scales of the MMI primary stand. The MMI primary stand is used to calibrate the reference meters. The reference meters are used to calibrate manufactured flowmeters.

The uncertainty analysis can be split into five main parts:

A. Uncertainty of the scales in the MMI primary stand;

B. Uncertainty of the MMI primary stand (best measurement capability of the MMI primary stand);

C. Uncertainty of the reference meters, calibrated on the primary stand;

D. Uncertainty of the manufactured flowmeter at ambient temperature;

E. Uncertainty of the manufactured flowmeter at cryogenic working conditions.

The first four points of this analysis give a measurement capability of the Coriolis meter of 0.25 % of full scale mass flow for worst case conditions (DeBoom et al, 2000).

The fifth point gives an overall uncertainty of 1 %, depending on the Young's modulus absolute accuracy at 5 K.

The total uncertainty of the cryogenic Coriolis flowmeter is calculated as the root of the sum of the squares of each of the individual contributions to the uncertainty and is therefore close to 1 %. A better calibrator or a better measurement of the Young's modulus could lower this absolute accuracy down to 0.25 % while the repeatability of 0.2 % is preserved. These results obtained with different geometries and sizes showing similar calibrations errors are consistent with a shift caused primarily by a change in Young's modulus from the one obtained by Ledbetter, 2000.

8.9 Radiation compatibility tests

Selected flowmeters were subsequently installed in existing accelerator test areas where the integrated level and type of radiation is comparable with the future LHC accelerator. They were metering a constant flow of air at ambient

conditions with a thermal mass flowmeter in a shielded zone providing the reference flow.

One of the prototype Coriolis mass flowmeters was exposed to a radiation dose comparable to the LHC of few Gy/day to investigate failures, zero deviation and flow accuracy.

As the level of radiation is such that does not allow the use of standard electronic components only two choices were possible:

1. Radiation hard components

2. Remote electronics

As the first solution would have been too expensive, the meters were tested with several hundred meters cabling between the sensors and the transmitter to be able to shield all active electronic components in protected areas along the tunnel. In the radiation areas only passive electromagnetic devices therefore had to cope with the specified radiation levels.

Figure 61 shows the results of several months testing with an accumulated dose of more than 1000 Gy. No sign of deterioration or drift was detected.

8.10 Long-term testing and reliability

The LHC Test String described in chapter 7 was used as a final validation test bench for the most promising flowmeters and in particular the Coriolis prototype meter CMF025 which is shown in figure 62 in its final position inside the insulation vacuum of the cryogenic distribution line cryostat just before final closure and cooldown. An additional by-pass valve below it was installed to reduce the pressure drop during the cooldown phase.

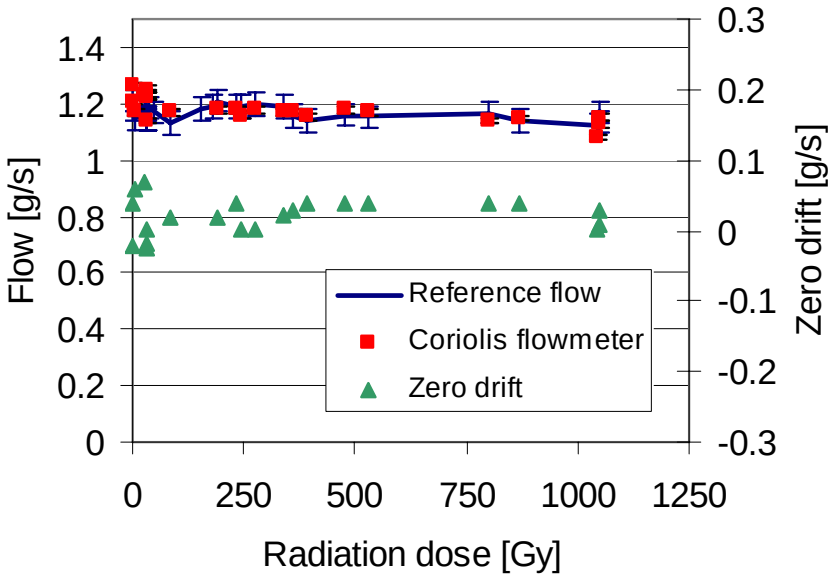

Figure 61: Radiation tolerance tests of a Coriolis meter at CERN test facilities

The long-term overall performances during more than 2-year operation and reliability testing, confirmed the performance of the prototype Coriolis meter and its intrinsic robustness.

Three Coriolis flowmeters have been extensively tested with cryogenic helium down to 1.7 K and show superior performance in terms of absolute accuracy, repeatability and robustness to other meters. The meters were calibrated on water at 20 °C and tested on liquid and supercritical helium, indicating a high degree of insensitivity to fluid properties. Several flowmeters ranging from 0.5 g/s up to 1.2 kg/s are now installed. The modifications described earlier in the chapter and the calibration factors taking into account the new values of Young's modulus have been introduced and the meters are successfully operating in the CERN cryogenic test facilities to assess performance of superconducting devices and liquid helium pumps and to meter cryogenic cooling power distribution.

Figure 62: Coriolis meter installed in the LHC Test String cryogenic distribution line insulation vacuum envelope

Two qualifying prototypes were installed in the LHC Test String and have been in operation since August 2001. In the Test String, their performance and their use by the operation team have been confirmed as the two meters have been constantly used to monitor consumption on the main cooling loops and to verify operating conditions during transients. The heat loads of the LHC Test String have also been assessed more precisely than previously and are constantly being monitored during different operating conditions and extrapolated for the LHC machine. A few watts increase above the expected heat loads of the 1.9 K superfluid helium loop have been discovered confirming the higher than

budgeted heat loads mainly due to the prototype magnet instrumentation feed through system and the presence of prototype magnets with an old type of superinsulation.

Comparisons have been made between the Coriolis meters and the mass flow inferred by the valves opening. Errors up to 20 % were observed in the mass flow calculated with the valve opening when compared to the calibrated Coriolis meter. These larger than expected errors are probably due to variation in time of the opening characteristics and offsets of the valves.

The CMF025 used for cryogenic diagnostics was previously tested at the factory against thermal cycling: no component failures or calibration shifts were found after 30 thermal cycles down to liquid nitrogen temperatures and 4 thermal cycles down to liquid helium temperatures.

Metallurgical tests have confirmed that the lifetime of the mechanical system (oscillating tubes and case) is several orders of magnitude larger than the LHC lifetime. Therefore, the worst accident would be the loss of signal from one of the pick-up coils or the driving coil, with no effect on the operation of the LHC machine. To increase even further the reliability against a leak to the insulation vacuum, the external case that protects the oscillating tubes (now open to insulation vacuum) could be eventually filled with gaseous helium and sealed.

Chapter 9

9. ANALYSIS AND INTERPRETATION OF EXPERIMENTAL RESULTS

Extensive tests have shown that only a few cryogenic flowmeters based on heat transfer or on the Coriolis force can be successfully employed at cryogenic temperatures and in particular with supercritical helium.

Temperature and density oscillations of supercritical helium near the critical point have been observed in the measurements of the Coriolis meter and have increased the difficulty of measuring correctly a cryogenic flow rate, the measurement needing to be performed on a fluid of varying density.

The calibration of the Coriolis meters has shown an error close to 1 % consistent primarily with a shift in the Young's modulus from the one obtained by an acoustic method.

Recommendations and alternative solutions to meter cryogenic flow in the LHC machine are presented and discussed.

9.1 Cryogenic flowmeters performances

Table 15 summarises advantages and disadvantages of different methods of flow measurement for cryogenic helium applications. Accuracy is based upon only a room temperature calibration and is in % of the full-scale of the instrument. For the thermal probe flowmeters accuracy is based only on comparison with theoretical heat transfer correlations. Ultimate accuracy can only be reached with calibration at working conditions.

The results of the "in-house" built thermal probe flowmeters are promising in terms of robustness and achievable performances but require individual calibration at working conditions (expensive and time consuming) in order to achieve the expected performances. The limitations due to the temperature fluctuations can be overcome with filtering and continuous computing of the heat transfer. Otherwise they will better perform away from the critical region of instabilities.

Turbine flowmeters have definitely shown poor performances and in particular lack of robustness for long term operation. The Venturi flowmeter tested has confirmed a good achievable accuracy (with individual cryogenic calibration) but also lack of robustness and long term zero stability.

On the basis of the flowmeter specification, but in general taking into consideration the performances achievable at cryogenic temperature without expensive calibration at nominal operating conditions, the best device is undoubtedly a Coriolis flowmeter. Its price is relatively high in terms of capital cost but does not require a "cryogenic" calibration to achieve the required performances. The main advantage is the direct measurement of the mass flow rate with an accuracy of 0.5 % and repeatability of 0.2 %. Its extremely high reliability and practically zero cost of operation makes this instrument a valuable and extremely useful diagnostic for cryogenic installations. Its robustness, precision and repeatability make it an alternative control parameter for the cryogenic cooling power sharing among large installations and distribution transfer lines.

Type of meter	Recommended application	Accuracy [ultimate]	Repeatability	Rangeability Press. Drop	Cost capital/ operation
Coriolis	Mass flow, industrial, high accuracy	± 0.5 % [± 0.25 %]	± 0.2 %	Very good Medium	Med/high Low
Venturi	Volumetric, laboratory	10 % [± 2 %]	± 2 %	Medium Good	Medium High
Thermal probe: heated sensor	Mass flow, laboratory, low cost flow monitor	± 15 % [± 10 %]	± 5 %	Low Very good	Low Medium
Turbine Levitated	Volumetric, laboratory	± 20 % [± 0.8 %]	± 0.8 %	Medium Good	High Medium
Time-of-Flight	Volumetric, laboratory, flow monitor	± 20 % [± 10 %]	± 10 %	Medium Very good	Medium High
Turbine Classical	Volumetric, laboratory, or industrial	± 20% [± 10 %]	± 10 %	Medium Good	Medium High
Thermal probe: wire grid	Mass flow, laboratory, flow monitor	± 25 % [± 10 %]	± 5 %	Low Very good	Low Medium
Thermal pulse	Mass flow, laboratory, flow monitor	± 25% [± 10 %]	± 10 %	Low Very good	Med/low Medium

Table 15: Qualitative comparison of various cryogenic flowmeters tested

9.2 Supercritical helium instabilities

Giarratano et al, 1971, report that in their experimental set-up to measure heat transfer to supercritical helium (as well as a number of other investigations), there is an appearance of oscillations during heat transfer to near critical fluids as is the case in our installation. An apparent criterion for the onset of oscillations is the presence of vastly differing states of the fluid within the system (a kind of void area in the high density fluid). This situation can be encountered in the near critical region and along the transposed critical line, where large changes in density occur with small changes in temperature (due to heat loads), or in the region away from the critical, under high heat flux or high wall-to-bulk temperature ratio conditions. The frequency of the oscillation varies from about 0.05 to 0.1 Hz with amplitude in temperature varying from 0.01 to 1 K.

In our test station we have experienced similar oscillations with various types of flowmeters: thermal probe, turbine and Coriolis.

Oscillations onset appears to occur at a certain critical heat that varies mainly with the mass flow (the larger the mass flow, the larger will be the critical flux at which the oscillation appears for a defined geometry and helium properties). Once the oscillation in temperature has started, it provokes oscillation in density that can be seen with the Coriolis flowmeter as real oscillation in mass flow about a mean value. The same frequency oscillation can be seen with a differential pressure transducer and is very much reduced and damped in an external reference "warm" flowmeter. The oscillation in mass flow increases the temperature fluctuations and therefore the density variations. Thus the oscillations of the system diverge. To reduce the oscillation the only solution is to increase the mass flow and/or decrease the heat load (switch off the thermal probe).

The oscillations or instabilities in the fluid temperature and flow encountered during the tests were therefore investigated with additional tests and a literature search.

Further tests have shown that the onset of the oscillations in temperature and mass flow happens to be at around 5.5 K and 3 bar in the zone where the variability of most of the physical parameters of helium is drastic.

A similar behaviour of helium near the critical point or the transposed critical line has already been observed in other experiments and in particular in the test set-up for the beam screen cooling loops at CERN. The beam screens are cooled between 5 and 20 K by forced flow of weakly supercritical helium in order to avoid two-phase flow in long and narrow channels but a risk of thermohydraulic instabilities is present as observed in experiments performed on test loops.

There are various types of instability as found in the literature:

1. Acoustic oscillations at high frequencies due to a large temperature gradient along the cryogenic tubes. Heat is transferred from the warm side to the cold one and this can develop an oscillatory movement of the fluid;

2. Thermal oscillations associated with the interaction of the heat transfer coefficient and the fluid flow; their period is defined by the tube inertia;

3. Wave of density due to the change of density and positive feed-back in the controlled cooling loop.

Experimental and theoretical work has given sufficient evidence to support the view that the main type of dynamic instability in channels is caused by the propagation of density waves due to multiple regenerative feedback. A small flow

fluctuation creates an enthalpy perturbation in the "liquid-like" density region and travels along the channel until it reaches the "gas-like" density region caused by heat loads and pressure drop along the channel. With correct timing the perturbation can therefore acquire appropriate phase and become self-sustaining.

An oscillating helium flow in the LHC conduit or two parallel tubes of a Coriolis mass flowmeter can therefore create large variations of pressure and temperature and therefore cause significant operational problems as well as measuring errors.

9.3 Coriolis meter mass flow oscillation perturbations

Cheesewright et al, 1999, have identified and listed external factors which can influence the calibration of Coriolis mass flowmeters. The work has mainly been performed to show how flow pulsations and/or mechanical vibrations can affect the calibration of Coriolis meters. In our case, density waves in supercritical helium can give rise to flow pulsations and even mechanical vibrations.

The conclusions of the work performed by Cheesewright et al, 1999, are that for disturbances at the Coriolis frequency (natural frequency of the Coriolis twisting mode of the tube) Coriolis meters may fail completely. For disturbances at a frequency close to the meter drive frequency all the meters showed a significant oscillation in their output signal but the mean value of the output signal agreed well with the calibration. At other frequencies the disturbances can excite the Coriolis frequency error mechanism due to the presence of higher harmonics.

In our tests low frequency oscillations of the signals have been observed with instantaneous incorrect measurement values but by setting the electronics to average over several seconds, the mean value was found to be true within 0.5 %. Density changes and flow pulsation do not affect the flowmeter performances as long as there is no need of fast acquisition rates (above 0.5 Hz).

9.4 The modulus of elasticity at cryogenic temperatures

The coefficients of proportionality in the Coriolis meter are related to the dimensions and flow tube shape (taken into account during the water calibration) and to the modulus of elasticity. Using the ratio of the Young's modulus value below 20 K and the value at 293 K we can use the Coriolis meter for mass flow measurement with the precision of the measurement of the Young's modulus by acoustic methods, (± 1 % accuracy error band). Figure 63 shows the Young's modulus as found in the literature (Ledbetter, 1980 and 2000) compared with the measurements inferred from the IMGC calibration test facility with a Coriolis meter (± 0.5 % accuracy error band). The low temperature measurements based on mass flow calibration seem to suggest a further small decrease of the Young's modulus below 20 K. This is further supported by consistent performances of meters with different geometries and sizes.

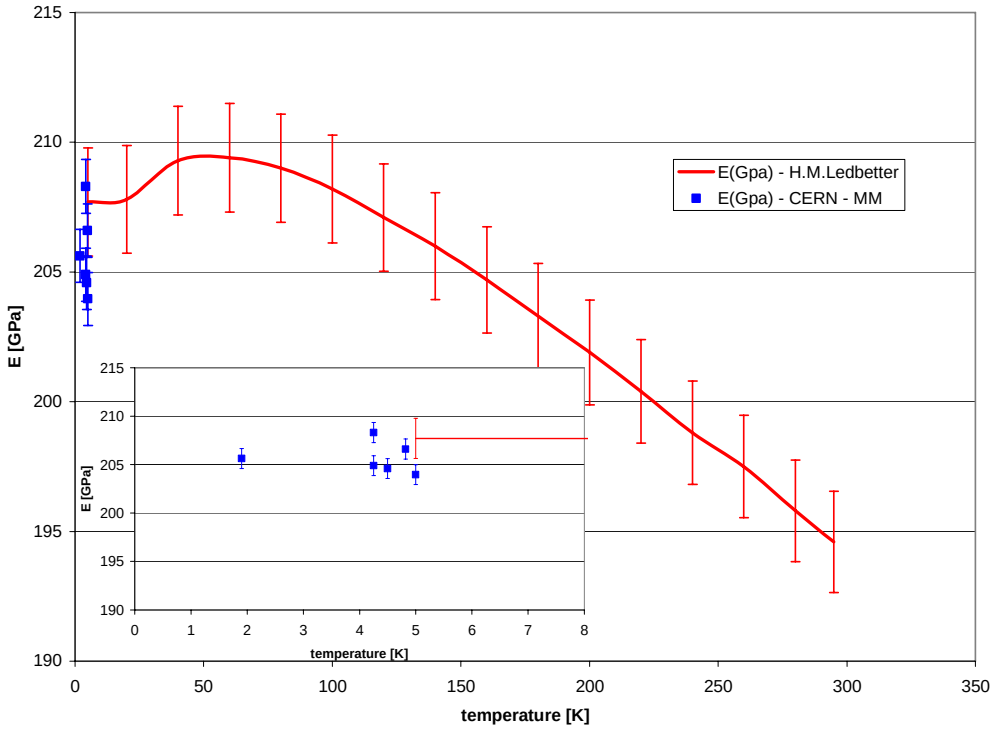

Figure 63: Temperature dependence of Young's modulus for stainless steel 316 L as found in literature and measured via mass flow calibration of Coriolis meters

There is therefore a possible correction of the Young's modulus based on mass flow measurements at low temperatures based on mass flow calibration of Coriolis meters in the IMGC calibration facility.

Further and more extensive tests at low temperatures will be useful and recommended to confirm if the systematic offset between the calibration facility at IMGC and the Coriolis meters under test is due to the inaccuracies of the Young's modulus inferred by the acoustic method below 20 K, to the existence of a further decrease of Young's modulus below 5 K or to other low temperature effects.

9.5 Heat transfer correlations

The experimental results of the heat transfer based flowmeter have validated the heat transfer correlations in steady state and to a smaller extent the dynamic heat transfer theory. The correlations found in the literature have been verified and seem to be in accordance with experimental results as long as the temperature dependent physical properties of the fluid are taken into account as in equation 5.10. A better constant for this equation has been found which gives the following correlation valid for the heat transfer from a heated temperature sensor of about 4 mm diameter in the middle of a 20 mm diameter conduit:

$$Nu = 0.022\,\mathrm{Re}_D^{4/5}\,\mathrm{Pr}^{2/5}\left(\frac{T_s}{T_m}\right)^{-0.716}$$

9.6 Analysis of the added value of a cryogenic flowmeter

It was strongly recommended to install Coriolis meters in all the LHC cooling loops because of the proven performance and reliability demonstrated in the field at ambient temperature and at the LHC operating conditions in our installations and IMGC calibration facility.

The flowmeters are indeed a diagnostic tool and not an active component of the cryogenic system, but would be a valuable instrument during the commissioning and operation of the LHC machine.

The operating teams of the machine are mainly composed of technicians and industrial support operators for whom on-line measurements of cooling flow distribution can allow early diagnosis and faster troubleshooting as well as better identification of the process.

Economic constraint have excluded the possibility of installing such devices and alternative but less accurate methods based on the flow inferred by valves opening with pressure and temperature measurements have been implemented.

9.7 Proposed alternative solutions to meter a cryogenic flow

The valve opening measurements to infer the mass flow have given larger than the expected 12 % mass flow error when compared with the Coriolis meters. This difference takes probably into account variation with time of the opening characteristics and offsets of the valve.

The Coriolis accuracy allows to measure flow rates of a few g/s with better than 0.05 g/s or about a 1 W resolution at 1.9 K.

Even the best valve accuracy of 12 % for a nominal flow of 5 g/s would allow about 0.6 g/s accuracy or about a 12 W resolution at 1.9 K.

A typical measurement of the arc cell splice resistances would give an increase of about 10 W to the static heat loads on the 1.9 K circuit, while the beam screen minimum flow increase is 1.4 g/s. The valve measurement would therefore give only a rough indication of the process performance while a Coriolis flowmeter would allow precise and reliable monitoring of the process. In case of missing or

broken instrumentation (temperature sensors), the Coriolis flowmeter would even allow "blind" operation for the control of the valve based on historic data of flow versus magnet current and beam intensity.

Chapter 10

10. CONCLUSIONS

Mass flow measurements can be achieved with expensive calibration at cryogenic working conditions of lower manufactured cost devices depending on the final precision required. Nevertheless, if ultimate accuracy, reproducibility and reliability are required, there is a superior and clear advantage in using a true mass flow measurement and in particular a flowmeter based on the Coriolis force.

To date, using Coriolis meters, better than 0.5 % absolute accuracy and 0.2 % reproducibility have been achieved. It may be possible, with further testing, to achieve a better absolute accuracy with no need of individual calibration but only by measuring at working temperature the Young's modulus of a sample of a chosen stock of the flow tubes material used to manufacture the meters.

In particular, tests have shown the insensitivity of the Coriolis flowmeters to the type (water, helium) and thermodynamic state (superfluid, liquid, supercritical, gas) of the fluid metered.

These meters chosen for the LHC (CMF025) will be able to measure a variation of less than 0.02 g/s, thus less than 0.5 W at 1.9 K, with an absolute accuracy of about 1 W.

After extensive testing, two Coriolis prototype meters were installed in the LHC Test String and have permitted the assessment and monitoring of the thermal performance of components of the LHC machine.

Temperature variations in the refrigerator supply, causing density oscillation and therefore oscillations in the cooling flow, without an accurate flow measuring device and are not clearly understandable from temperature and pressure sensor analysis. The Coriolis flowmeter however allows clear identification and on-line monitoring of these phenomena. Therefore it seemed to be a necessary tool for the operation crew.

The cost of the flowmeters, that appeared to be a disadvantage at the beginning, has been reduced by a joint effort of CERN and the supplier to reduce requirements and complexity of the meter electronics and manufacturing costs.

Nevertheless, due to budgetary cuts and the elevated number of required flowmeters, the installation of this diagnostic equipment in the LHC machine was reassessed and an alternative and cheaper solution identified.

Alternative flowmeter such as the Venturi, turbine and thermal probe flowmeters have much lower accuracy and their behaviour with oscillating flow is not proven. Under these circumstances an alternative method to infer the mass flow from the valves opening would be more adequate.

The method to infer mass flow from the on-line measurement of the valve opening and pressure drop, together with the density measurement, has been proposed, tested, calibrated and validated on the LHC Test String with Coriolis meters. It is used in the LHC for on-line measurement of flow with about 15 to 20 % accuracy.

Flow metering based on Coriolis devices might in future be used for special zones where heat loads have not yet been finally assessed or, if larger than expected, could hamper the correct functioning of the machine.

The Coriolis flowmeters modified and tested for cryogenic operation are being used continuously in test facilities at CERN and for cryogenic component acceptance. Having been calibrated at the IMGC recognized metrological laboratory they are also considered to be working secondary standards for cryogenic flow measurements.

The Coriolis flowmeters will allow further investigation of supercritical helium oscillations with a direct measurement of mass flow pulsation. Calibrating Coriolis meters made of the material of interest in the IMGC facilities or using the calibrated flowmeters as secondary standards, would allow the assessment of the Young's modulus of material at cryogenic temperature with better accuracy than the acoustic method.

Is the cost of an accurate mass flow measurement worth the benefit? Would the measurement of the valve opening give sufficiently accurate information on the process performance and diagnose on time possible problems or system limitations? Unfortunately, the comparison will not be made but, hopefully, the system would not require precise metering at least for the first years of operation. When and if the limit of cryogenic power is reached, the lack of precise metering might increase the cost of the cryogenic system upgrade because of the lack of local information (around the ring).

The use of flowmeters as an operation diagnostic tool seems to be driven by short term economic reasons based on investment costs rather than operational savings. Nevertheless, accurate and repeatable flowmeters are always required during the R&D phase of a project to assess and improve the performance of the system to be built.

10.1 Recommendations for future work

In this section proposals for further work triggered or not fully completed by the present research are given.

10.1.1 Cryogenic flowmeters

Although the results of the Coriolis flowmeter tests are very good and its long-term capabilities very promising, there is no experience on the long-term behavior in terms of robustness, accuracy and drifting. It would be advisable to install in a cryogenic facility a second flowmeter to continuously verify its performance on a longer period than the one observed during this research.

The improved version of the thermal probe flowmeter presented in 8.2.1 should be manufactured, tested and validated for use as a simple and inexpensive flow indicator in cryogenic installations. Independently from the heat transfer correlation, the reproducibility of several manufactured thermal probe flowmeters should be verified. This could improve the expected accuracy (after calibration) of these devices.

10.1.2 Supercritical helium oscillations

Further work should be performed on the possibility of using Coriolis meters to measure density oscillations and pulsating flow at frequencies close to the Coriolis natural frequency and the meter drive frequency. The extent of the disturbances in meter reading and the analogy with the influence of mechanical vibration on the calibration of Coriolis mass flowmeters should be verified.

10.1.3 Young's modulus

Additional tests on the difference in Young's modulus measurements at low temperature between the IMGC calibrator and the acoustic method should be performed to confirm the findings. Possible improvements of the IMGC or other calibrators should be envisaged to use it as a Young's modulus measuring bench.

The possible application for other temperature ranges should be investigated together with effects of temperature changes on static stress levels within the flow tubes that could modify its stiffness.

REFERENCES

Bager T. et al, Instrumentation, field network and process automation for the cryogenic system of the LHC Test String, Proceedings ICALEPS, 2001

Baker R. C., Flow Measurement Handbook, Cambridge University Press, 2000, (a)

Baker R. C., Flow Measurement Handbook, Cambridge University Press, 99, 2000, (b)

Baker R. C., Flow Measurement Handbook, Cambridge University Press, 166, 2000, (c)

Baker R. C., Flow Measurement Handbook, Cambridge University Press, 398-421, 2000, (d)

Baker R. C., Flow Measurement Handbook, Cambridge University Press, 421-423, 2000, (e)

Baker R. C., Flow Measurement Handbook, Cambridge University Press, 117,134,148,158,198,228,264,381,409,428, 431,435, 2000, (f)

Barre C., Private communications, 1999

Benda V. et al, Conceptual Design for the Cryogenic System for the Large Hadron Collider, LHC Project Report 12, CERN, July 1996

Bird R. B., Stewart W. E., Lightfoot E. N., Transport Phenomena, Wiley, New York, 1966

Bloem W. B., Transient Heat Transfer to a Forced Flow of Supercritical Helium at 4.2 K, Cryogenics, Vol. 26, 300-308, 1986, (a)

Bloem W. B., Transient heat transfer to a forced flow of supercritical helium at low temperatures, Netherlands Energy Research Foundation ECN, Petten, NL, 1986, (b)

Bon Mardion G., Claudet G. and Seyfert P., Practical data on steady state heat transport in superfluid helium at atmospheric pressure, Cryogenics 19, 45-47, 1979

Bordry F. et al, The LHC Prototype Full-Cell: Design Study, LHC Project Report 170, CERN, March 1998

Carlslaw H.S., Jaeger J.C., Conduction of heat in solids, Clarendon Press, Oxford, 1959

Casas-Cubillos J. et al, Operation, Testing and Long Term Behaviour of the LHC Test String Cryogenic System, LHC Project Report 210, CERN, July 1998

Casas J. and Serio L., Gas Flow Rate Meters, Handbook of Applied Superconductivity, IOP Publishing UK, chapter E2, 897-907, 1998

Chapman J., Heat Transfer, Macmillan Publishing Co., 1984

Cheeswright R. and Clark C., The effect of flow pulsations on Coriolis mass flowmeters, Journal of Fluids and Structures, 12, 1025-1039, 1998

Cheeswright R. et al, Understanding the experimental response of Coriolis mass flowmeters to flow pulsations, Flow Measurement and Instrumentation, 10, 207-215, Elsevier, 1999

Cheeswright R. et al, The identification of external factors which influence the calibration of Coriolis mass flowmeters, Flow Measurement and Instrumentation, 11, 1-10, Elsevier, 2000

Chorowski M. et al, A Simplified Cryogenic Distribution Scheme for the Large Hadron Collider, LHC Project Report 143, CERN, August 1997

Claudet G. and Aymar R., Tore Supra and helium-II cooling of large high-field magnets, Adv. Cryo. Eng. 35A, 55-67, 1990

Claudet S., Erdt W., Frandsen P., Gayet Ph., Solheim N. and Winkler G., Four 12 kW / 4.5 K cryoplants at CERN, Cryogenics 34 ICEC Supplement, 99-102, 1994

Claudet S., Gayet Ph. and Wagner U., Specification of four new large 4.5 K refrigerators for the LHC, paper presented at CEC '99 Montreal, 1999

Coughlan G. D. and Dodd J. E., The ideas of particle physics, an introduction for scientist, Cambridge University Press, second edition, 1991

Cryodata Inc., www.cryodata.com, P.O. Box 173, Louisville, Colorado 80027, USA

Cumming R. D. and Smith J. L., Liquid Helium Technology, Pergamon Press, Oxford, 1966

DeBoom R. et al, Traceability and Uncertainty Analysis for a Calibration Process for Flowmeters, Using Coriolis Flowmeters as Reference, Micro Motion, Inc., Boulder, Colorado, USA, internal report, 2000

Dittus F. W. and Boelter L. M. K., University of California, Berkeley, Publ. Eng., vol. 2, p. 443, 1930

Erdt W., Riddone G., Trant R., The Cryogenic Distribution Line for the LHC: functional specification and conceptual design, Proceedings CEC-ICMC '99, Montreal - Quebec, Canada, 1999

Evans L. R., The Large Hadron Collider, Proceedings ICEC16 Elsevier, Amsterdam, 1997

Evans L. R., The Large Hadron Collider, present status and prospects, MT16, Ponte Vedra Beach, Florida, USA, 1999

Giarratano P. J. et al, Forced convection heat transfer to supercritical helium, Cryogenics, 385-394, 1971

Giarratano P. J. et Steward W. G., Transient forced convection heat transfer to helium during a step in heat flux, Journal of heat transfer, Vol. 105, 350-357, 1983

Hatchadourian E., Stability and control of supercritical helium flow in the LHC circuits, Proceedings CEC '99, Montreal, 1999

Hatchadourian E. et al, Supercritical helium cooling of the LHC beam screens, proceedings ICEC 17, Bournemouth UK, 1997

Hauviller C. et al, The Electrical Distribution Feed Box for the LHC Prototype Cell, LHC Project Report 416, September 2000

Hebral B. et al, Cryogénie, ses applications en supraconductivité, Techniques de l'ingénieur, IIF, Paris, 1995

Hebral B., Private communications, 1999

Khalatnikov I. M., Introduction to the Theory of Superfluidity, Chap. III, W.A. Benjamin, New York, 1965

King L. V., On the convection of heat from small cylinders in a stream of fluid, Phil. Trans. Roy. Soc., A214-373, 1914

Kramers H., Physica, Vol. 12, 61, 1946

Kuper C. G., Physica, Issues 6-10, 1009-1017, 1958

Landau L. and Lifchitz E., Mécanique de Fluides, MIR, Moscow, 1971

Lebrun Ph., Tavian L. and Claudet G., Development of large-capacity refrigeration at 1.8 K for the Large Hadron Collider, Proceedings Kryogenika'96, Icaris, Praha, Czech Republic, 54-59, 1996

Lebrun Ph., Superfluid helium as a technical coolant, presented at 15th UIT National Heat Transfer Conference, Torino, Italy, 61-77, June 19-20 1997

Lebrun Ph. et al, Demands in refrigeration capacity for the Large Hadron Collider, Proceedings ICEC16 Elsevier, Amsterdam, 1997

Lebrun Ph., Serio L., Tavian L. and van Weelderen R., Cooling Strings of Superconducting Devices below 2 K: The Helium II Bayonet Heat Exchanger, LHC Project Report 144, CERN, September 1997

Lebrun Ph. et al, Cool-down and Warmup Studies for the Large Hadron Collider, LHC Project Report 214, CERN, July 1998

Lebrun Ph., Advanced Superconducting Technology for Global Science: the Large Hadron Collider at CERN, CEC-ICMC 2001 Conference, Madison, Wisconsin, USA, 16-21 July 2001

Ledbetter H. M. et al, Low-temperature elastic properties of four austenitic stainless steels, J. Appl. Phys. 46(9), 3855-3860, 1975

Ledbetter H. M., Stainless-steel elastic constants at low temperatures, J. Appl. Phys. 52(3), 1587-1589, 1980

Ledbetter H. M., Private communications, 2000

Livingston M. S., High-energy accelerators, Interscience Publishers Inc., New York, USA, 1954

McAdams W. H., Heat Transmission, McGraw-Hill, New York, 1954

MicroMotion Inc., Elite Sensor Instruction Manual, July 1999

Murakami M. and Shimizu Y., Asymmetric swirling flows in composite pipe bends, bulletin of JSME, Vol. 21, n. 157, 1144-1151, 1978

Murakami M. et al, Studies on fluid flow in three-dimensional bend conduits, bulletin of JSME, Vol. 12, n. 54, 1369-1379, 1969

Ower E. and Pankhurst R. C., The measurement of air flow, Oxford, Pergamon Press, 1966

Rausch R., Pignard C., Wijnands T., Qualification of Electronic Components and Systems in a LHC Tunnel Radiation Environment, 8th European Particle Accelerator Conference : a Europhysics Conference, La Vilette, Paris, France, 263, 3 - 7 Jun 2002

Rausch R. and Tavlet M., On-line Radiation Test Facility for Industrial Equipment Needed for the Large Hadron Collider at CERN, Proceedings ICALEPS, 1999

Reader-Harris M. J. and Keegans W., The equation of expansibility factor for orifice plates, FLOWMEKO '98 9th Int. Conf. on flow measurement, Lund, Sweden, 209-214, 1998

Rivetti A., Martini G., Birello G., A Flowrate Calibrator for Cryogenic Helium, Adv. Cryo. Eng., Vol. 39, 1043-1050, Plenum Press, New York, 1994, (a)

Rivetti A., Martini G., Birello G., Metrological Performances of Venturi Flowmeters in Normal, Supercritical and Superfluid, Helium, Adv. Cryo. Eng., Vol. 39, 1051-1058, Plenum Press, New York, 1994, (b)

Rivetti A., Martini G., Birello G., LHe flowmeters: state of the art and future developments, Adv. Cryo. Eng., Vol. 41, 1789-96, 1996

Rivetti A. et al, An Accurate Rotor-Levitated Turbine Flowmeter for Cryogenic Service, to be published in Adv. Cryo. Eng., 2004

Sandborn V. A., Resistance Temperature Transducers, Metrology Press, Fort Collins Colorado, USA, 1972

Schmidt C., Proc. Stability of Superconductors, International Institute of Refrigeration, Paris, 1981

Seeber B., Handbook of Applied Superconductivity, IoP Publishing, Bristol UK, 1998

Serio L. et al, The Superfluid Helium Cryogenic System for the LHC Test String: Design, Construction and First Operation, Adv. Cryo. Eng., Vol. 41, 777-784, Plenum Press, New York, 1996, (a)

Serio L. et al, Development of a mass flowmeter based on the Coriolis acceleration for liquid, supercritical and superfluid helium, Proceedings of the Nineteenth International Cryogenic Engineering Conference, Grenoble, France, 647-650, 2002, (b)

Serio L. et al, The cryogenic system for the LHC Test String 2: design, commissioning and operation, Proceedings of the Nineteenth International Cryogenic Engineering Conference, Grenoble, France, 63-66, 2002, (c)

Spitzer D. W., Flow Measurement, Instrument Society of America, 1991, (a)

Spitzer D. W., Flow Measurement, Instrument Society of America, 335-345, 1991, (b)

Spitzer D. W., Flow Measurement, Instrument Society of America, 406-407, 1991, (c)

Spitzer D. W., Flow Measurement, Instrument Society of America, 395-398, 1991, (d)

Spitzer D. W., Flow Measurement, Instrument Society of America, 539-573, 1991, (e)

Spitzer D. W., Flow Measurement, Instrument Society of America, 56-58, 1991, (f)

Tavlet M. and Leon Florian M. E., Dose and neutron-fluence measurements in mixed gamma-neutron fields by means of semi-conductor dosimeters, Radecs'93, IEEE Cat. N. 93TH0616-3, pp 27-32, 1994

van Sciver S. W., Helium Cryogenics, Plenum Press, New York, 54, 1986 (a)

van Sciver S. W., Helium Cryogenics, Plenum Press, New York, 1986, 89-137, (b)

van Sciver S. W., Helium Cryogenics, Plenum Press, New York, 1986, 89-96, (c)

van Sciver S. W., Helium Cryogenics, Plenum Press, New York, 1986, 199-235, (d)

van Sciver S. W., Helium Cryogenics, Plenum Press, New York, 1986, 142-146, (e)

Vance R. W. and Duke W. M., Applied Cryogenic Engineering, John Wiley & Sons Inc., New York, 1962

VELAN Inc., www.velan.com, 7007 Cote de Liesse, Montreal, QC, H4T 1G2, Canada

Weisend J. G., Handbook of Cryogenic Engineering, Taylor and Francis, Philadelphia, 1998

Wilks J., The properties of liquid and solid helium, Clarendon Press, Oxford, 1967

Wilson M. N., Superconducting Magnets, Clarendon Press, Oxford, 1983

Zeppenfeld D., Nikitenko A., Richter-Was E., Measuring Higgs boson couplings at the LHC, Phys.Rev., D : 62, 13009, 2000